1993

In Situ Determination of Capillary Pressure and Relative Permeability Curves Using Well Logs.

Adel Afifi Ibrahim
Louisiana State University and Agricultural & Mechanical College

Recommended Citation

Ibrahim, Adel Afifi, "In Situ Determination of Capillary Pressure and Relative Permeability Curves Using Well Logs." (1993). *LSU Historical Dissertations and Theses*. 5517.
https://digitalcommons.lsu.edu/gradschool_disstheses/5517

INFORMATION TO USERS

This manuscript has been reproduced from the microfilm master. UMI films the text directly from the original or copy submitted. Thus, some thesis and dissertation copies are in typewriter face, while others may be from any type of computer printer.

The quality of this reproduction is dependent upon the quality of the copy submitted. Broken or indistinct print, colored or poor quality illustrations and photographs, print bleedthrough, substandard margins, and improper alignment can adversely affect reproduction.

In the unlikely event that the author did not send UMI a complete manuscript and there are missing pages, these will be noted. Also, if unauthorized copyright material had to be removed, a note will indicate the deletion.

Oversize materials (e.g., maps, drawings, charts) are reproduced by sectioning the original, beginning at the upper left-hand corner and continuing from left to right in equal sections with small overlaps. Each original is also photographed in one exposure and is included in reduced form at the back of the book.

Photographs included in the original manuscript have been reproduced xerographically in this copy. Higher quality 6" x 9" black and white photographic prints are available for any photographs or illustrations appearing in this copy for an additional charge. Contact UMI directly to order.

In situ determination of capillary pressure and relative permeability curves using well logs

Ibrahim, Adel Afifi, Ph.D.

The Louisiana State University and Agricultural and Mechanical Col., 1993

In-Situ Determination of Capillary Pressure and Relative Permeability Curves Using Well Logs

A Dissertation

Submitted to the Graduate Faculty of the
Louisiana State University and
Agricultural and Mechanical College
in partial fulfillment of the
requirements for the degree of
Doctor of Philosophy

in

The Department of Petroleum Engineering

by
Adel A. Ibrahim
B.Sc., Suez Canal University, 1984
M.Sc., Suez Canal University, 1988
May 1993

ACKNOWLEDGMENTS

TABLE OF CONTENTS

LIST OF TABLES

LIST OF FIGURES

ABSTRACT

Capillary pressure and relative permeability characteristics of a reservoir rock are presently determined through core analysis. The process of core handling and cleaning can result in significant alteration in core wettability; consequently, tests conducted on these altered cores can produce non-representative reservoir rock characteristics. This dissertation documents a study of the possibility of in-situ determination of capillary pressure and relative permeability using pressure data in the transition zone and open hole well logs.

A pressure profile obtained from the formation tester defines the wettability, free water level, and hydrocarbon and water densities as well as the capillary pressure above the free water level. Correlating the pressure values to the water saturation values determined from the resistivity logs results in a capillary pressure/water saturation, $P_c(S_w)$, curve characteristic of the reservoir. A relative permeability curve then can then be derived from this $P_c(S_w)$ curve using empirical relationships.

This approach was tested in the laboratory using an eight-foot vertical sandstone core to simulate the formation. The core was fitted with electrode arrays, and resistivity measurements were used to construct the water saturation profile. The capillary pressure values were calculated from both the densities and the height above the free water level values. The free water level was indicated by a tube connected to the core setup. Chapter III documents the laboratory details of this experimental work together with its results and conclusions.

ix

A technique that can be used to extrapolate existing core data to cases where such data is absent or not representative of in-situ conditions is of interest. Chapter IV of this dissertation documents a new approach that has been developed and is based on using log data to derive a water saturation versus depth profile in the transition zone of the formation of interest. The log derived water saturation distribution is then correlated to generalized capillary pressure curves typical of the formation studied. This curve matching yields, by comparison, a capillary pressure curve specific to the formation of interest. The capillary pressure type curves are generated from already available core data and other petrophysical information. Relative permeability curves are subsequently generated using correlations based on Purcell's model. The technique is successfully applied to several field examples.

Special attention is given to cases of tight sands where relative permeability measurements on core samples are very complex, time consuming, and inaccurate due to the very small pore space available to the fluid to move through the tight sand cores. In Chapter V, the above mentioned technique is extended to tight sand cases where a special relationships characteristic of tight sands are developed and mathematically manipulated to adapt already existing relative permeability equations.

CHAPTER I

FLUID FLOW CHARACTERISTICS IN POROUS MEDIA

1.1   General

The coexistence of two or more immiscible fluids within the voids of a porous rock gives rise to capillary forces. Because an interfacial tension exists at the boundary between two immiscible fluids in a pore space, the interface is curved, and there is a pressure differential across the interface.

The magnitude of capillary pressure between two immiscible liquids in a porous medium is attributed to a number of factors, the most important of which are:

- The texture of the porous medium

- Wettability

- Relative saturation of the two fluids

- Saturation history

The proceeding factors can also be considered as the most important factors that affect the relative permeability curve for the same system. Since both the capillary pressure curve and the relative permeability curves are affected mainly by the same factors, there should be a direct relationship between the two that will allow the determination of one curve from the other.

1

The direct relationship between wettability and both the capillary pressure curve and the relative permeability curves comes from the fact that the location, distribution, and the flow of fluids inside the core are strongly affected by the wettability of the core.

The following sections review the development of measurements of the capillary pressure curve and the relative permeability curves. Some advantages and disadvantages of these methods are also mentioned. Special attention is given to the effect of wettability on both the capillary pressure and the relative permeability curves.

1.2   Determination of Capillary Pressure Curve

Four methods for measuring the capillary pressure on small core samples are presently in use. These methods are the porous diaphragm method of Bruce and Welge, the mercury injection method of Purcell, the dynamic method of Brown, and the centrifuge method. These methods are discussed below:

1.2.1 Porous Diaphragm Method

In the restored state method, developed by Bruce and Welge [1947], the core sample, saturated with a wetting fluid, is placed on a porous diaphragm that is permeable to the wetting phase. By the application of a known pressure to the non-wetting phase, which is confined above the diaphragm, a portion of the wetting phase is expelled from the core sample. By the use of successively higher pressure values in this procedure, a relation between the capillary pressure curve and the fluid saturation can be established.

The advantage of this technique is that either the actual fluids or any combination of fluids can be used. A drawback is that as the core approaches equilibrium, the pressure differentials which cause flow are vanishingly small. To go to final equilibrium and complete determination of the capillary pressure curve may take several weeks.

1.2.2 Mercury Injection Method

In the Mercury Injection technique, as proposed by Purcell [1949], mercury is injected under pressure into an evacuated core sample. The amount of mercury (the non-wetting phase) injected into the core sample is recorded at each injection pressure to determine the capillary pressure curve.

As compared to the porous diaphragm method, the mercury injection method requires a much shorter measuring time. Also, a higher pressure range is available with mercury injection. The main disadvantage of this method is the difference in the wetting properties of mercury and the real reservoir fluids. Permanent loss of the core is also a significant disadvantage.

1.2.3 Dynamic Method

The dynamic method was proposed by H. W. Brown, [1951] using a Hassler tube. In this technique, both wetting and non-wetting phases are introduced into the core. When the pressure difference between the non-wetting and the wetting phase are equal at the inlet and the outlet, equal capillary pressure exists, and a homogeneous water saturation inside the core is attained. The pressure difference equals the capillary pressure at the average saturation of the core which is determined by weighing the core.

1.2.4 Centrifuge Method

High acceleration in a centrifuge increases the effective force on the fluids, subjecting the core, in effect, to an increased gravitational force. When the sample is rotated at an incremental number of constant speeds, a complete capillary pressure curve can be obtained. The speed of rotation is converted into force units in the center of the core sample.

1.2.5 Using Wireline Formation Tester Data

In a homogenous water-wet reservoir with an oil water contact, the variation of saturation and phase pressure from the water zone through the capillary transition zone into the oil zone is shown in **Figure 1.1**. In the transition zone, the phase pressure difference is given by the capillary pressure which is a function of the wetting phase saturation. For an oil-water system, the capillary pressure is calculated as:

$$P_c (S_w) = P_o - P_w \qquad (1.1)$$

where:

P_o is the pressure in the oil phase; and

P_w is the pressure in the water phase.

At hydrostatic equilibrium, the capillary pressure equals:

$$P_c(S_w) = \Delta\rho * g * h \qquad (1.2)$$

where:

$\Delta\rho = \rho_w - \rho_o$ (The density difference)

ρ_w is the water density;

ρ_o is the oil density; and

h is the vertical height above the free water level.

On the depth-pressure diagram the intersection of the continuous phase pressure lines occurs at the free water level as shown in **Figure 1.1**.

The oil-water contact corresponds to the depth at which the oil saturation starts to increase from zero. The free water level is the depth at which the capillary pressure is zero. The oil-water contact lies above (for water-wet reservoir), or below (for oil-wet reservoir) the free water level by an amount depending on the threshold pressure, which in turn depends on formation parameters such as grain size, permeability, and porosity.
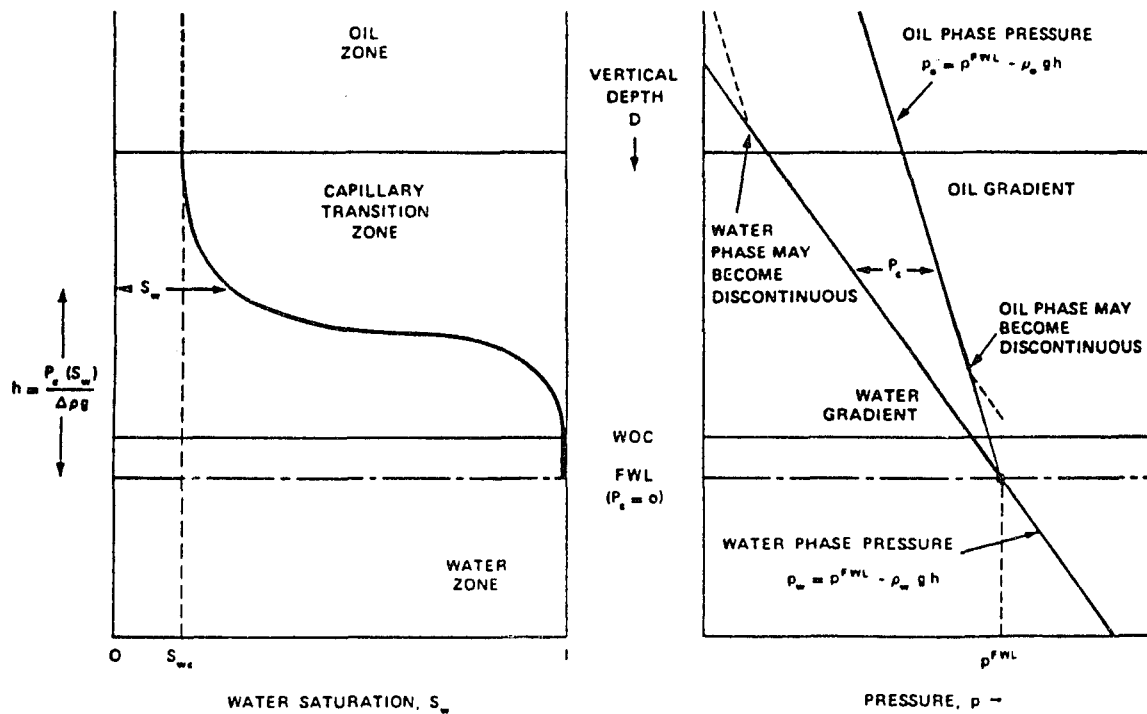
Figure 1.1 Capillary pressure in the transition zone of a water-wet reservoir.

1.3 Laboratory Measurement of Relative Permeability

In steady state methods, a mixture of fluids of fixed proportions is forced through the test sample until the saturation and the pressure equilibria are established. The primary concern in designing the experiment is to eliminate or reduce the saturation gradient which is caused by capillary pressure effects at the outflow boundary of the core [Honarpour et al., 1986]. Some of the more commonly used laboratory methods for steady-state relative permeability measurements are briefly described below:

1.3.1 Single Sample Dynamic Method

The Single Sample Dynamic Method method was developed by Richardson et al. [1952]. Two immiscible test fluids are injected simultaneously through a single core. End effects are minimized by using a relatively high flow rate, therefore, the region of high wetting-phase saturation at the outlet face of the core is small.

The theory which has been developed is mainly a combination of Darcy's equations for wetting and non-wetting phases, with the equation defining the capillary pressure.

1.3.2 Penn-State Method

The version of the apparatus that was described by Geffen et al [1951], is shown in Figure 1.2. In order to reduce the end effect due to capillary forces, the sample to be tested is mounted between two rock samples that are similar to the test sample. This arrangement also promotes thorough mixing of the two fluids before they enter the test sample.
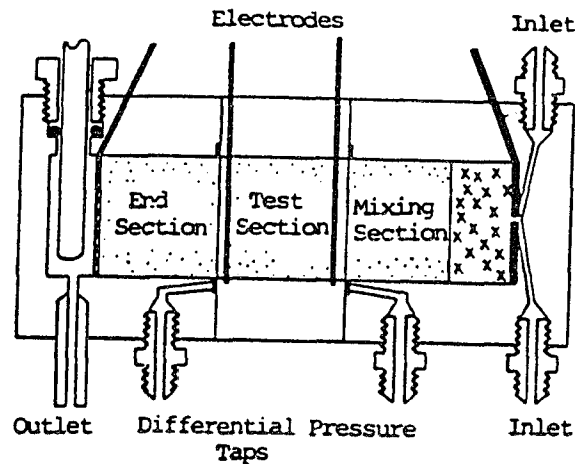
Figure 1.2 Three-section core assembly.

The laboratory procedure begins by flooding the sample with one fluid phase and adjusting the flow rate of this phase through the sample until a predetermined pressure gradient is obtained. Injection of the second phase at a low rate is then started, and the flow of the first phase is reduced slightly so that the pressure differential across the system remains constant.

After reaching a condition of equilibrium, the two flow rates and the pressure drop are recorded. The percentage saturation of each phase within the test sample is determined by removing the test sample from the assembly and weighing it. This procedure is repeated sequentially at higher saturations of the second phase until a complete relative permeability curve is established.

Honarpour **[1986]** questioned the accuracy of the weighing technique since it represents a potential source of errors. Many other methods for in-situ determination of the saturation in cores have been used, the most common of which are :

- Resistivity measurement

- Electric capacitance

- X-ray absorption (CT Scanner)

- Vacuum distillation

1.3.3 Hassler Method

This method was described by Hassler **[1944]**, and subsequently was modified by Osabo and Richardson **[1951]**. The proposed apparatus has the capability of measuring the pressure drop in each liquid separately. This measurement is achieved by the use of special membranes that can keep the two fluid phases separated at the outlet of the core, but still allow both phases to flow simultaneously through the core. By adjusting the flow rate of the non-wetting phase, the pressure gradients in the two phases can be made equal, equalizing the capillary pressure at both the inlet and outlet of the core.
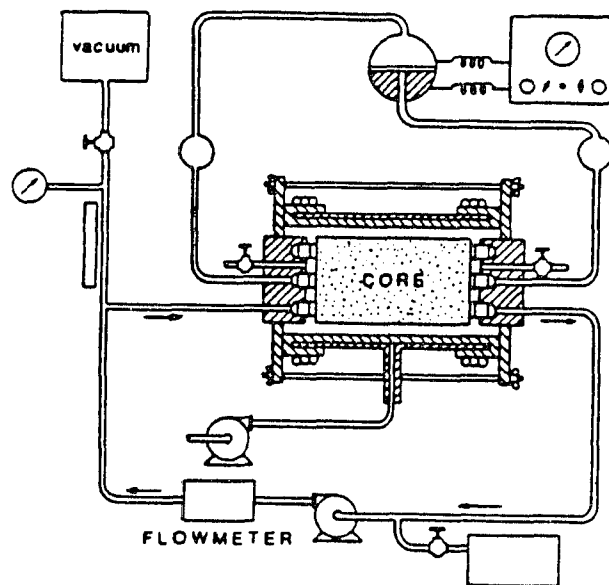
Figure 1.3 Two-phase relative permeability apparatus.

The Hassler technique is designed to provide a uniform saturation throughout the length of the core.

1.3.4 Stationary Fluid Method

Very low flow rates must be used in the Stationary Fluid technique as recommended by Leas et al. [1950]. Leas described his technique for measuring permeability to gas with the liquid phase held stationary in the core by capillary forces. As reported by Rapoport and Leas [1951], semi-barriers that are permeable to gas, but not permeable to liquid, may be used to hold the liquid phase stationary within the core.

Osoba et al. [1951], observed that relative permeability to gas determined by the stationary fluid method was in agreement with values measured by other techniques for the cases examined. However, they found that relative permeability to gas determined by the stationary fluid technique was generally lower than data obtained by other methods in the region of equilibrium gas saturation.

1.3.5 Dispersed Feed Method

In the Dispersed Feed method, the wetting fluid enters the test sample by first passing through a dispersing section made of porous material similar to the test sample [Richardson et al. 1952]. This dispersing section evenly distributes the wetting phase into the test sample. The non-wetting phase is introduced into radial grooves machined into the outlet face of the dispersing section. Pressure gradients used for the tests are high enough that the boundary effect at the outlet face of the core is not significant.

1.3.6 Unsteady State Relative Permeability

Buckley and Leverett [1942] developed the theory of this technique. Their model was based primarily on Darcy's law and the definition of capillary pressure in differential form. For an oil-water system, they developed the formula:

$$F_{o2} = \frac{1}{1 + \dfrac{K_{rw}\,\mu_o}{K_{ro}\,\mu_w}} \tag{1.3}$$

where:

K_{rw} is the relative permeability to water;

K_{ro} is the relative permeability to oil;

F_{o2} is the oil rate at the outlet of the core;

μ_w is the water viscosity; and

μ_o is the oil viscosity.

Since μ_w, and μ_o are known, K_{rw} and K_{ro} could be calculated from the production data at the outlet.

Welge [1952] extended Buckley and Leverett's model for calculating individual phase relative permeability curves from unsteady state test data. The equation they derived is:

$$\frac{F_o}{K_{ro}} = \frac{d\left\{\dfrac{1}{w_i\,I_r}\right\}}{d\left\{\dfrac{1}{w_i}\right\}} \tag{1.4}$$

where:

F_o is the fraction of displacement phase in flooding stream;

W_i is the cumulative injection in pore volume;

I_r is the relative injectivity; and

K_{ro} is the relative permeability of displaced phase.

The relative injectivity is defined as:

$$I_r = \frac{(u - \Delta P)_{\text{at any time}}}{(u - \Delta P)_{\text{at start of injection}}}$$ (1.5)

where u is the average velocity.

The expression for relative permeability of the displacing phase is:

$$K_{rw} = \frac{(1 - F_0)}{F_0} \frac{\mu_w}{\mu_o} K_{ro}$$ (1.6)

where

μ_w is the viscosity of displacing phase;

μ_o is the viscosity of displaced phase; and

K_{ro} is the relative permeability for displacing phase.

Johnson et al. **[1959]** got an excellent match when they compared results of the relative permeability tests to the calculated ones from gas flood experiments on short and long sandstone cores.

1.4   Effect of Wettability on Reservoir Fluid Flow Properties

1.4.1   General

Wettability is the main factor responsible for microscopic fluid distribution in porous media.   It determines to a great extent the amount of residual oil saturation and the ability of a particular phase to flow.

The direct relationship between wettability and relative permeability comes from the fact that the location, distribution, and even the flow of fluids inside the core are all strongly affected by the wettability of the core.

1.4.2 Factors Affecting Wettability, and the Effect of Core Handling

Wettability is an important factor that affects almost all types of core analysis. Since wettability controls the location, distribution, and flow of fluids in the reservoir rocks, the wettability directly affects capillary pressure, relative permeability, electric properties, and water flood behavior.

Water-wet cores can become oil-wet cores by the adsorption of polar compounds and/or the deposition materials that may be found in some crude oils.

1.4.3 Native-State, Cleaned, and Restored-State Cores

The four different states of preservation used in core analysis are:-

- Native-state cores;

- Fresh-state cores;

- Cleaned cores; and

- Restored-state cores.

The term "native" is used for any core that was obtained and restored by methods that preserve the wettability of the reservoir. Treiber et al. [1972] referred to "native-state" cores as those that were taken with a suitable oil-filtrate-type drilling mud which maintains the original connate water saturation.

When a core is obtained using water-base drilling mud that contains no compounds capable of altering core wettability, the core is said to have "fresh-state" unaltered wettability.

The term "cleaned-state" is used when an attempt is made to remove all of the original and intruded drilling fluids while cutting the core. Flooding the core with several pore volumes of different solvents is a common technique. Cleaned cores cannot be used for measuring relative permeability or electric properties of the reservoir; however, they can be used for measuring wettability-independent parameters such as porosity and air permeability.

The term "restored-state" is used when the following three steps are completed:
- Cleaning the core with strong solvents, and drying.
- Saturating the core with brine, followed by crude oil.
- Aging the core under reservoir conditions.

1.4.4 Factors Affecting Wettability In the Reservoir

The original strong water-wetness of most reservoir rocks can be altered by certain factors related to the chemistry of the flowing fluids, the rock mineralogy, and the reservoir conditions. These factors can be summarized as follows:-

a. Surface-active Compounds in Crude Oil

The surface-active agents in crude oil are believed to be polar compounds that contain oxygen, nitrogen, and/or sulphur, and possesses a polar and a hydrocarbon end. The polar end adsorbs on the rock surface, exposing the hydrocarbon end, making the surface

more oil-wet. The surface-active compounds in the crude oil are more prevalent in the heavier fractions of crude, such as resins and asphaltenes.

b. Brine Composition.

A. C. Lowe, et al. **[1973]** experimentally showed that natural surfactants in crude oils are often soluble enough in water to adsorb onto the rock surface after passing through a thin layer of water. After comparing the asphaltene adsorption in cores with and without water, V. M. Berezin et al. **[1982]** discovered that in many cases, a water film may reduce but not completely inhibit the adsorption of the surface-active compounds in the oil.

The salinity and pH of brine are very important in determining wettability because they strongly affect the surface charges on the rock surface and fluid interface, that in turn can affect the adsorption of surfactants. Positively charged cationic surfactants are attracted to negatively charged surfaces, and the negatively charged anionic surfactants are attracted to positively charged surfaces.

Brine pH directly affects the wettability by changing the surface charge of the minerals. P. Sumasundaran **[1975]** reports that the surface charge of silica and calcite in water is positive at low pH, and negative at high pH.

c. Mineral Surface

Wettability is a function of the type of mineral surface in the reservoir. Chilingar and Yen **[1983]** found that carbonate reservoirs are typically more oil-wet than sandstone reservoirs. The mineral surface interacts with the crude oil components to determine the wettability.

1.4.5 Native Wettability Alteration

Many factors can significically alter the wettability of undisturbed reservoir rock. These factors are categorized by W. G. Anderson [1986] as follows:-

- Factors that affect core wettability before the test.
- Factors that affect core wettability during the test.

a. Factors that affect core wettability before testing

1. While cutting the core, the flushing action of the drilling fluid disturbs and replaces the original fluid distributions which causes a change in wettability. More importantly, drilling fluids containing surfactants or having a pH different from that of the reservoir fluids, also changes the wettability.

2. If any changes of core pressure and temperature occur while extracting the core from the reservoir and transporting it to the surface, fluids will be expelled from the core, particularly the light hydrocarbons, and the distribution of the fluids will change.

Furthermore, the asphaltenes and other heavy ends may deposit on rock surface, making the core more oil-wet. Oxidation is another factor that contributes to wettability alteration along with core cleaning and preparation which result from changing the original fluids proportionalities.

b. Factors that affect core wettability during testing

Reservoir conditions should be simulated while testing a native-state core. Cores that are run at atmospheric conditions are more oil-wet than those run at reservoir conditions because of the reduction in solubility of the surface-active compounds.

Testing fluids may also introduce some source of error. Tests run with air-brine or mercury-brine combinations instead of oil-brine implicitly assume that wettability effects are negligible.

1.4.6 Determination of Wettability

The wettability of a rock can either be evaluated experimentally or estimated qualitatively. Laboratory-measured wettability has been used to evaluate in-situ wettability. Since many of the widely used experimental methods of wettability evaluation utilize either the reservoir rock or the reservoir fluids, but not both, a laboratory wettability evaluation should be related to actual reservoir conditions.

1.4.6.1   Qualitative determination of wettability

A number of qualitative methods for wettability determination can be found in literature. Those discussed below include the fractional surface area method, the dye adsorption method, the drop test method, the Bobek et al. method, the permeability method, the relative permeability method, the resistivity index method, and the capillary pressure method. They are discussed below.

a. Fractional Surface Area Method

This method uses mixtures of untreated sand and sand rendered oil-wet by organosilane vapors to obtain wetting conditions ranging from completely water-wet to completely oil-wet [Brown and Fatt 1956]. Wettability is determined by the fraction of solid surface made artificially oil-wet.

b. Dye Adsorption Method

This method is based upon the ability of reservoir rock to adsorb a dye such as methylene blue from aqueous solution, while rock surface areas covered by contaminants from the oil phase remain unaffected **[Holbrook and Bernard 1958]**. Wettability is determined by comparing the adsorption capacity of the test sample with that of an adjacent sample in which the fluids have been extracted by choloroform and methanol.

c. Drop Test Method

This method, as reported by Rapoport et al. **[1986]**, is used to confirm rock wettability. Drops of oil and water are placed on the surface of a fresh break in the core. The fluid that is imbibed into the core is the wetting phase while the fluid that forms a ball and does not wet the the surface is non-wetting.

d. Bobek et al. Method

Bobek et al. **[1958]** proposed a laboratory technique that determines which fluid will displace the other from a core sample by imbibition. The results of this imbibition test are compared with those of a reference imbibition test on the same core sample after the core has been rendered completely water-wet through cleaning and extreme heating for a long period of time. The rate of imbibition and relative amounts of imbibed fluids are the qualitative measure of wettability.

e. Permeability Method

The determination of wettability of a sample from permeability data is accomplished by comparing the ratio of water permeability at residual oil saturation with oil permeability at connate water saturation. If the ratio is less than 0.3, the sample is considered to be water-wet, while a value near unity indicates that the sample is oil-wet

[Keelan, D. K.1972]. Rocks with low connate water saturation are considered to be oil wet, while rocks with high connate water saturation are normally designated as water-wet.

f. Relative Permeability Method

Figure 1.6 shows a comparison between the shape of the relative permeability curves for oil-wet and water-wet systems [Craig, F.F. 1971]. The correlation parameters are summarized in the following table:

Table 1.1 Craig's rules of thumb to differentiate between water-wet and oil-wet relative permeability curves.

	WATER-WET	OIL-WET
Swi	> 20 to 25 %	<15 %, usually 10 %
Krw = Krow	@ Sw > 50 %	@ Sw < 50 %
Krw at Sorw	< 0.3	> 0.5. approaching 1.0

In a water-wet rock, residual oil globules in the large flow channels slow the flow of water and cause a low water relative permeability; however, the oil in an oil-wet system occupies smaller flow channels and coats the walls of the large ones, causing a minimum disturbance to water flow and a higher water relative permeability. This explains why an oil-wet reservoir will water flood poorly, with early water breakthrough, rapid increase in water cut, and high residual oil saturation.

g. Resistivity Index Method

Formation resistivity obtained from electric logs can be used as a qualitative technique for wettability identification. Resistivity index is defined as the ratio of true formation resistivity to resistivity of the formation when it is 100% saturated with formation brine. A high resistivity index indicates low water saturation or a discontinuous water phase, which characterizes an oil-wet system. There is considerable uncertainty concerning the nature of the wettability characteristics of reservoir rock in-situ. Tests of wettability made on cores taken from reservoirs are not necessarily valid indicators of subsurface conditions, since the coring process itself may alter wettability. Cores cut in oil-base mud are reported to be rendered entirely or partially preferentially oil-wet **[Amott, E. 1959]**.

h. Capillary Pressure Method

Both displacement pressure and the ratio of drainage to imbibition displacement pressure have been proposed as qualitative indicators of preferential wettability of porous media. An increase in displacement pressure or in the ratio of drainage to imbibition displacement pressure signifies a tendency of the core to become oil-wet. The above technique is applicable when oil-wet capillary tests are made on native-sate cores. However, most capillary pressure tests are either of the mercury injection or air-brine type, which provide little information concerning wettability **[Anderson, W.G. 1987]**.

1.4.6.2   Quantitative Determination of Wettability

The three main methods presently in use to determine core wettability quantitatively are:

- 　　　The contact Angle Method;

-     The Amott Method; and

-     The U.S.M.B Method.

a. Contact Angle Method

For most porous media, the equations for interfacial curvature are much too complicated to be solved analytically, therefore, the capillary pressure must be determined experimentally. In such cases, a simple relationship between the contact angle and the capillary pressure cannot be derived. One simple system, where P_c can be calculated as a function of geometry, wettability, and interfacial tension is a capillary tube.

On a surface, it is impossible to measure a single equilibrium value for the contact angle. A range of contact angles will be measured in most systems with reproducible maximum and minimum values. Maximum angle is obtained by pushing the liquid over the surface, while minimum angle is obtained by pushing the liquid back. These two angles are referred to as the advancing angle and the receding angle.

Three main reasons are reported for contact angle hysteresis :-

    1- Surface roughness.

    2- Surface heterogeneity.

    3- Surface motion.

b. Amott Method

The Amott method combines imbibition and forced displacement to measure the average wettability of core. The major advantage of this method over the contact angle method is that both reservoir core and fluids are used in the test. This method is based on the fact that the wetting fluid will generally imbibe spontaneously into the core, displacing the non-wetting fluid. The ratio of spontaneous imbibition to forced imbibition is used to

reduce the influence of other factors, such as relative permeability, viscosity, and initial saturation of the rock.

As reported by E. Amott [1959] the test results are expressed by the displacement-by-oil ratio and the displacement-by-water ratio. These two ratios are explained as follows:

Displacement-by-oil ratio

"The ratio of the water volume displaced by spontaneous oil imbibition, V_{wsp}, to the total water volume displaced by imbibition and centrifugal (forced) displacement, V_{wt}."

$$\delta_o = \frac{V_{wsp}}{V_{wt}} \quad\quad (1.7)$$

Displacement-by-water ratio

"The ratio of the oil volume displaced by spontaneous water imbibition, V_{osp}, to the total oil volume displaced by imbibition and centrifugal (forced) displacement, V_{ot}."

$$\delta_w = \frac{V_{osp}}{V_{ot}} \quad\quad (1.8)$$

A displacement-by-water ratio larger than zero and a zero value for the displacement-by-oil ratio indicate water wet rock. The displacement-by-water ratio approaches 1 as the water wetness increases. Similarly, oil wet cores have a larger than zero displacement-by-oil ratio and a zero displacement-by-water ratio. Both ratios are zero for neutrally-wet cores

c. U.S.M.B. Wettability Method

The U.S.M.B. Wettability test was developed by Donaldson et al. [1969]. Like the Amott method, it measures the average wettability of the core but in a relatively rapid way.

The U.S.M.B. wettability test compares the work necessary for one fluid to displace the other. Because of favorable free-energy in the core, the work required for the wetting fluid to displace the non-wetting fluid from the core is less than the work required for the opposite displacement. It has been shown that the required work is proportional to the area under the capillary pressure curve.

1.4.6.3   Comparison of the Three Quantitative Methods for Wettability Determination.

1 - The contact angle method for wettability determination has three main limitations as reported by Anderson, W.G. [1986]. These limitations are:

a. The Hysteresis in the Readings

It has been found experimentally that a liquid drop on a surface may have a number of different stable contact angles. Even though it is possible, with great care, to get reproducible contact angle measurements, the question of how representative these results are of the wettability of the reservoir arises. Treiber et al. [1972] in an 1800-hour experiment found that time is an important factor that affects contact angle readings. **Figure 1.4** shows cases where the contact angle changes with time.

b. Rock heterogeneity

Rock heterogeneity is also an important factor that is neglected. Contact angles are

measured on a single smooth mineral crystal representing the reservoir rock (silica or quartz is used to represent a sandstone; calcite is used to represent a carbonate or reef reservoir), while a core contains many different constituents.
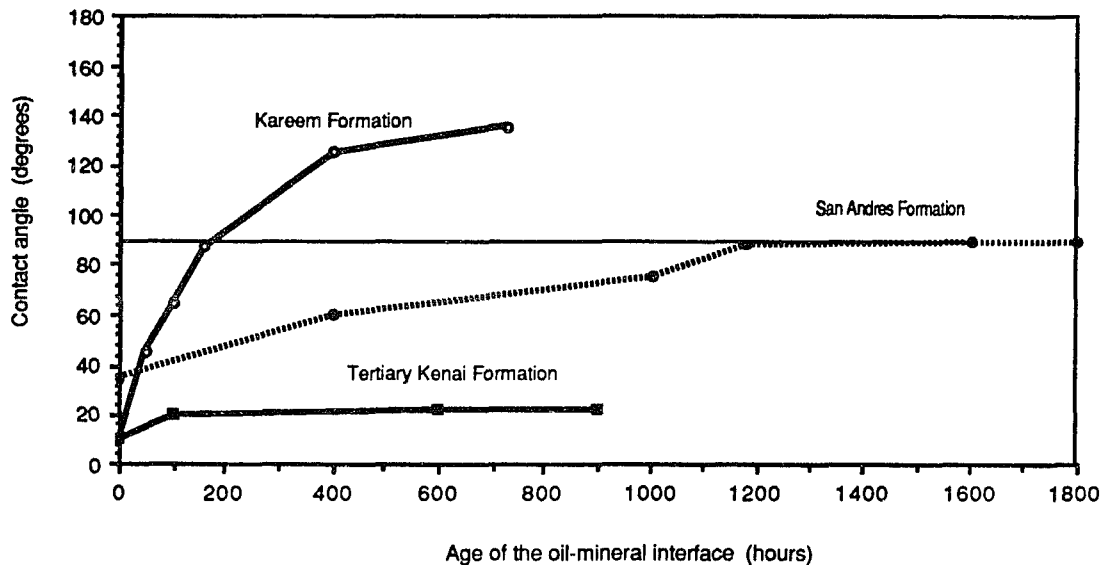
Figure 1.4 Contact angle measured for different formation crystals.
[Treiber et al., 1972]

c. Lack of Information

The third limitation of the contact angle method is that no information can be obtained about the presence or absence of permanent organic coatings on a reservoir rock.

2 - The Amott, and U.S.M.B. methods are superior to the contact angle method for determining wettability because they use the reservoir rock and the reservoir fluid, and the resultant wettability is the average wettability for the particular core being tested.

3 - A major advantage of the U.S.M.B. method over the Amott method is that the U.S.M.B. method is more sensitive in the neutral wettability range.

4 - In the Amott and U.S.M.B. methods, the native-state core should be used and reservoir conditions should be simulated. **Figure 1.5** shows the difference in the capillary pressure curves on a single core when measured in the native and cleaned states **[Richardson et al., 1955]**. From this figure, it is obvious that the native-state or restored-state core should be used.

5 - Neither the Amott nor the U.S.M.B. methods can determine whether a system has fractional or mixed wettability.

1.4.7   Effect of Wettability on Relative Permeability

Relative permeability is defined as a direct measure of the ability of the porous system to let one fluid flow when one or more fluids are present. The flow properties are found to be the composite effect of several factors as stated by Craig **[1971]**, These factors are:

- Pore geometry
- Wettability
- Fluid distribution
- Saturation history
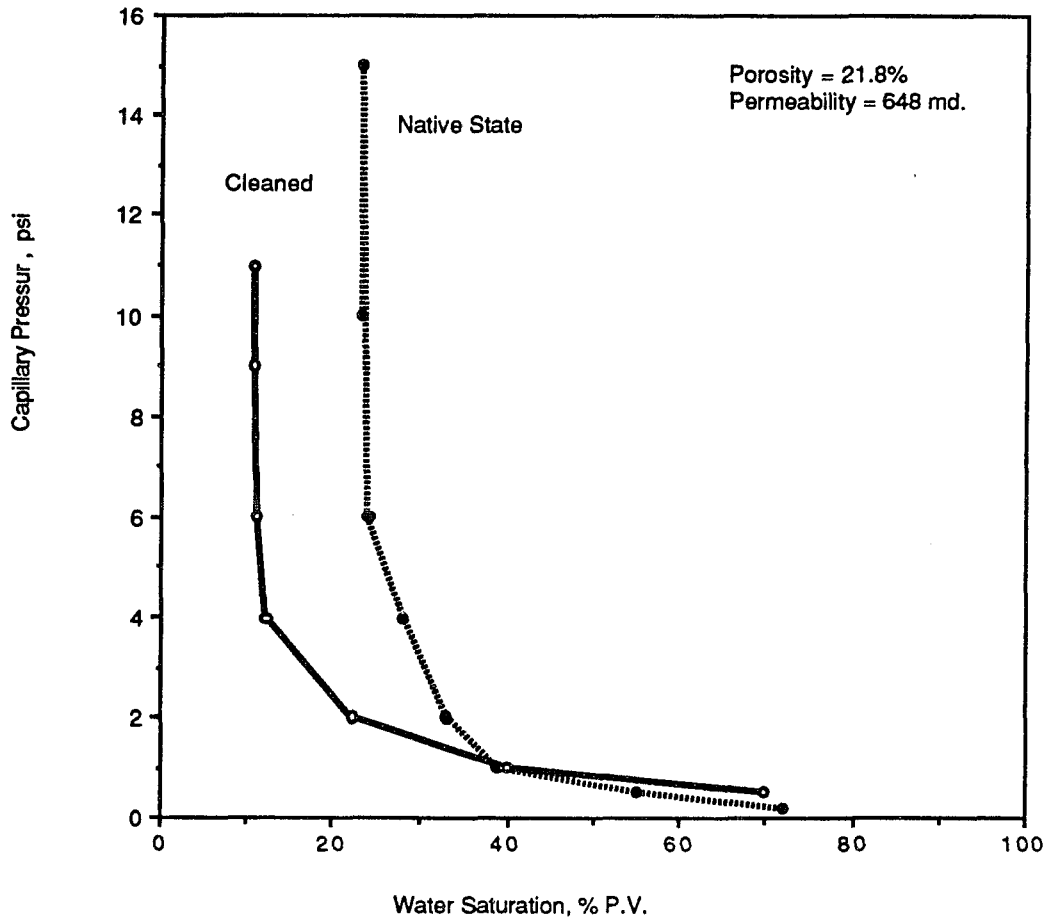
Figure 1.5 Comparison of capillary pressure curve measured on a single
core in the native and cleaned states.
[Richardson et al. 1955].

Craig presented three rules of thumb that can qualitatively differentiate between the relative permeability characteristics of strongly water-wet, and strongly oil-wet systems. These rules of thumb are as follows:

1 - There is a difference in the connate water saturation values for water-wet, and oil-wet systems. Usually it is greater than 20 - 25 % pore volume (PV) in water-wet systems, while it is generally less than 15 % PV in oil-wet systems.

2 - The water saturation at which the water and oil relative permeability are equal is greater than 50% in strongly water-wet systems, while in strongly oil-wet cores it is less than 50%.

3 - The value of the relative permeability to water at the maximum water saturation is less than 30 % for water-wet systems, and ranges between 50%-100% in oil-wet systems.

Figure 1.6 shows the typical relative permeability curves for both oil-wet and water-wet systems, and the three rules of thumb are marked 1, 2, and 3 respectively. Explanations of why these values are affected by wettability are well documented by W. G. Anderson [1987].
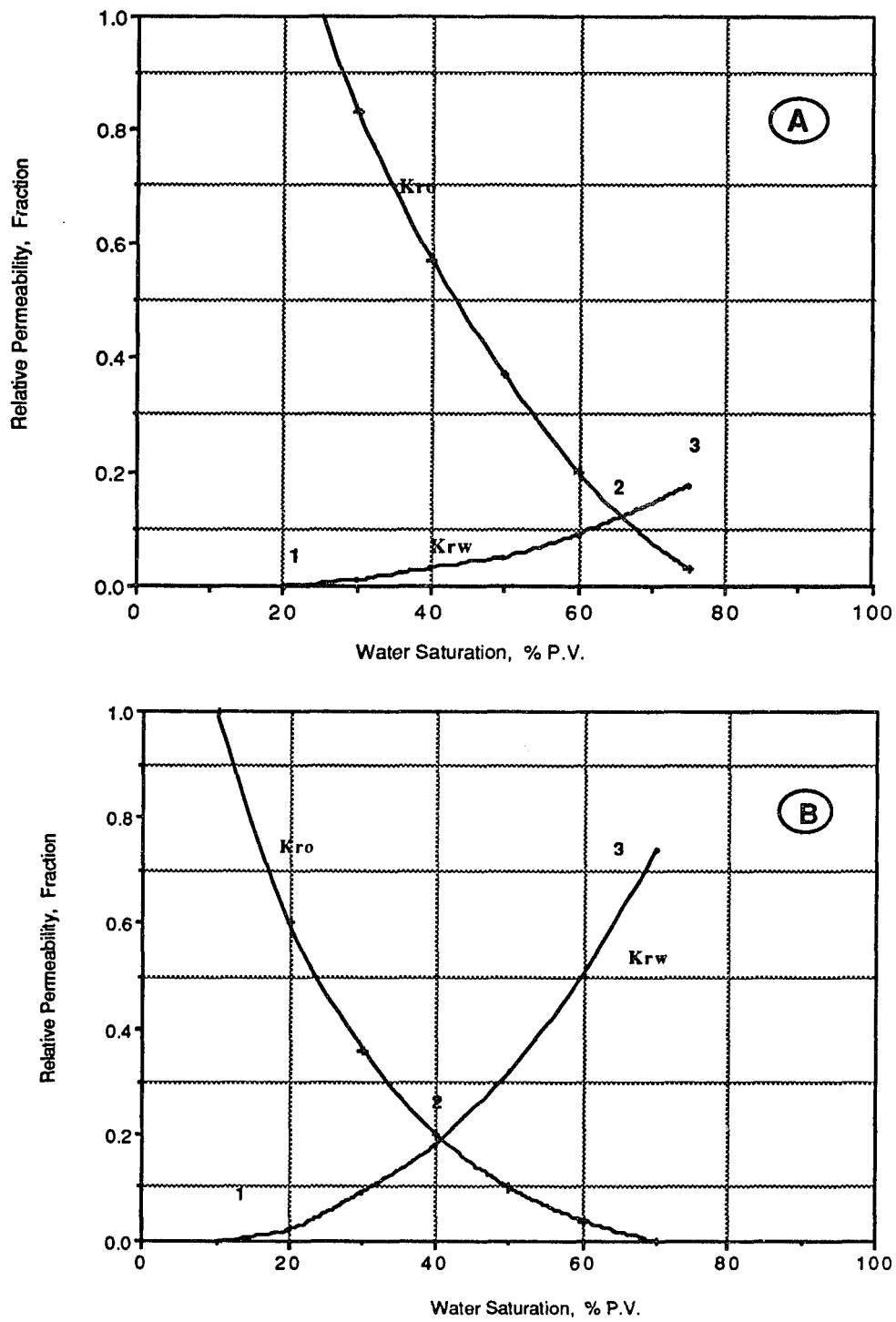
Figure 1.6 Typical relative permeability curves for strongly water-wet, (A) and strongly oil-wet systems, (B). **[Craig, 1971]**

1.4.8   Effect of Wettability on Electric Properties of Porous Media

Three main assumptions are implied in Archie's empirically determined saturation equation :

$$S_w^{-n} = \frac{R_t}{R_o} = I_R \qquad (1.9)$$

where:

S_w is the water saturation;

n   is the saturation exponent;

R_t is the formation resistivity;

R_o is the formation resistivity at 100% water saturation; and

I_R is the resistivity index.

These assumptions, as reported by W. G. Anderson [1986], are:

a: The saturation/resistivity relation is unique, i.e., only one resistivity will ever be measured at a given saturation.

b: The saturation exponent is constant for a given porous medium.

c: All the brine contributes to the flow of electric current.

These three assumptions are true for water-wet conditions because the brine is almost continuous in water-wet cores and thus all the brine contributes to the flow of current and the water saturation/resistivity relation is unique. Consequently, the saturation exponent is constant and depends on the core structure. However, for the oil-wet core

case the fluid distribution will change (water will occupies the center of the large pores). Consequently, the length and cross-sectional area of the conductive path will be changed and the resistivity will be changed. Therefore, water saturation/resistivity relation is not unique when the wettability is altered, since different resistivities can be measured at the same saturation.

W.G. Anderson [1986] reported that the saturation exponent is considerably higher in oil-wet rock than in water-wet rocks, and because it depends on wettability, this exponent must be measured at reservoir wettability conditions. Otherwise invalid water saturations may be obtained from the logs. The effect of wettability on the saturation exponent becomes more important as the brine saturation decreases because, in oil-wet systems, there is more disconnection and insulation of globules of brine. The isolated brine is surrounded by oil, which acts as an insulator that makes it impossible to conduct electric current.

In water-wet rocks, most of the increase in the resistivity as the water saturation decreases is caused by the decrease in the cross section area available for conduction, not by an increase in the path length or brine trapping.

In oil-wet rocks, at high water saturation, the brine is continuous and located in the center of the large pores. Even though, the location is different than in water wet rocks, the Archie's saturation/resistivity relation behaves as it does in the water-wet case, with (n) around 2.0. As water saturation decreases, two factors contribute to the exponential increase in resistivity:

a: A portion of the brine is trapped and no longer contributes to the local current.

b: Some of the brine will be located in pseudo-dead end pores (also known as fingers or dendritic structures).

These fingers consist of brine that is connected to the continuous brine in only one location.   The brine cannot conduct electricity because of the interface oil-water in the remainder of the pore throats, so the length of the conducting path is increased.

Figure 1.7 shows the exponential behavior of the resistivity in an oil-wet core as the water saturation decreases **[V. Ong, 1990]**.   Ong concluded that the saturation exponent varies inversely with the water saturation according to the equations:

$$S_w^{n = f(S_w)} = \frac{R_o}{R_t} \qquad (1.10)$$

$$n = a \, S_w^{-b} \qquad (1.11)$$

where a and b are constants specific to the reservoir and can only be determined in the laboratory.
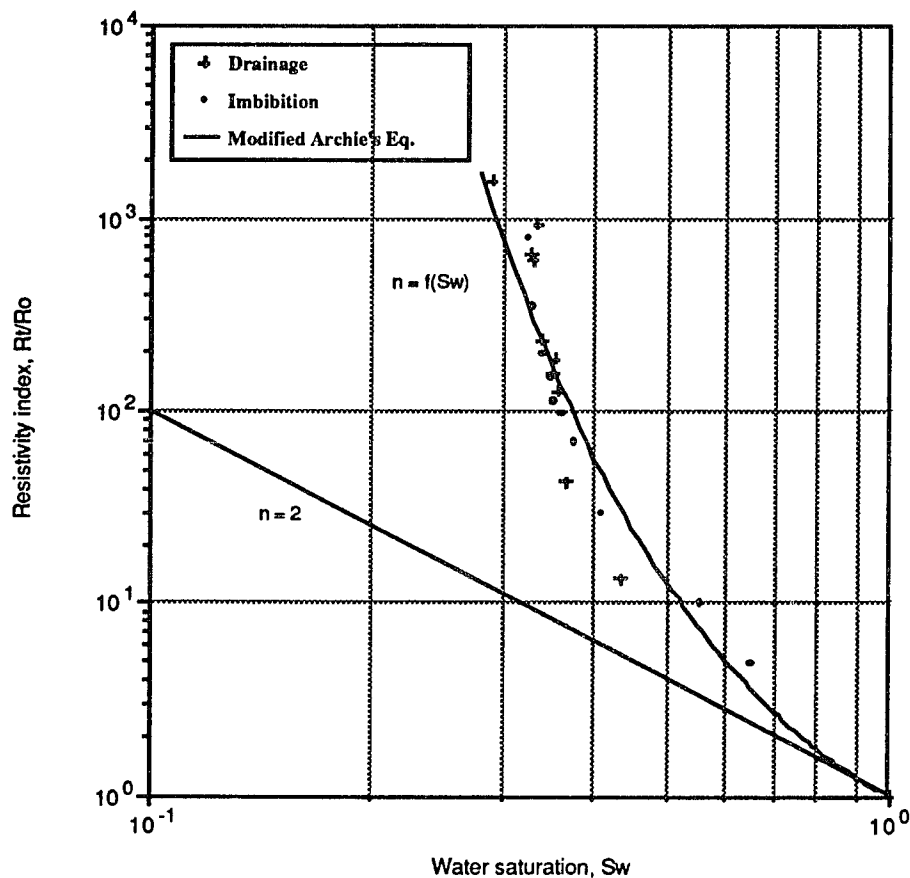
Figure 1.7   Saturation exponent/resistivity index relationship in oil-wet sands.
[Ong, 1990]

1.4.9   Effect of Wettability on Saturation Exponent

Morgan and Pirson **[1964]** made fractionally wetted bead packs with a variation in the proportions of oil-wet and water-wet beads.   They measured the resistivity as the proportion of oil-wet beads was varied from 0 to 100% of the total beads.   In each run, they started with 100% brine, and flooded the core with oil until irreducible water saturation and then they proceeded to measure the resistivity.   Archie's saturation exponent for each pack was found by plotting the resistivity index versus the saturation and then calculating the average saturation exponent on the assumption that the

resistivity index varies linearly with the saturation. **Figure 1.8** shows the summary of their results, with the saturation exponent varying from 2.5 for strongly water-wet to 25 for strongly oil-wet beads.
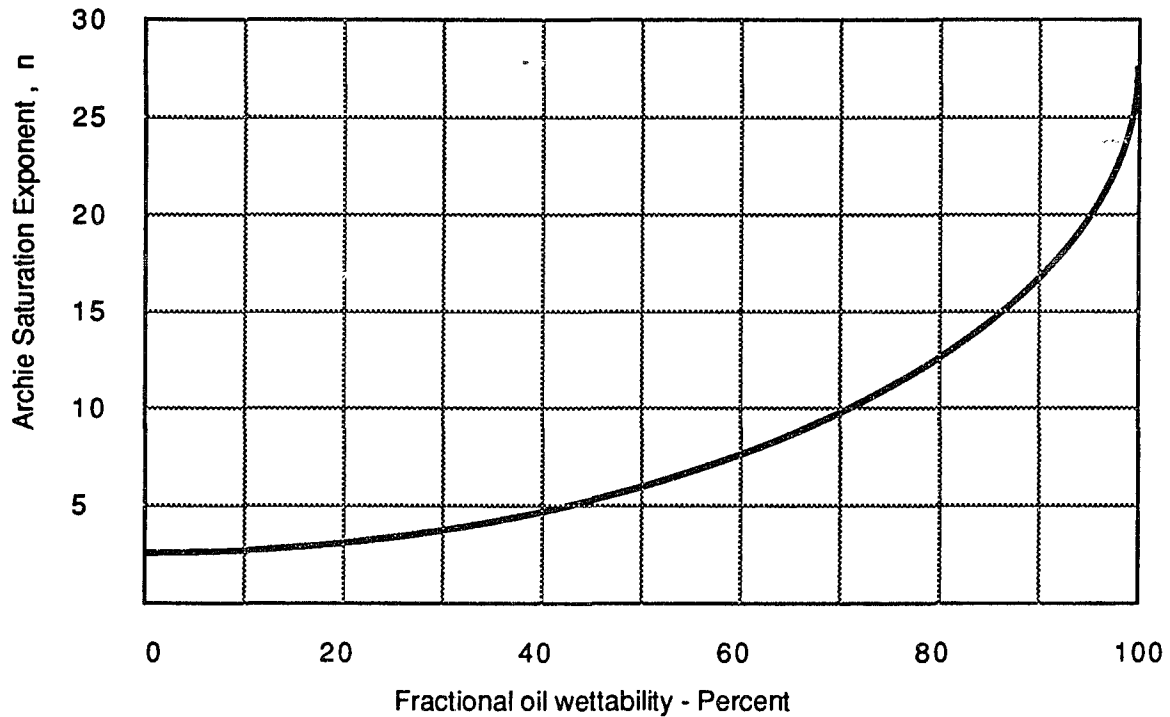
Figure 1.8 Archie's saturation exponent versus oil-wet fraction.
[Morgan et al., 1964]

The results from the experiments performed using uniformly wetted cores (teflon or sandstone treated cores) showed n ranges from 9.0 to 13.0 for oil-wetted cores and about 2.0 for water-wetted cores. The experiments performed using native-state cores showed the same wettability response for n, but very high values for uniformly wetted systems where never reached. These results may be attributed to variations in mineral composition that may make the reservoir cores fractionally wet (making a portion of their surface water wet).

1.4.10   Effect of Wettability on Capillary Pressure

There is no existing simple relationship that relates the capillary pressures determined at two different wettabilities. Consequently, the most accurate measurements are made with cores that have native reservoir wettability using native reservoir fluids.

There are two basic types of capillary pressure: drainage and imbibition. In a drainage process, the non-wetting fluid displaces the wetting fluid, while the reverse occurs for imbibition. Generally, there is hysteresis in capillary pressure as the saturation is varied, making the drainage and imbibition curves different.

1.4.11   Fractional and Mixed Wettability Systems

Salathiel [1973], introduced the term "mixed wettability" for a special type of fractional wettability in which the oil-wet surfaces form continuous paths throughout the large pores. The small pores remain water-wet, containing no oil.

The main distinction between mixed and fractional wettability is that the latter does not imply either specific locations for the oil-wet and water-wet surfaces or continuous oil-wet paths. **Figure 1.9** shows a schematic drawing for the mixed wettability that is formed due to the flow of oil containing surface active compounds through the pore space.

water-wet

Oil-wet
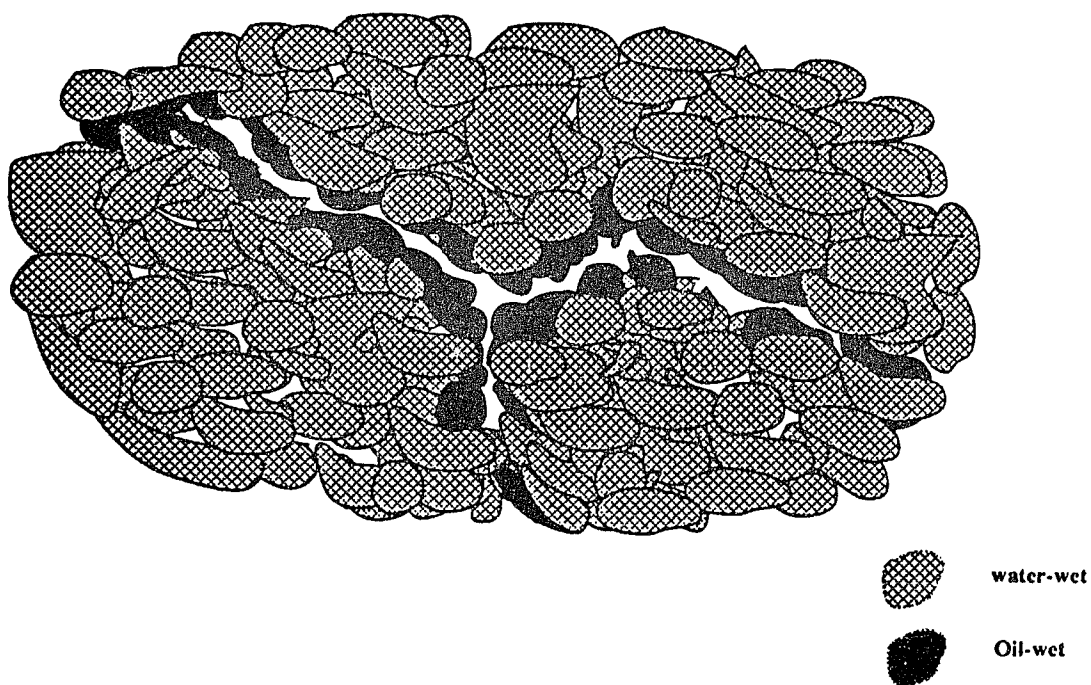
Figure 1.9 Formation of mixed wettability in oil pathes due to surface active components in the oil.

Fatt and Klikoff **[1959]** studied the effect of fractional wettability on capillary pressure. Fractionally wetted sand packs were formed by mixing various proportions of treated (oil-wet) and untreated (water-wet) sand grains. The sand packs were placed in a porous-plate apparatus, then saturated with water. Kerosene was used to measure the capillary pressure. **Figure 1.10** shows the results of such experiments. Increasing the amount of oil-wet sand decreases the area under the Pc-Sw curve, indicating less work is required for kerosene to displace the water.

To study the effect of the location of oil-wet versus water-wet surfaces, Fatt and Klikoff measured the capillary pressure curve for the following three sand categories:

- 100% water-wet sand

- 50% of all the grain sizes are oil-wet sands

- 58% of the smallest the sand grains are oil-wet sands.

The results are presented in **Figure 1.11**. At low capillary pressure, the 58% fines-treated sand curve lies below the curve for uniformly treated grains. As the capillary pressure increases, the fines-treated curve becomes nearly vertical at a much higher water saturation. The figure shows the importance of the locations of the oil-wet sands.
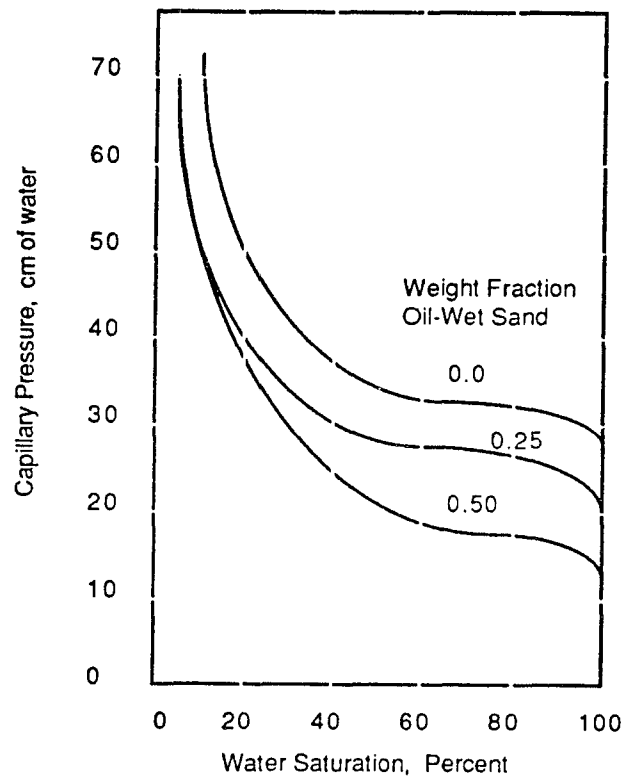
Figure 1.10 Wettability effect on capillary pressure using sandpacks.
[Fatt et al., 1959]
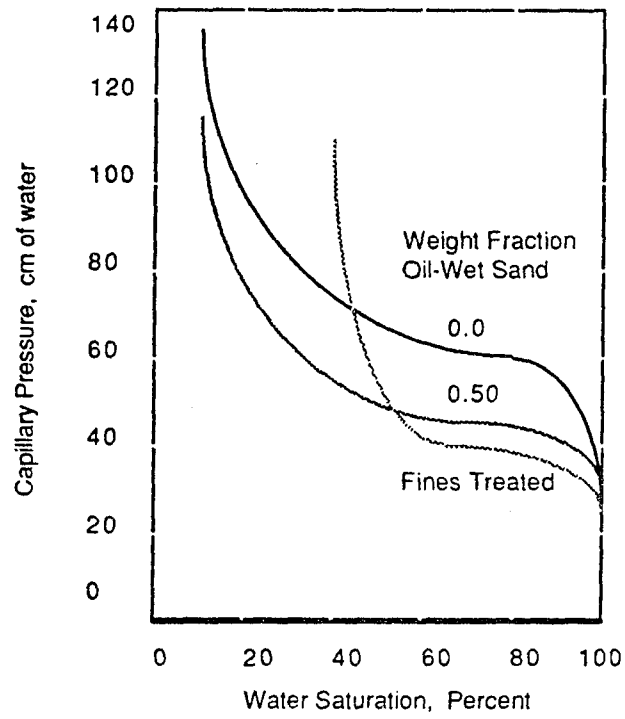
Figure 1.11 Importance of the location of the oil-wet versus the water-wet surfaces on capillary pressure. **[Fatt et al., 1959]**

CHAPTER II

CALCULATION OF RELATIVE PERMEABILITY CURVES USING CAPILLARY PRESSURE DATA

2.1 Drainage Models

The following paragraphs review the most common models presented in the area of calculating the relative permeability using the laboratory determined capillary pressure curves.

2.1.1 Purcell's Model

W. R. Purcell [1949] introduced a theoretical derivation to calculate permeability using capillary pressure data obtained by mercury injection. The capillary pressure for a single tube is given by :

$$P_c = \frac{2 \, \sigma \cos (\theta)}{r} \qquad (2.1)$$

where:

σ is the interfacial tension;

r is the radius of the tube; and

θ is the contact angle.

Poiseuille's law for flow of viscous fluid of viscosity (μ) in a cylindrical tube of length (L), and radius (r) is given by:

$$Q = \frac{\pi r^4 \Delta p}{8 \mu L}$$ (2.2)

where ΔP is the pressure drop across the tube.

For a cylindrical tube of length L and radius r, the volume is:

$$v = \pi r^2 L$$ (2.3)

Equation 2.2 may be written as:

$$Q = \frac{v r^2 \Delta p}{8 \mu L^2}$$ (2.4)

Solving Equation 2.1 for r and substituting in Equation 2.4 gives:

$$Q = \frac{(\sigma \cos \theta)^2 \, v \, \Delta P}{2 \mu L^2 P_c^2}$$ (2.5)

Assuming that the porous medium is composed of n capillary tubes of the same length L, but different radius r:

$$Q = \frac{(\sigma \cos \theta)^2 \Delta P}{2 \mu L^2} \sum_1^n \{\frac{v_i}{P_{ci}^2}\}$$ (2.6)

The rate of flow Q through the same system of capillaries is also given by Darcy's Law:

$$Q = \frac{K\,A\,\Delta P}{\mu\,L}$$ (2.7)

where:

K is the absolute permeability;

A is the area of flow;

ΔP is the pressure drop due to flow;

μ is the flowing fluid viscosity; and

L is the length of the medium.

Equating the right hand side of the previous two equations (2.6 and 2.7), we get:

$$K = \frac{(\sigma \cos \theta)^2}{2\,A\,L} \; \Phi \sum \left\{ \frac{S_i}{P_{ci}^2} \right\}$$ (2.8)

where:

Φ is the porosity.

If Vt is the total void volume, and Vi is the volume of each capillary expressed as a fraction S_i of the total void volume Vt, then:

$$S_i = \frac{V_i}{V}$$ (2.9)

and since the amount (A L) gives the bulk volume, then:

$$\Phi = \frac{V_t}{A * L}$$ (2.10)

Substituting in Equation 2.8,

$$K = \frac{(\sigma \cos \theta)^2}{2} \Phi \sum_1^n \{\frac{S_i}{P_{ci}^2}\} \qquad (2.11)$$

The quantity $\sum_1^n \{\frac{S_i}{P_{ci}^2}\}$ is equal to the integral of the reciprocal of the square of the capillary pressure expressed as a function of liquid saturation which also represents the area under the $1/P_c^2$ curve as explained by Purcell. Consequently, the equation will take the form:

$$K = \frac{(\sigma \cos \theta)^2}{2} \Phi \, F \int_{s=0}^{s=1} \frac{dS}{P_c^2} \qquad (2.12)$$

The constant F accounts for the assumption which considers the reservoir rock as a bundle of tubes (Poiseuille's formula).

Applying the formula for the wetting and non-wetting phase in a two phase flow:

$$K_{rwt} = \frac{K_{wt}}{K} = \frac{\int_{s=0}^{s=s_{wt}} \frac{dS}{P_c^2}}{\int_{s=0}^{s=1} \frac{dS}{P_c^2}} \qquad (2.13)$$

and

$$K_{rnwt} = \frac{K_{nwt}}{K} = \frac{\int_{s=s_{wt}}^{s=1} \frac{dS}{P_c^2}}{\int_{s=0}^{s=1} \frac{dS}{P_c^2}} \qquad (2.14)$$

where:

S   is the saturation;

K_{rwt} is the relative permeability of the wetting phase; and

K_{mwt} is the relative permeability of the non-wetting phase.

2.1.2   Burdine's Model

N. T. Burdine **[1950 and 1953]** introduced an equation which was later reviewed by W. J. Amyx **[1960]** that includes tortuosity as a factor in the model proposed by Purcell. Burdine introduced the two following definitions:

λ the tortuosity factor for a pore when the porous medium is saturated with only one fluid; and

λ_{wt} the wetting phase tortuosity factor when two phases are present.

Burdine also defined tortuosity as:

$$\lambda_{rwt} = \frac{\lambda}{\lambda_{wt}} \qquad (2.15)$$

Given that λ_{rwt} is constant for the porous medium and depends only on the final saturation, the equations proposed by Burdine are as follows:

$$K_{rw} = \lambda_{rwt}^2 \; \frac{\displaystyle\int_{S=0}^{S=S_{wt}} \frac{dS_w}{P_c^2}}{\displaystyle\int_{S=0}^{S=1} \frac{dS_w}{P_c^2}} \qquad (2.16)$$

for the wetting phase; and

$$K_{mw} = \lambda_{mwt}^2 \quad \frac{\displaystyle\int_{S=S_{wt}}^{S=1} \frac{dS_w}{P_c^2}}{\displaystyle\int_{S=0}^{S=1} \frac{dS_w}{P_c^2}} \qquad (2.17)$$

for the non-wetting phase.

where:

K_{rwt} is the relative permeability for the wetting phase;

K_{mwt} is the relative permeability for the non-wetting phase;

λ_{rwt} is the wetting phase tortuosity factor defined as:

$$\lambda_{rwt} = \frac{S_w - S_{wi}}{1 - S_{wi}} \qquad (2.18)$$

and

λ_{mwt} is the non-wetting phase tortuosity factor defined as:

$$\lambda_{mwt} = 1 - \frac{S_w - S_{wi}}{S_c - S_{wi}} \qquad (2.19)$$

where:

S_c is the critical saturation. For $S_w > S_c$, the non-wetting phase is discontinuous;

S_w is the water saturation; and

S_{wi} is the irreducible water saturation.

2.1.3   Corey's Model

A.T. Corey [1954] made an observation, based on experiments on capillary pressure-oil desaturation measurements, that generally a linear relationship exists between the capillary pressure and the effective saturation in the form:

$$\frac{1}{P_c^2} = \begin{cases} \dfrac{c\ (S_o - S_{or})}{1 - S_{or}} & \text{for } S_o > S_{or} \\[3mm] 0 & \text{for } S_o < S_{or} \end{cases} \tag{2.20}$$

where:

S_o is oil (wetting-phase in a gas-oil system) saturation;

S_{or} is residual oil saturation;

c   is constant; and

P_c is capillary pressure.

Based on this relationship, Burdine's equations developed to calculate the relative permeability curves in the drainage regime could be written in a simple form as follows:

$$K_{rwt} = \left(\frac{S_o - S_{or}}{1 - S_{or}} \right)^4 = S_{oe}^4 \tag{2.21}$$

$$K_{rnwt} = \left(1 - \frac{S_o - S_{or}}{1 - S_{or}} \right)^2 \left[1 - \left(\frac{S_o - S_{or}}{1 - S_{or}} \right)^2 \right]$$

$$= (1 - S_{oe})^2 \ (1 - S_{oe}^2) \tag{2.22}$$

where S_{oe}, the effective wetting phase saturation, is defined as:

$$S_{oe} = \frac{S_o - S_{or}}{1 - S_{or}} \tag{2.23}$$

Equations 2.21 and 2.22 are used to calculate the relative permeability curves using only saturation data without the need for capillary pressure data.

Brooks and Corey **[1964]**, modified Corey's original capillary pressure versus saturation relationship (Equation 2.20) into a two-parameter expression:

$$S_e = \left(\frac{P_b}{P_c} \right)^{\lambda} \tag{2.24}$$

$$K_{rwt} = \left(S_e \right)^{(2+3\lambda)/\lambda} \tag{2.25}$$

$$K_{mwt} = (1 - S_e)^2 \left(1 - S_e^{(2+\lambda)/\lambda} \right) \tag{2.26}$$

where:

K_{rwt} is the relative permeability for the wetting phase;

K_{mwt} is the relative permeability for the non-wetting phase;

λ is the pore size distribution index;

S_e is the effective saturation, defined as:

$$S_e = \frac{S - S_r}{1 - S_r} \tag{2.27}$$

P_b is the Bubbling pressure (approximately the minimum Pc on the drainage cycle at which a continuous non-wetting phase exists in a porous medium); and

P_c is the capillary pressure.

It is noteworthy that Equations 2.25 and 2.26 reduce to Equations 2.21 and 2.22 for λ = 2. However, Equations 2.25 and 2.26 are more reliable because they contain a descriptive term driven from the capillary pressure curve which reflects the pore structure distributions for the rock under consideration.

2.1.4   Wyllie's Model

Wyllie [1958] introduced his model starting with Kozeny and Carman's equation [1948]. This equation relates the rock's properties to its permeability as:

$$K = \frac{\Phi^3}{2.5 \ (L_e/L)^2 \ S^2}$$

(2.28)

where:

K	is the permeability;
Φ	is the internal volume / unit bulk volume, or porosity;
L_e	is the apparent length;
L	is the actual length of fluid flow;
S	is the internal surface/unit bulk volume, or specific surface area;
2.5	is the shape factor;
L_e/L	is the tortuosity; and
$2.5 \ (L_e/L)^2$	is known as Kozeny constant, k.

The main assumptions made in the derivation of the above equation, as stated by Wyllie, are :

1. A porous medium consists of one straight capillary of complex shape oriented in a direction parallel to that of macroscopic flow.

2. The mean hydraulic radius equals the internal volume divided by the unit bulk volume

$$\text{Mean hydraulic radius} = \frac{\text{Internal vol./ Unit bulk vol.}}{\text{Internal surface / Unit bulk vol.}} = \frac{2 * \Phi}{S}$$

(2.29)

3. A porous medium is uniform and isotropic, so the area available for flow normal to

the direction of fluid flow is Φ per unit bulk area.

4. The actual average velocity within the pores is given by the equation:

$$u_e = (u/\Phi)\,(L_e/L) \qquad (2.30)$$

where u is the apparent velocity.

Wyllie and Spangler [1952] incorporated the capillary pressure curve as a descriptive term of pore sizes and their distribution to the equation of flow stated above (Equation 2.28). Based on experimental data, they proposed the following equation for uniform pore size (sand packs):

$$S = P_c\,(\Phi/\gamma) \qquad (2.31)$$

where:

S   is the internal surface area per unit bulk volume;

γ is the surface tension; and

P_c is the capillary pressure.

Incorporating Equation 2.31 into Equation 2.28, and equating with Darcy's law gives:

$$K = \frac{\Phi\,\sigma^2}{k}\int_0^1 dS_w/P_c^2 \qquad (2.32)$$

where:

K   is the permeability; and

k   is the Cozeny constant = 2.5 $(L_e/L)^2$.

In order to account for the assumption that the porous medium may be represented by a bundle of tubes of different diameter, Wyllie assumed that the main difference between

the porous medium and a tube bundle is the length of the fluid flow used to calculate the tortuosity factor. In order to calculate this tortuosity factor, Wyllie assumed the following model that relates the hydraulic conductivity of a porous medium to its electrical conductivity.

The resistance of a homogeneous porous medium saturated with conducting fluid of resistivity R_w, may be considered to be the resistance of a volume of fluid of length, L_e, and area, ΦA, where $L_e > L$. Therefore, the resistance of the 100% saturated porous medium can be described as follows:

$$R = \frac{R_w L_e}{\Phi A} \qquad (2.33)$$

The resistance of a fluid having a resistivity of R_w, and the same geometry will be:

$$R = \frac{R_o L}{A} = \frac{R_w L_e}{\Phi A} \qquad (2.34)$$

where:

A   is the apparent cross sectional area; and

R_o is the 100% water saturated formation resistivity.

By definition, the formation resistivity factor F is:

$$F = \frac{\text{Resistance of saturated porous medium}}{\text{Resistance of fluid}} = \frac{R_o}{R_w} \qquad (2.35)$$

combining Equations 2.34 and 2.35 gives:

$$F = \frac{L_e}{L \, \Phi} \tag{2.36}$$

$$T = \left\{\frac{L_e}{L \, \Phi}\right\}^2 \tag{2.37}$$

$$T = \Phi^2 \, F^2 \tag{2.38}$$

where T is the tortuosity.

Wyllie's model involves some questionable assumptions. The main assumption is that the tortuosity pertaining to the flow of electrical current through the conducting fluid in porous media is closely related to the tortuosity which appears in equations describing the flow of fluids in the same media.

The equivalence of hydraulic and electrical tortuosity seems to depend to some extent on the degree of uniformity of the pore structure. Wyllie, in his treatment, for simplicity assumed T_{hyd} (hydraulic resistance) and T_{elec} (electric resistance) having the same value. He stated that there may be a constant connecting both tortuosities , but assumed the constant equal to one.

In a porous medium composed of both conducting and non-conducting solids, the similarity between fluid flow and electrolytic conduction can only be presumed to exist through the liquid phase. Any conductivity resulting from the presence of conducting solids in the matrix must first be accounted for by independent processes.

By incorporating the tortuosity factor, Wyllie ended up with the following equations to calculate the relative permeability curve.

$$K_{rwt} = \frac{1}{I^2 S_w^2} \frac{\int_0^{S_w} \frac{dS_w}{P_c^2}}{\int_0^1 \frac{dS_w}{P_c^2}} \qquad (2.39)$$

$$K_{rnwt} = \frac{1}{I_n^2 (1 - S_w)^2} \frac{\int_{S_w}^1 \frac{dS_w}{P_c^2}}{\int_0^1 \frac{dS_w}{P_c^2}} \qquad (2.40)$$

where:

I, I_n are the wetting and non-wetting resistivity index, respectively;

K_{rwt} is the relative permeability for the wetting phase; and

K_{rnwt} is the relative permeability for the non-wetting phase.

Wyllie did not provide data that tests for the accuracy of the proposed equations; nor did his model account for the fact that at S_{wi} electrical resistivity is finite, but the thin films of liquid that are able to conduct electrically are unable to support a laminar flow of fluid.

In the same year [1958], Wyllie modified the model by considering that the bundle of tubes, which represents the porous medium, are cut into a large number of thin slices. These slices are imagined to be rearranged randomly, and then reassembled. Using this model, Wyllie introduced the following two equations to calculate the relative permeability curves for a porous medium as a function of its capillary pressure distribution and the irreducible water saturation.

$$K_{rw} = \left(\frac{S_w - S_{wi}}{1 - S_{wi}}\right)^2 \frac{\displaystyle\int_{S_{wi}}^{S_w} \frac{dS_w}{P_c^2}}{\displaystyle\int_{S_{wi}}^{1} \frac{dS_w}{P_c^2}} \tag{2.41}$$

$$K_{mw} = \left(\frac{1 - S_w}{1 - S_{wi}}\right)^2 \frac{\displaystyle\int_{S_w}^{1} \frac{dS_w}{P_c^2}}{\displaystyle\int_{S_{wi}}^{1} \frac{dS_w}{P_c^2}} \tag{2.42}$$

Wyllie investigated the accuracy of his proposed model, and his results agree with the measured gas-oil relative permeability curves for Berea sandstone core.

2.1.5 Fatt and Dykstra's Model

Following the method of Purcell for calculating the permeability, Fatt and Dykstra [1951] developed an expression for relative permeability considering the lithology factor as a function of saturation. The lithology factor provides a correction for the inequality of the path length of the proposed tube bundle from the length of the porous medium. Fatt and Dykstra assumed that the inequality of the path was a function of the radius of the conducting pores so that:

$$\lambda = \frac{a}{r^b} \tag{2.43}$$

where:

λ is the lithology factor;

a, b   are constants for the material; and

r   is the pore radius.

The final equation presented is:

$$K_{rw} = \frac{\int_{S=0}^{S=S_{wt}} dS/P_c^{2(1+b)}}{\int_{S=0}^{S=1} dS/P_c^{2(1+b)}}$$

(2.44)

where b is usually assumed to be 0.5. When this equation is tested, a significant difference occurs between the computed results and the core data.

2.2   Imbibition Models

2.2.1   Naar's Model

Naar and Henderson [1961] developed a model to calculate the relative permeability curves for the imbibition condition. Their model extends Wyllie and Grander's model to the imbibition case by accounting for the entrapment of the non-wetting phase during the imbibition process of the wetting phase. The authors relate the drainage and imbibition saturation for equal values of non-wetting relative permeability as:

$$S_{w\,(Imb.)}^* = S_{w\,(drg.)}^* - 0.5\, S_{w\,(drg.)}^{*\,2}$$

(2.45)

where:

$S_{w\,(Imb.)}^*$ is the effective water saturation for imbibition; and

$S_{w\,(drg.)}^*$ is the effective water saturation for drainage.

The relative permeability of the wetting phase can also be calculated under imbibition conditions with this model using:

$$K_{rw \; (imb.)} = \frac{\Phi^{*3} \sigma^2}{K} S^*_{w \; (imb)} \int_0^{S^*_{w \; (imb)}} \frac{S^*_{w \; (imb)} - S}{P_c^2} \; dS \qquad (2.46)$$

where:

Φ^* is the reduced porosity;

$$\Phi^* = \Phi \; (\; 1 - S_{wi} \;)$$

σ is the interfacial tension;

K is the absolute permeability; and

$S^*_{w \; (imb)}$ is the imbibition effective water saturation.

The effective water saturation is defined as:

$$S^*_w = \frac{S_w - S_{wi}}{1 - S_{wi}} \qquad (2.47)$$

where S_{wi} is the irreducible water saturation.

2.2.2   Pirson's Model

From petrophysical considerations, Pirson [1952] derived theoretical equations that can be used to calculate the wetting and non-wetting phase relative permeability under both the imbibition and drainage conditions. For a gas-water system under imbibition

process these equations are:

$$K_{rwt} = S_w^3 \sqrt{S_e} \tag{2.48}$$

$$K_{mwt} = \left(1 - \frac{S_w - S_{wi}}{1 - S_{wi} - S_{nwtr}} \right)^2 \tag{2.49}$$

where:

S_e is the effective water saturation;

K_{rwt} is the relative permeability for the wetting phase; and

K_{mwt} is the relative permeability for the non-wetting phase.

S_{nwtr} is the residual non-wetting phase saturation.

Equations 2.48 and 2.49 were derived for clean water-wet rocks of intergranular porosity. Laboratory experiments conducted by Pirson et al. **[1964]** confirmed the validity of the theoretical petrophysical concepts involved in predicting relative permeability values by use of the above equations . These experiments suggested, however, that to obtain a closer fit between theoretical and experimental curves, Equation 2.48 should be changed to:

$$K_{rwt} = S_w^4 \sqrt{S_e} \tag{2.50}$$

2.3 Generalizing Capillary Pressure Data

Experimentally determined capillary pressure curves (Pc/Sw) and water saturation profiles derived from well logs (Sw/depth) are two independent ways to determine the water saturation distribution inside the transition zone.

In order to correlate the capillary pressure data to well logs, capillary pressure curves obtained from different cores must be generalized. To generalize these curves, the

capillary pressure data must be related to the corresponding rock and fluid properties. M.C Leverett.[1941] pioneered such generalizations based on an experimental study of sand pack columns. According to Leverett's work the capillary pressure is related to reservoir porosity, permeability, and interfacial tension in a dimensionless factor known as the J-function.

$$J_{(S_w)} = \frac{P_{c\,(S_w)}}{\sigma} \sqrt{\frac{K}{\Phi}} \qquad (2.51)$$

where:

$J_{(S_w)}$	is called Leverett's J-function	(dimensionless)
$P_{c\,(S_w)}$	is the capillary pressure	(dyne/cm^2)
σ	is the interfacial tension	(dyne/cm)
K	is the permeability	(cm^2)
Φ	is the porosity	(fraction)

To include the wettability effect, the contact angle (θ) has been added by Rose et al. [1949] to the above equation to become:

$$J_{(S_w)} = \frac{P_{c\,(S_w)}}{\sigma \cos \theta} \sqrt{\frac{K}{\Phi}} \qquad (2.52)$$

H.W. Brown [1951] applied Leverett's relationship to cores of various porosities, permeabilities, and lithologies. His conclusions support the use of the J-function in correlating capillary pressure data obtained from core samples and he states that the correlation could be improved by restricting its use to specific lithologic types from the same formation.

Aufricht and Koepf [1957] introduced the idea of using the measured capillary pressure and the relative permeability data for some cores to generate capillary pressure type curves that can be used to determine the water saturation in the transition zone of the reservoir. They developed two type curves to estimate the water saturation and water cut as a function of the height above the "bottom of the transition zone" with the porosity or permeability as a correlating parameter. (At the time Aufricht and Koepf were developing their technique, the concept of the free water level was not clear) . The technique is applied at a certain depth with a known porosity or permeability and is implemented as follows:

- Type curves, which are developed by interpolation using cores from the same reservoir, are used to estimate the water saturation and the water cut at this depth.

- A water saturation profile can be obtained, using the type curves, and plotted as a function of depth, when the technique is applied to a sequence of depths of known porosity and permeability in the transition zone.

Aufricht and Koepf recommend using permeability as a correlating parameter in relatively homogeneous reservoirs, whereas porosity should be used in fractured and/or vuggy formations.

In recent work, Heseldine [1974] improved Aufricht and Koepf's technique to generalize the capillary pressure type curves. The improvement is simply curve fitting the experimentally determined capillary pressure data and then using the fitting equation to generate a set of capillary pressure curves for different porosities. Since porosity is always available through well logs, it is used as a correlation parameter rather than using the permeability. Heseldine used capillary pressure data from

mercury injection and he expressed the saturation in terms of bulk rather than pore volume, which improved the scatter of saturation values usually observed at low porosity. **Figures 2.1 and 2.2** (taken from Heseldine) show examples of the fitting process and the development of capillary pressure type curves respectively.

The bulk volume of water, BVW, may be expressed as:

$$BVW = \Phi \ (1 - S_{Hg}) \qquad (2.53)$$

where:

Φ is the porosity; and

S_{Hg} is the saturation of mercury.

Heseldine developed these type curves to determine the water saturation in the transition zone. The technique requires knowledge of both the exact location of the free water level and the porosity of the point at which the water saturation is to be calculated. Although the curve fitting technique enhances the accuracy of the developed capillary pressure type curves, a large number of core data is necessary to get a reasonable fit. Alger et al. [1987] replaced the curve fitting in Heseldine's technique with multi-linear regression analysis and extended the benefits of the technique.
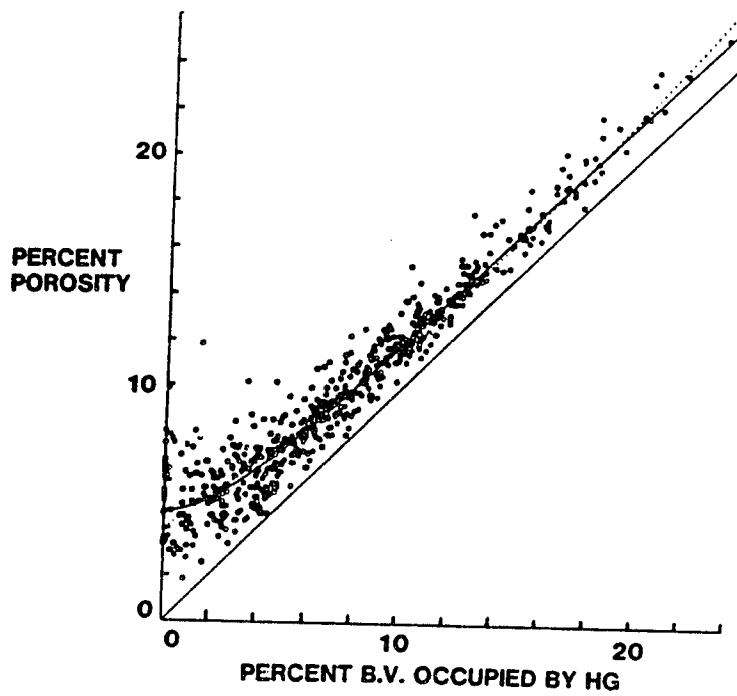
Figure 2.1 Example Air/Hg capillary pressure data at Pc = 400 psia.
[Heseldine, 1974]
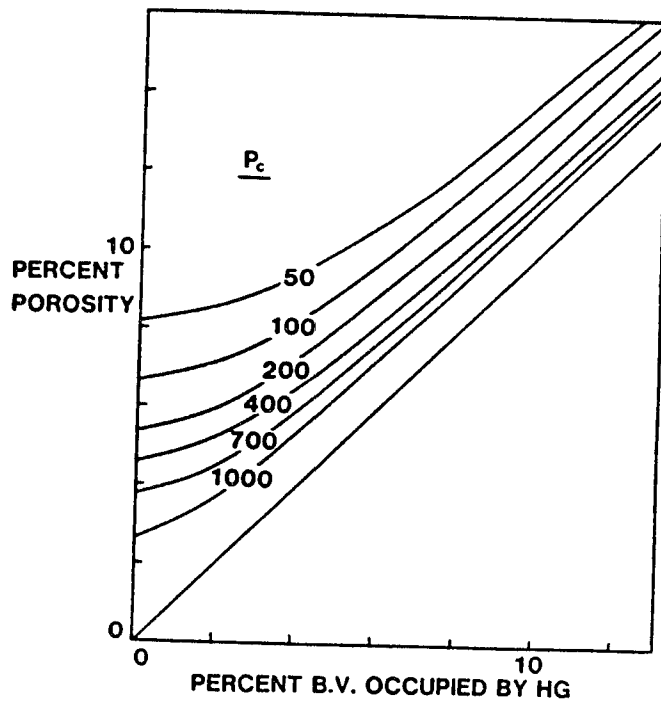
Figure 2.2 Air/Hg capillary pressure relationships for various values of Pc.
[Heseldine, 1974]

CHAPTER III

EXPERIMENTAL INVESTIGATION

3.1   Introduction

When the well bore cuts through both the hydrocarbon and the water in a homogeneous transition zone, by means of pressure measurements taken at various levels within this zone, the mobile fluid pressure recorded with the Repeat Formation Tester can be used to calculate the densities of the saturating fluids and to define the free water level. These measurements also permit the calculation of the threshold pressure and the capillary pressure at any level of the reservoir. Once the densities of the saturating fluids and the free water level are known, a capillary pressure/depth profile can be established. On the other hand, water saturation/depth profile can be obtained through the resistivity measurements in the same zone. The two preceding profiles (P_c/depth and S_w/depth) can be used to determine the capillary pressure/water saturation curve (P_c/S_w) for the zone. This technique provides the in-situ capillary pressure curve (P_c/S_w) in reservoirs with homogeneous transition zone in cases where core samples are not available.

This chapter documents a laboratory study of the possibility of in-situ determination of capillary pressure and relative permeability curves using open hole well logs.

3.2 Preliminary Runs

To establish the in-situ capillary pressure curve, and to study the effect of saturation history on the shape of the resistivity profile, measurements of resistivity along the height of a long core in which a transition zone is established through water imbibition or drainage was needed. Brine imbibition rate is expected to vary with the variation of the pore structure of the core. Consequently, the rate of brine imbibition was monitored both visually and electrically in small, less expensive, cores of different permeabilities. The purpose of such experiments was also to examine the electrical method best suited for monitoring the brine imbibition into the core. A sketch and photograph of the laboratory setup for the preliminary experiments is shown in **Figure 3.1** and **3.2** respectively.
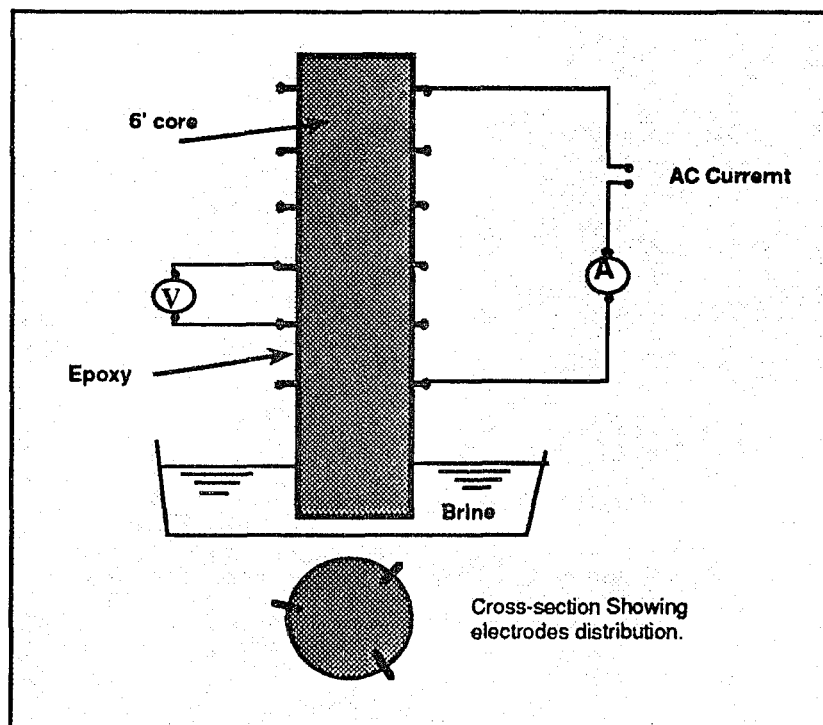
Figure 3.1 Sketch of the preliminary laboratory setup.
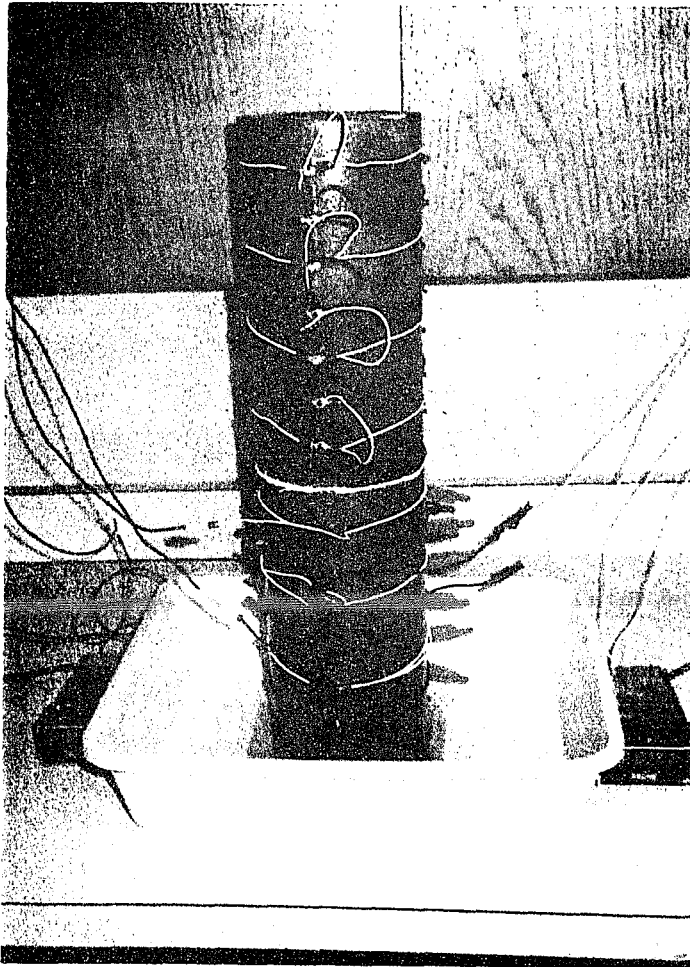
Stainless steel electrodes inserted 1/8" deep into a 6" core that has a permeability of 100 md. Electrode arrays are placed 1.5" apart along the axis of the core at 120°. Electrodes are connected externally and the core is insulated with epoxy.

Figure 3.2 Photograph showing the preliminary setup.

The resulting imbibition rate curves for different permeability cores are shown in Figure 3.3. These preliminary runs were promising, and through them it was found that electrical measurement (when compared to visual observation) accurately monitor the water imbibition rate. Also, water saturation could be calculated using the voltage drop across each section of the core. To provide better contact with the fluid in the core, the stainless steel current electrodes were replaced with a molten alloy of lead and

silver poured in the shallow holes drilled in the core. The thickness of the epoxy layer on the core surface was also increased for better isolation of the core. Finally, to assure brine homogeneity, the open brine basin was replaced with a closed one in the long core experiments .
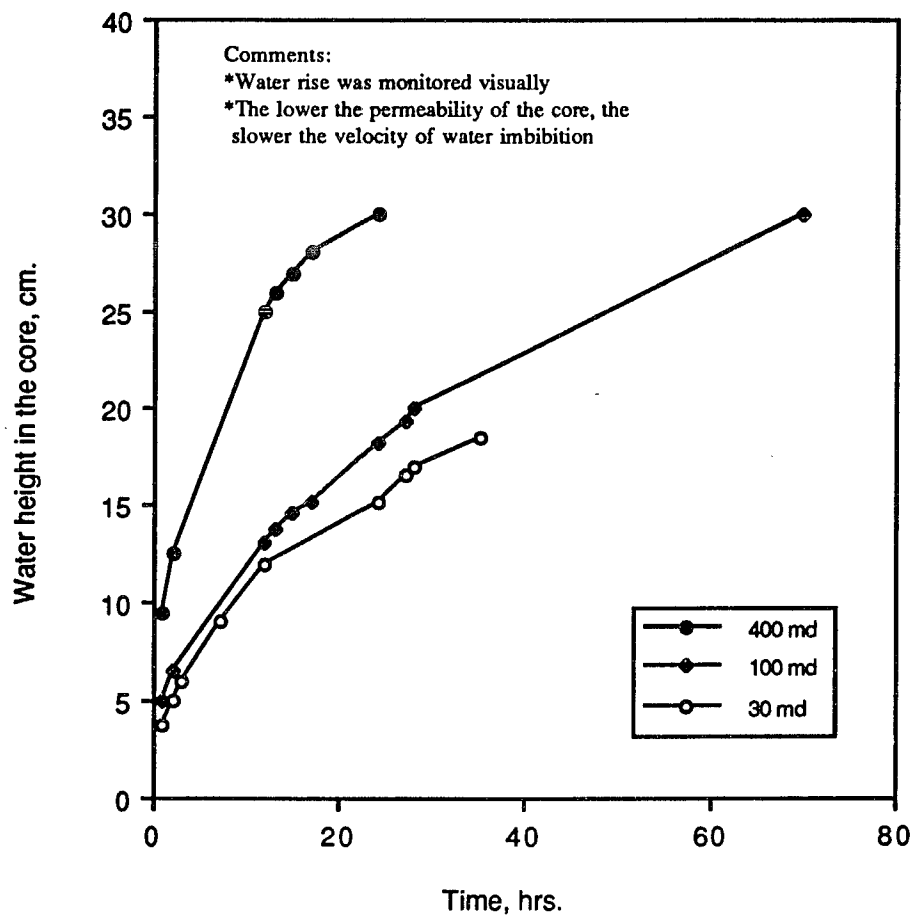
Figure 3.3 Brine imbibition in different permeability cores.

3.3 Long Core Model

A laboratory model was constructed using an eight-foot long Berea sandstone core. Electrode arrays were fitted along the core. These electrodes were used to determine the

saturation profile along the core. The core was connected to a tube to monitor the free water level necessary to determine the capillary pressure profile along the core. **Figures 3.4** and **3.5** show a photograph and sketch of the described model respectively.
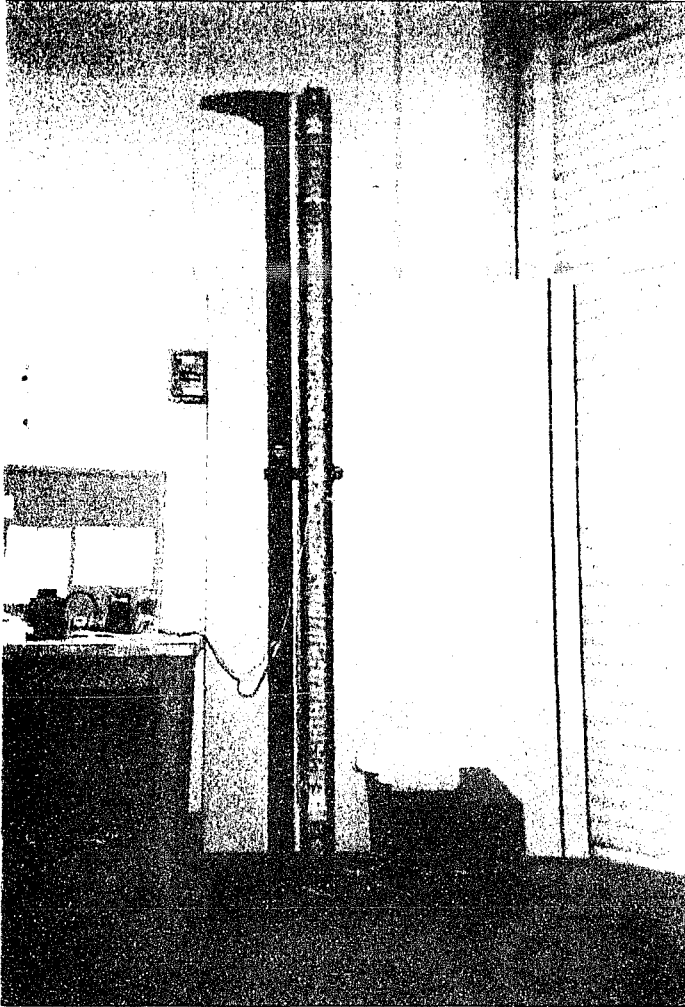
Figure 3.4 Photograph for the experimental setup for the long Berea sandstone core.
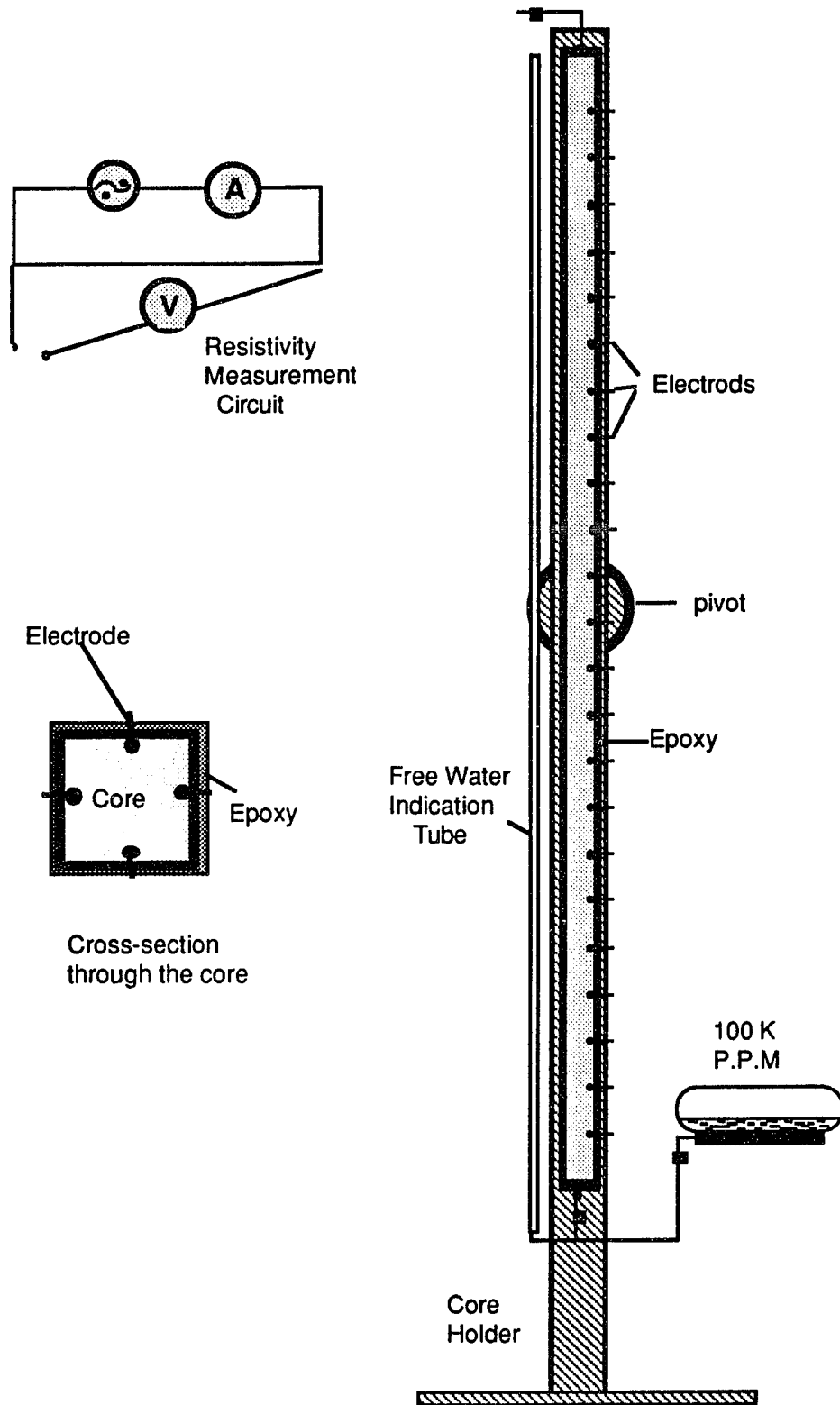
Figure 3.5 Schematic of the experimental setup.

3.4 Imbibition Regime

The core was allowed to imbibe NaCl brine of 100 kppm concentration. Three months were needed for complete imbibition as indicated by fluid stabilization inside the core. The brine imbibed to about 55 inches in the core with a transition zone of about 30 inches. Resistivity measurements were taken and used to calculate the water saturation profile along the core. During the imbibition period the reproducibility of the measurements was examined. **Figure 3.6** shows resistivity measurements at three different times. As shown in the figure, the lower 25 inches of the core shows stabilized water saturation as indicated by a constant resistivity; however, the upper part shows a decrease in resistivity with time as a result of increasing water saturation.
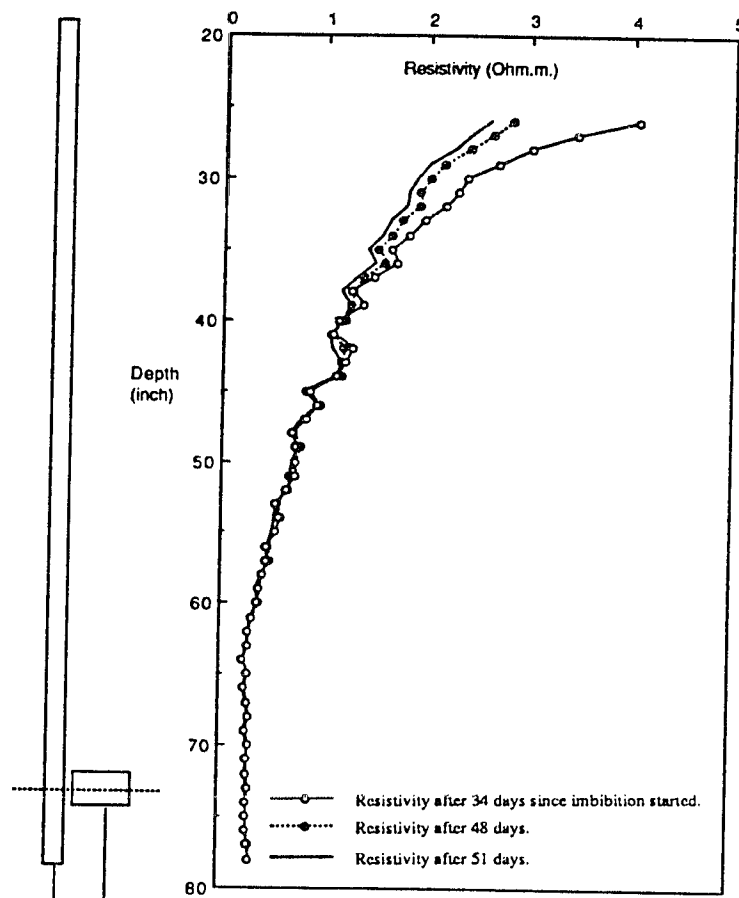
Figure 3.6 Resistivity measurements at different times during brine imbibition.

3.5 Drainage Regime

For the drainage run, the core was saturated under vacuum with the same brine until 100% brine saturation was assured. The core was then allowed to drain against the same free water level in the brine tank used in the imbibition run. Again resistivity readings were taken during the drainage run and a final set of measurements was recorded when the fluids reached stabilized conditions, i.e, when the gravity forces equal capillary forces.

Figures 3.7 and **3.8** show the resistivity and water saturation distribution, respectively, for both the imbibition and drainage runs. The resistivity profile in the drainage regime shows a straight line starting above the threshold pressure, while a curved line is observed in the imbibition regime. This observation concerning the shape of the resistivity profile may be used to indicate the saturation history of the reservoir which may help define its geologic development.

The vertical axis of **Figure 3.8** can be scaled in terms of capillary pressure using the following equation:

$$P_c = \frac{H}{2.3} (\rho_w - \rho_{air}) \qquad\qquad (3.1)$$

where:

P_c is the capillary pressure, psi;

H is the height above the free water level, ft;

ρ_w is the water density, gm/cc; and

ρ_{air} is the air density, gm/cc.
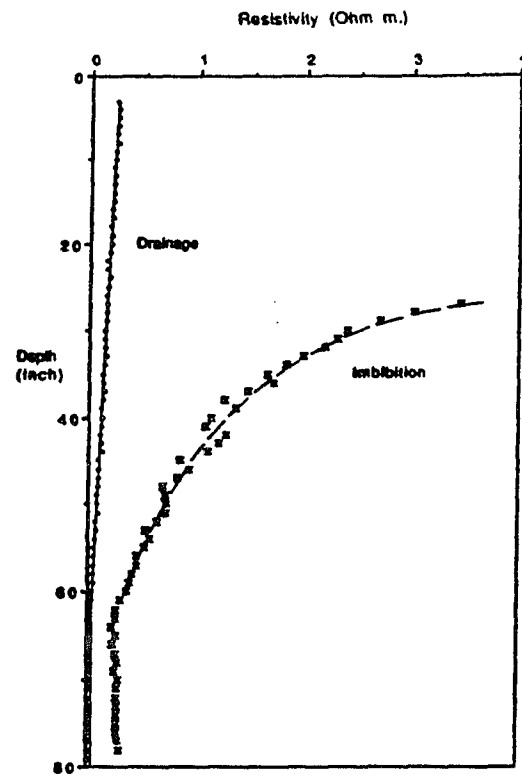
Resistivity (Ohm m.)

Figure 3.7 Resistivity profile for the long Berea sandstone core in both drainage and imbibition regimes.
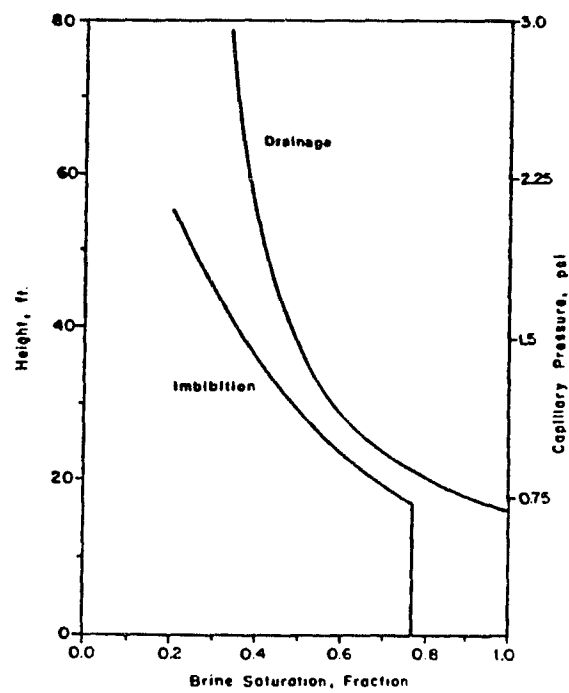
Figure 3.8 Saturation profile and capillary pressure for the long Berea sandstone core in both drainage and imbibition regimes.
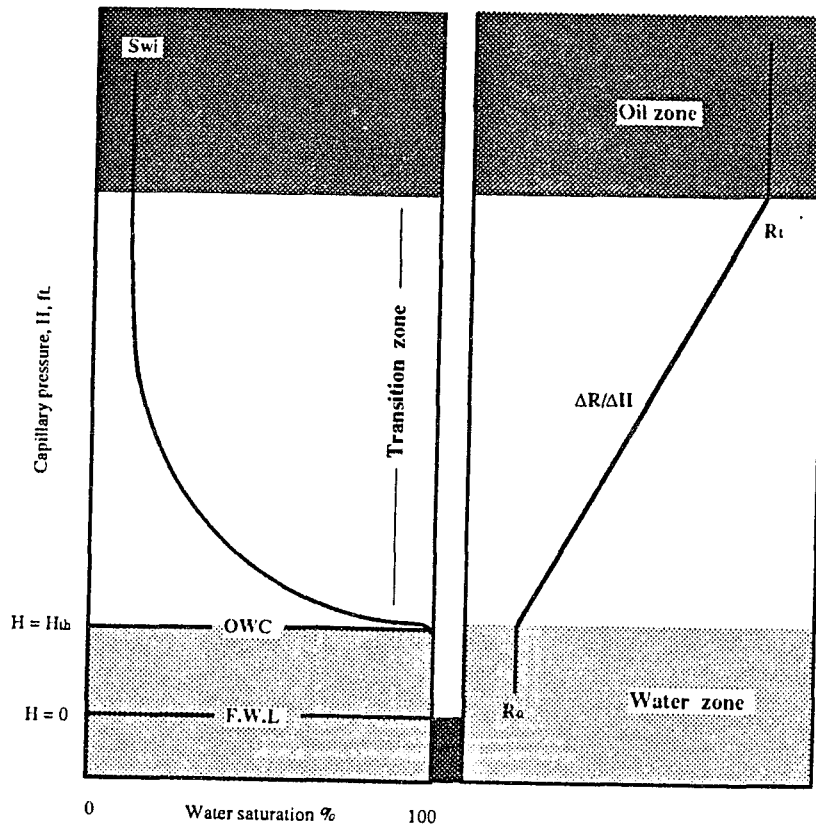
Figure 3.9 Resistivity profile under drainage regime in a homogeneous formation.

The resistivity/depth straight line relationship observed in the drainage conditions can be implemented to develop an equation that is used to calculate the in-situ capillary pressure in the transition zone for a homogeneous formation. **Figure 3.9** sketches the straight line relationship with respect to the different zones in the reservoir.

The straight line equation is:

$$R_t = R_o + \frac{\Delta R}{\Delta H} * (H - H_{th})$$

(3.2)

where:

R_o is the resistivity of the 100% water saturated formation;

R_t is the true formation resistivity;

$\dfrac{\Delta R}{\Delta H}$ is the resistivity gradient (slope of the line); and

H_{th} is the height of the water table above the free water level.

Archie's equation for clean sand states:

$$S_w = \sqrt[n]{\frac{R_o}{R_t}}$$

(3.3)

Substituting the term R_t from Equation 3.2 into Equation 3.3 gives:

$$S_w = \sqrt[n]{\frac{R_o}{R_o + \dfrac{\Delta R}{\Delta H} * (H - H_{th})}}$$

(3.4)

Solving for H, assuming n=2:

$$H = R_o \frac{\Delta H}{\Delta R} \left\{ \frac{1}{S_w^2} - 1 \right\} + H_{th}$$

(3.5)

Now, combining Equations 3.5 and 3.1, and solving for P_c gives:

$$P_c = R_o \frac{\Delta H}{\Delta R} \frac{(\rho_w - \rho_{hy})}{2.3} \left\{ \frac{1}{S_w^2} - 1 \right\} + \frac{(\rho_w - \rho_{hy})}{2.3} H_{th}$$

(3.6)

The second term in Equation 3.6 represents the threshold capillary pressure, P_{th}, consequently, the equation will take the form:

$$P_c = R_o \; \frac{\Delta H}{\Delta R} \; \frac{(\rho_w - \rho_{hy})}{2.3} \; \left\{ \frac{1}{S_w^2} - 1 \right\} + P_{th} \qquad (3.7)$$

Equation 3.7 is used to calculate the in-situ capillary pressure representative of the transition zone using data mainly derived from well logs. the boundary conditions of the equation are:

@ $S_w = 0$ $P_c = \infty$

@ $S_w = 1$ $P_c = P_{th}$

The general form of Equation 3.7 may be represented as:

$$P_c = A \; \left\{ \frac{1}{S_w^2} - 1 \right\} + B \qquad (3.8)$$

where:

$$A = R_o \; \frac{\Delta H}{\Delta R} \; \frac{(\rho_w - \rho_{hy})}{2.3}; \text{ and}$$

$$B = P_{th}$$

For the long Berea sandstone core, the measured resistivity profile together with the knowledge of the fluid densities used, provide the data necessary to solve Equation 3.7 to become:

$$P_c = 0.203 \; \left\{ \frac{1}{S_w^2} - 1 \right\} + 0.72 \qquad (3.9)$$

which reduces to:

$$P_c = \frac{0.203}{S_w^2} + 0.516 \qquad\qquad (3.10)$$

No information was found in the literature concerning the relation between the shape of the resistivity profile in the transition zone and the saturation history of the reservoir. Tixier **[1949]** presented some field examples where the resistivity log shows a fairly straight line through the transition zone in linear resistivity scale. Two of these examples are shown in **Figures 3.10** and **3.11**.

SELF - POTENTIAL	RESISTIVITY LOG	
$-$ –|20|– $+$	0 NORMAL 50	
	0 – – – LATERAL – – – – 50	
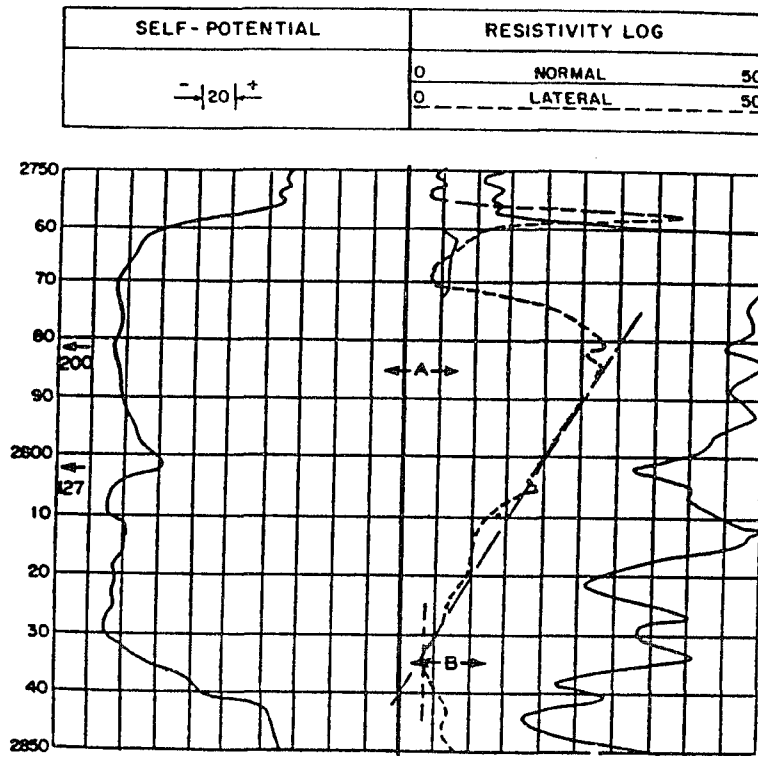
Figure 3.10 An example well log showing a straight line resistivity in the transition zone [Tixier 1949]

SELF - POTENTIAL	RESISTIVITY LOG
$-$ –|20|– $+$	0 NORMAL 50
	0 LATERAL 50
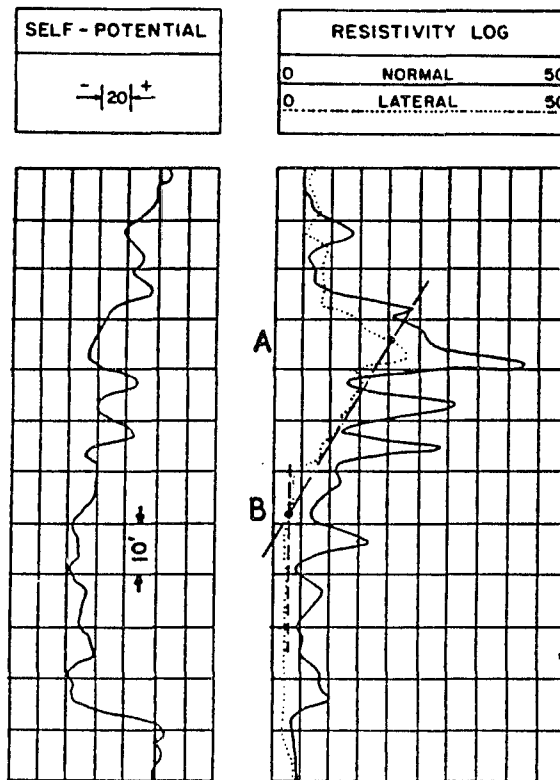
Figure 3.11 A second example showing a straight line resistivity in the transition zone [Tixier 1949]
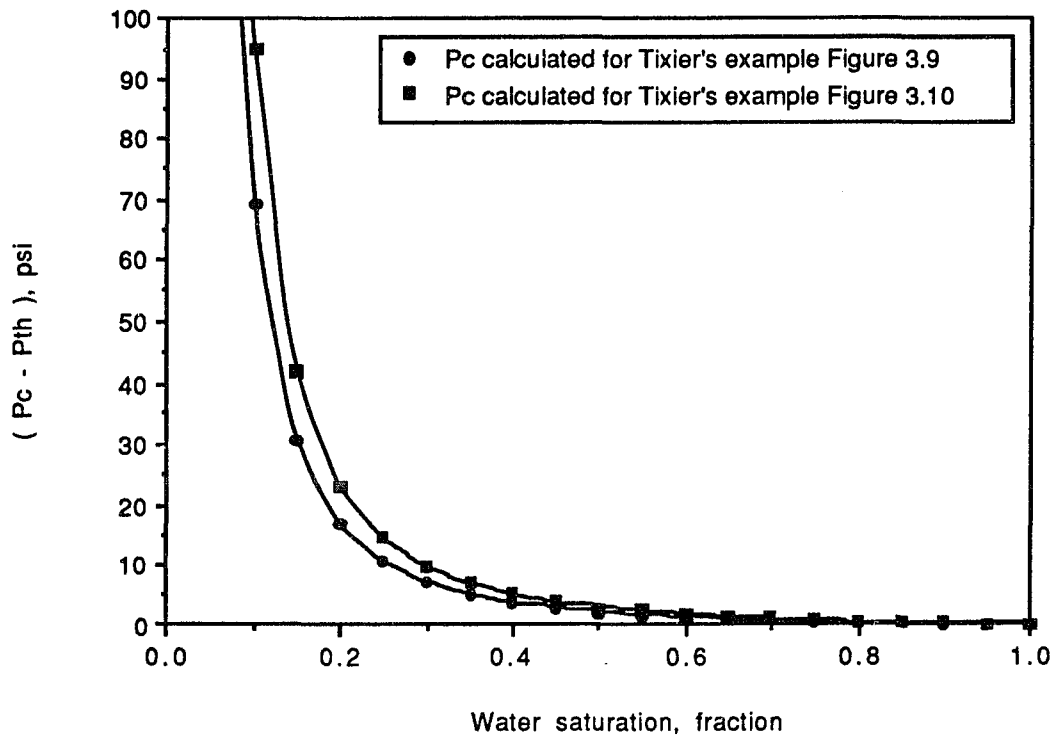
Figure 3.12 calculated capillary pressure curves for Tixier's examples.

Figure 3.12 shows the calculated capillary pressure curves for the two examples in **Figures 3.10** and **3.11** with zero threshold pressure assumption.

The curve calculated with Equation 3.10 is represented in **Figure 3.13**. The figure shows, as expected, that the curve represents the average capillary pressure for the long Berea sandstone core. **Figure 3.13** also shows a comparison between the in-situ capillary pressure curve measured on the long core in drainage condition with a drainage capillary pressure curve measured on a small core plug using a centrifuge. The capillary pressure curves agrees fairly well. The small difference between the curves

may be attributed to the following reasons:

1 - Centrifuge capillary pressure curve was conducted on a small volume of the rock (core plug), which may not be representative of the rest of the long core.

2 - Only five points determines the centrifuge capillary pressure curve. Consequently, any error in the measurement of the saturation affects the curve significantly.

3 - The calculation for the average water saturation at each stabilized capillary pressure value has some source of error: A homogeneous average water saturation is assumed along the core and the end effects are neglected.

For the above reasons, in-situ capillary pressure calculated using the resistivity log is believed to be more accurate and more representative of the long core.
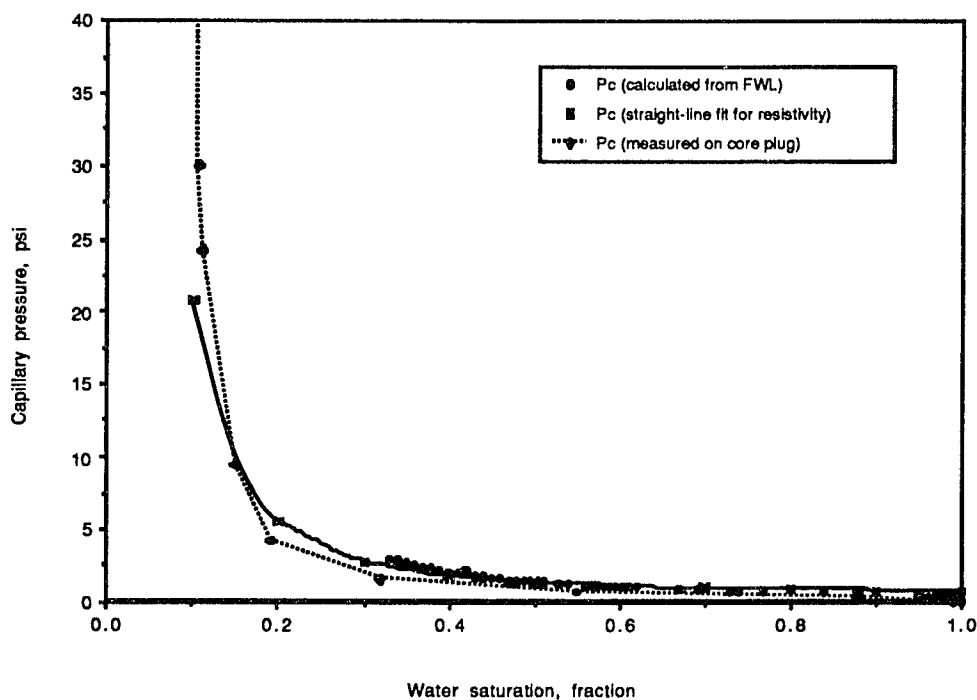
Figure 3.13 Capillary pressure comparison.

3.6 Relative Permeability Calculations

Corey's model was used to calculate the relative permeability curves in the drainage regime. **Figure 3.14** shows the calculation of the pore size distribution index, λ, which is used in Equations 2.25 and 2.26 to calculate the relative permeability curves in the drainage direction. To calculate the relative permeability in the imbibition regime, Pirson's model, Equations 2.49 and 2.50, was used. **Figure 3.15** shows the calculated relative permeability curves for both the drainage and imbibition regimes for the long Berea sandstone core
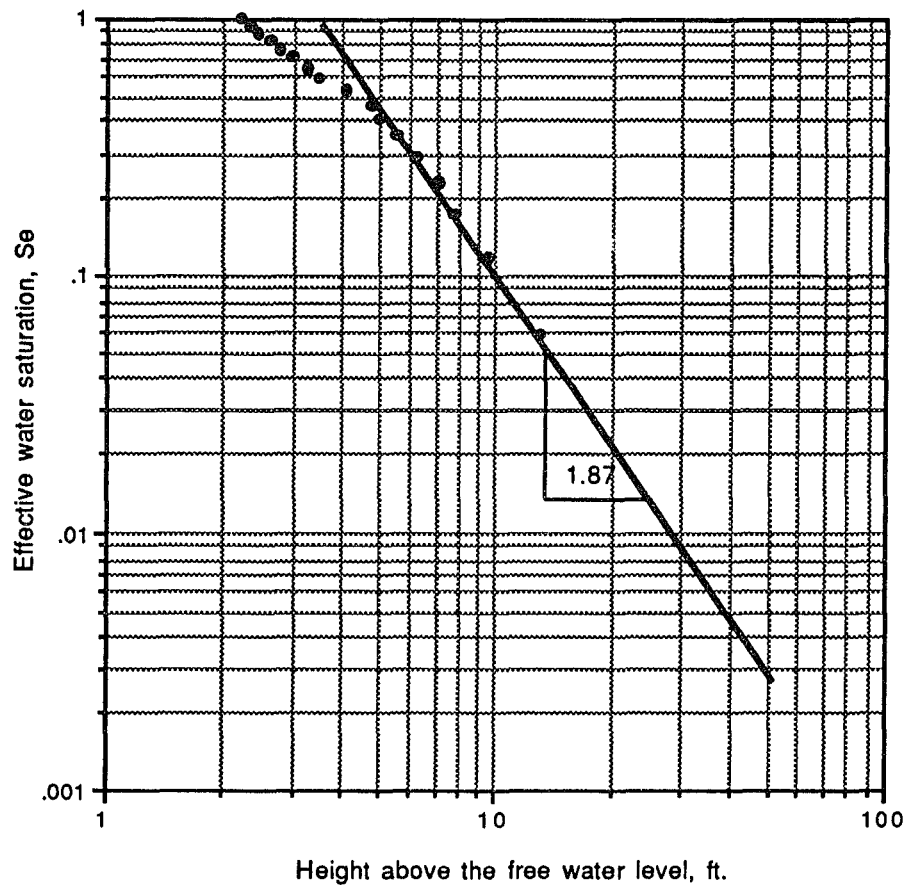
Figure 3.14 Calculation of the pore-size distribution index for Corey's model.
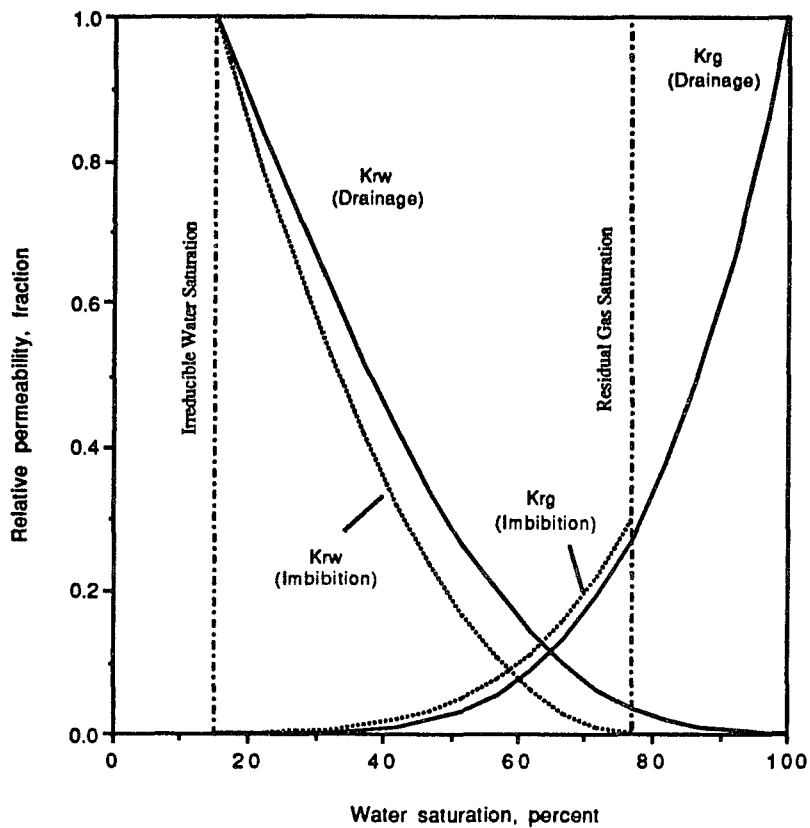
Figure 3.15 Calculated relative permeability curves for the long Berea sandstone core.

3.7 Conclusions

■ Experimental results show that correlating the well log-derived water saturation profile to the pressure data in the transition zone results in a capillary pressure/water saturation (P_c/S_w) curve. This technique when compared to the capillary pressure curve (P_c/S_w) measured on a core sample cut from the same rock showed good results. The developed capillary pressure curve can be used to generate relative permeability curves specific to the formation under study.

■ Experimental results show a linear resistivity gradient under drainage conditions, while a curved profile is observed under imbibition conditions. This observation can be used to indicate the saturation history, which would help to formulate an understanding of the geological history of reservoirs.

■ The linear resistivity gradient observed under the drainage regime is implemented to derive a formula that is used to calculate the in-situ capillary pressure curve for the transition zone using data from well logs.

CHAPTER IV

THEORETICAL

4.1 Technique Outline

The capillary pressure/saturation relationship is an inherent property of the rock-fluid system involved and represents the ability of the rock to retain the wetting phase against the pressure exerted by the non-wetting phase. The capillary pressure /saturation relationship determines the water saturation as a function of the height above the free water level. Besides the capillary pressure/saturation relationship, well log analysis provides another independent way to determine the water saturation profile along the transition zone either in clean or shaly formations. The distribution of water inside the transition zone is affected mainly by the capillary pressure between the water and the hydrocarbon. In a homogeneous transition zone with constant porosity, permeability, and lithology, the water saturation profile (Sw/depth) calculated from well logs is in fact a capillary pressure curve (Pc/Sw). This is true simply because the depth scale can be converted into capillary pressure once the free water level is located. This capillary pressure curve can be compared to the capillary pressure curve measured in core samples.

This chapter documents a new technique based on curve matching the log derived water saturation profile to generalized capillary pressure type curves in the transition zone. These capillary pressure type curves are generated using capillary pressure data measured on few core samples from the reservoir under consideration. A flow chart for the new technique is presented in the **Figure 4.1**. The major steps are discussed separately.

TECHNIQUE   OUTLINE

```
┌─────────────────┐                          ┌──────────────────────┐
│   OPEN HOLE     │                          │ CAPILLARY PRESSURE   │
│   WELL LOGS     │                          │ CURVES FROM CORES    │
└─────────────────┘                          │     (Pc / Sw)        │
        │                                    └──────────────────────┘
        ▼                                               │
┌─────────────────┐                                     ▼
│ WATER SATURATION│                          ┌──────────────────────┐
│    PROFILE      │                          │     J-FUNCTION       │
└─────────────────┘                          └──────────────────────┘
        │                                               │
        ▼                                               ▼
┌─────────────────────────┐                  ┌──────────────────────┐
│ WATER SATURATION PROFILE│                  │ CAPILLARY PRESSURE TYPE│
│ NORMALIZED TO A REFERENCE│                 │ CURVES NORMALIZED TO A │
│      POROSITY           │                  │  REFERENCE POROSITY    │
└─────────────────────────┘                  └──────────────────────┘
        │                                               │
        │                                               ▼
        │                                    ┌──────────────────────┐
        │                                    │ HEIGHT ABOVE FREE    │
        │                                    │ WATER LEVEL TYPE     │
        │                                    │     CURVES           │
        │                                    └──────────────────────┘
        │              ┌──────────┐                     │
        └─────────────▶│  MATCH   │◀────────────────────┘
                       └──────────┘
             ┌─────────────┼─────────────┐
             ▼             ▼             ▼
    ┌──────────────┐ ┌──────────┐ ┌──────────────┐
    │  CAPILLARY   │ │FREE WATER│ │  ABSOLUTE    │
    │  PRESSURE    │ │  LEVEL   │ │ PERMEABILITY │
    └──────────────┘ └──────────┘ └──────────────┘
            │
            ▼
    ┌──────────────────────┐
    │ TRANSFORMATION MODELS│
    └──────────────────────┘
            │
            ▼
    ┌──────────────────────┐
    │ RELATIVE PERMEABILITIES│
    └──────────────────────┘
```

Figure 4.1   Technique outline.

4.2   Normalized Water Saturation

Using the continuous data furnished by resistivity and porosity logs, water saturation inside the transition zone can be calculated. To exclude the effect of porosity, the water saturation values are normalized to a constant reference porosity, Φ_{ref} , in the transition zone.

For clean sands, the normalized water saturation value, S_{wn}, is related to the formation resistivity, R_t, and the reference porosity Φ_{ref} by:

$$R_t = \frac{a\,R_w}{\Phi^m\,S_w^n} = \frac{a\,R_w}{\Phi_{ref}^m\,S_{wn}^n} \qquad (4.1)$$

where:

a   is the formation factor coefficient;

R_w is the formation water resistivity;

m   is the cementation exponent; and

n   is the saturation exponent.

Solving for S_{wn}:

$$S_{wn} = S_w\sqrt[n]{\frac{\Phi^m}{\Phi_{ref}^m}} = \sqrt[n]{\frac{a\,R_w}{\Phi_{ref}^m\,R_t}} \qquad (4.2)$$

Equation 4.2 can be used to calculate the normalized water saturation, S_{wn}, for a chosen reference porosity using data from well logs only.

If m is assumed equal to n, the normalized water saturation, S_{wn}, can be calculated as:

$$S_{wn} = S_w\frac{\Phi}{\Phi_{ref}} \qquad (4.3)$$

The reference porosity may be chosen as the average reservoir porosity, provided that the calculated normalized water saturation does not exceed 100%. A higher reference porosity must be used if the normalized water saturation exceeds 100%.

4.3 Capillary Pressure Type Curves.

Figure 4.2, after W. R. Purcell[1949], shows capillary pressure data (P_c/S_w) measured on three core samples from the Frio formation. Applying the J-function transform to this capillary pressure data makes the data merges into one single curve as shown in **Figure 4.3**. The best fitting equation for the resulting curve is substituted in the J-function equation which is solved for capillary pressure as a function in water saturation for constant reference porosity and different permeabilities. The resultant of this calculations, when plotted, gives capillary pressure type curves that represents the reservoir as if it is composed of only one porosity, the reference porosity, and varying permeability. Consequently, these type curves can be used in a reservoir-wide scale as long as the lithology and the fluid properties do not change.

For comparison with the log-derived water saturation profile (S_w/depth), the capillary pressure will be expressed as height above the free water level using the equation below:

$$P_c = \frac{H}{2.3} (\rho_w - \rho_h) \tag{4.4}$$

where:

P_c Capillary pressure (psi)

H Height above free water level (ft.)

ρ_w Density of water (gm. / cc.)
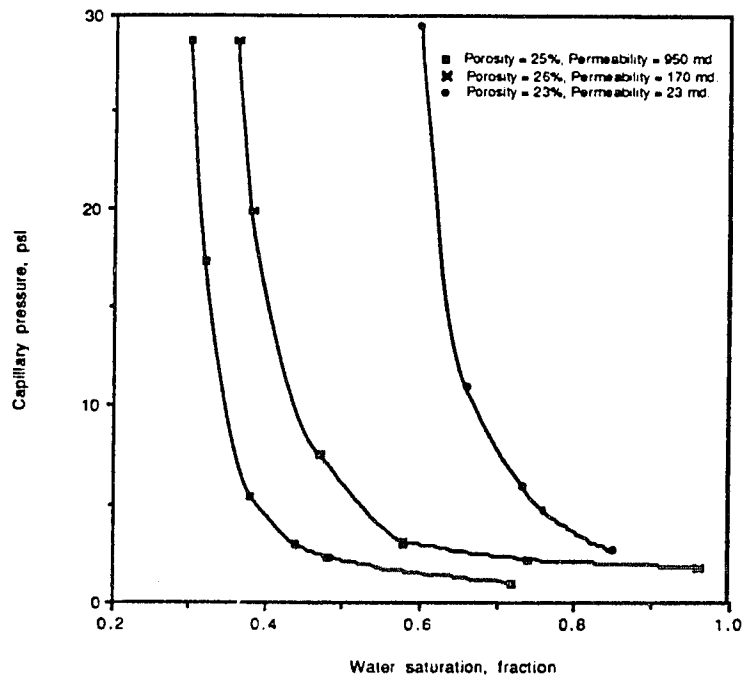
ρ_h Density of hydrocarbon (gm. / cc.)

Figure 4.2 Capillary pressure data for three cores from the Frio sandstone
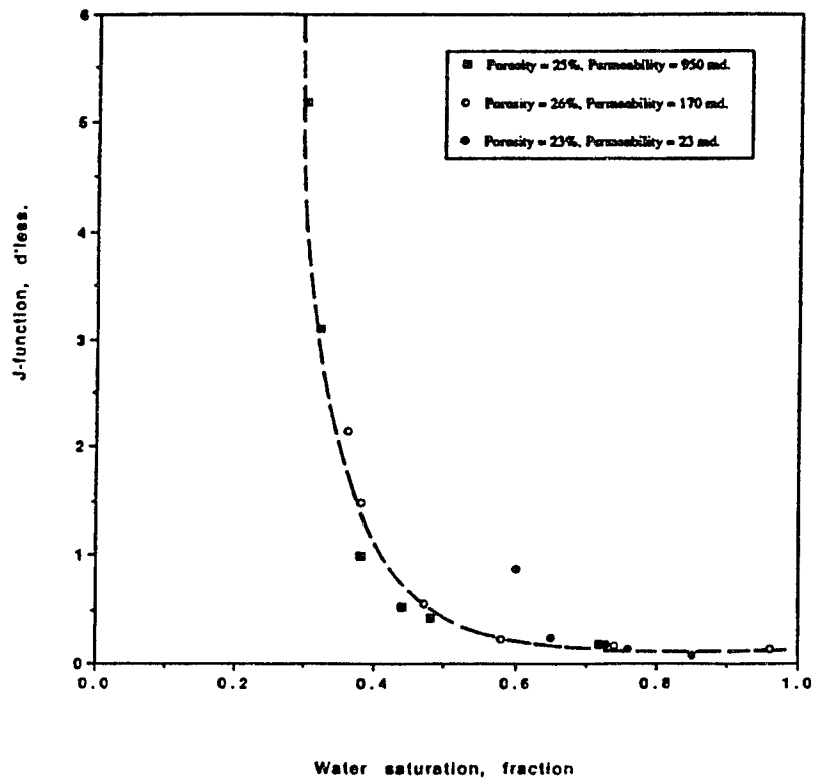[Purcell, 1949]

Figure 4.3 J-function for the three cores from the Frio sandstone.

Knowledge of fluids densities in reservoir conditions is necessary to apply the equation. However, reasonable estimation can be done for the water density when salinity, pressure, and temperature are known. Also, gas gravity can be used to estimate the gas density at reservoir conditions if the pressure and temperature are known.

Figure 4.4 shows an example of these type curves generated using a 25% porosity, zero degrees contact angle, and 0.874 gm/cc fluid densities difference.

Figure 4.5 shows another example the J-function calculated for capillary pressure data that was measured by H. Brown [1951]. Although the J-function generalizes the capillary pressure data, not all the capillary pressure curves coincide with one J-function curve. Brown enhanced the fit by plotting data for each lithology separately. The J-function can be subdivided, for the same lithology, into three categories based on the average pore radius of the rock, providing a representative J-function for low, medium, and high permeability sands. In Figure 4.6 the solid line shows Brown's estimated average J-function, and the dashed line shows the average J-function for core data from three tight sand formations: Cotton Valley, Travis Peak, and Falher. The figure shows that a trend specific to tight sands exists with a higher irreducible water saturation than that drawn by Brown. Consequently, the reduction in data scattering reported by Brown when he plotted the J-function for each lithology separately is due mainly to a smaller range of pore radii in each group.
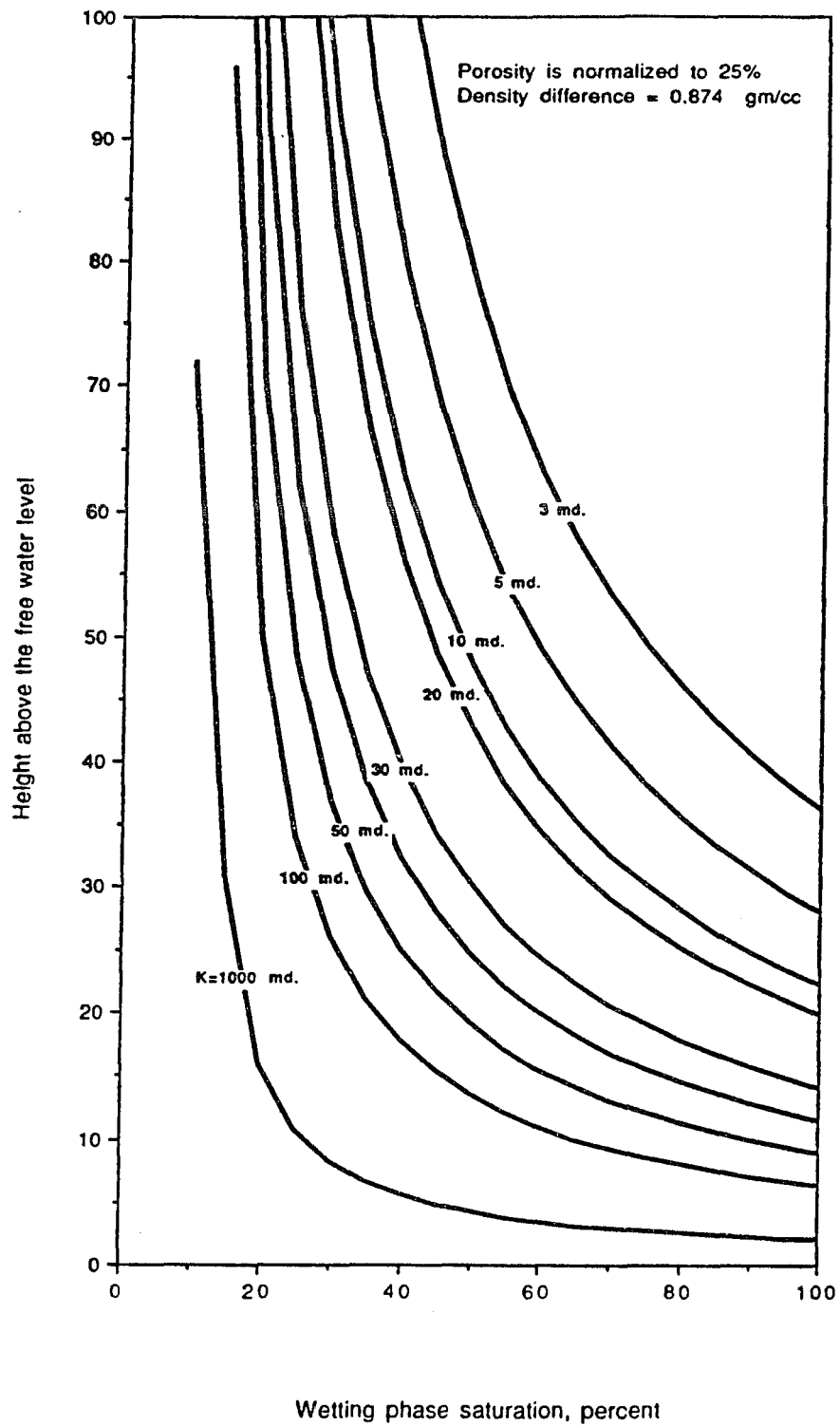
Figure 4.4 Capillary pressure type curves for the Frio sandstone.
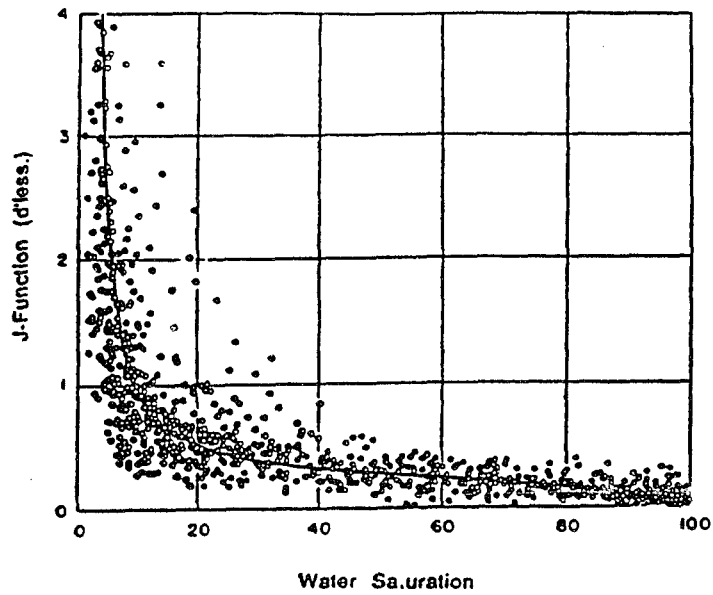
Figure 4.5 J-function for cores from Edwards Formation **[Brown, 1951]**
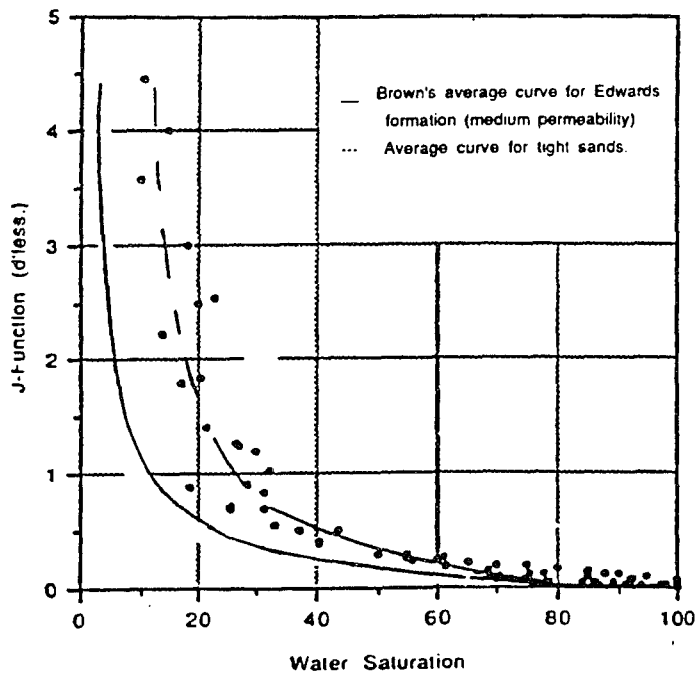
Figure 4.6 Leverette's J-function for different sandstone cores. Data from Edwards, Cotton Valley, Travis Peak, and Falher formations.

4.4   Application Methodology:

a.   Homogeneous Transition Zone

In a Homogeneous transition zone (fairly constant porosity, permeability, and lithology), the capillary pressure type curves, once established as a function of height above the free water level for the reference porosity, are laid over the normalized water saturation profile for which permeability is the correlating parameter. Since both curves have the same abscissa, only vertical shifting is necessary to obtain a match. When a match is found, the capillary pressure curve specific to the formation is defined, and the following parameters are estimated:

-Absolute permeability

-Depth of the free water level (H=0)

-Irreducible water saturation.

Since both the capillary pressure type curves and the water saturation profile are normalized to the same reference porosity, the value of this reference porosity will not affect the match results.

The capillary pressure curve is then used to generate the relative permeability curves for both the drainage and the imbibition conditions using the models mentioned in chapter II.

b.   Multi-layered Transition Zone

A transition zone composed of two layers of the same porosity and different permeabilities may be modeled by two bundles of tubes that are hydraulically connected. **Figure 4.7** shows two different variations of this model with the low permeability zone

(small diameter tubes) on top of the high permeability zone (large diameter tubes) in **Figure 4.7a**, and with the zones reversed in **Figure 4.7b**. The expected fluid distributions in the tubes and the corresponding capillary pressure curves are also schematized in the figures. The small-diameter tubes will show higher threshold pressures and higher residual water saturations than the tubes with larger diameters. If we consider **Figure 4.7a**, the capillary pressure curve above the free water level will correspond to the large tubes, up to the point at which the junction between the large and the small tubes is reached; beyond this point, the capillary pressure will correspond to the small tubes. The dashed extensions for the capillary curves describe the situation for the case in which the entire transition zone is composed of only one layer. For a multi-layered transition zone, a segmented water saturation profile results because of the changes in pore structure between layers. Each segment is matched separately to generate a capillary pressure and relative permeability characteristics specific to that segment. Only the free water level depth is common for all segments.

4.5 Gulf Coast Field Example

Figure 4.8, taken from the literature, shows the processed open hole logs for a well drilled in the Gulf Coast region. The figure shows the pressure data from the wireline formation tester. Since the formation is a clean sand of constant porosity (30.5%), the calculated water saturation presented in the third track is used directly to match capillary pressure data. Core data from this formation is not available. However, since the indicated porosity and permeability are in the same range as the Frio sands in the Gulf coast, capillary pressure type curves representative of the Frio sands were used.
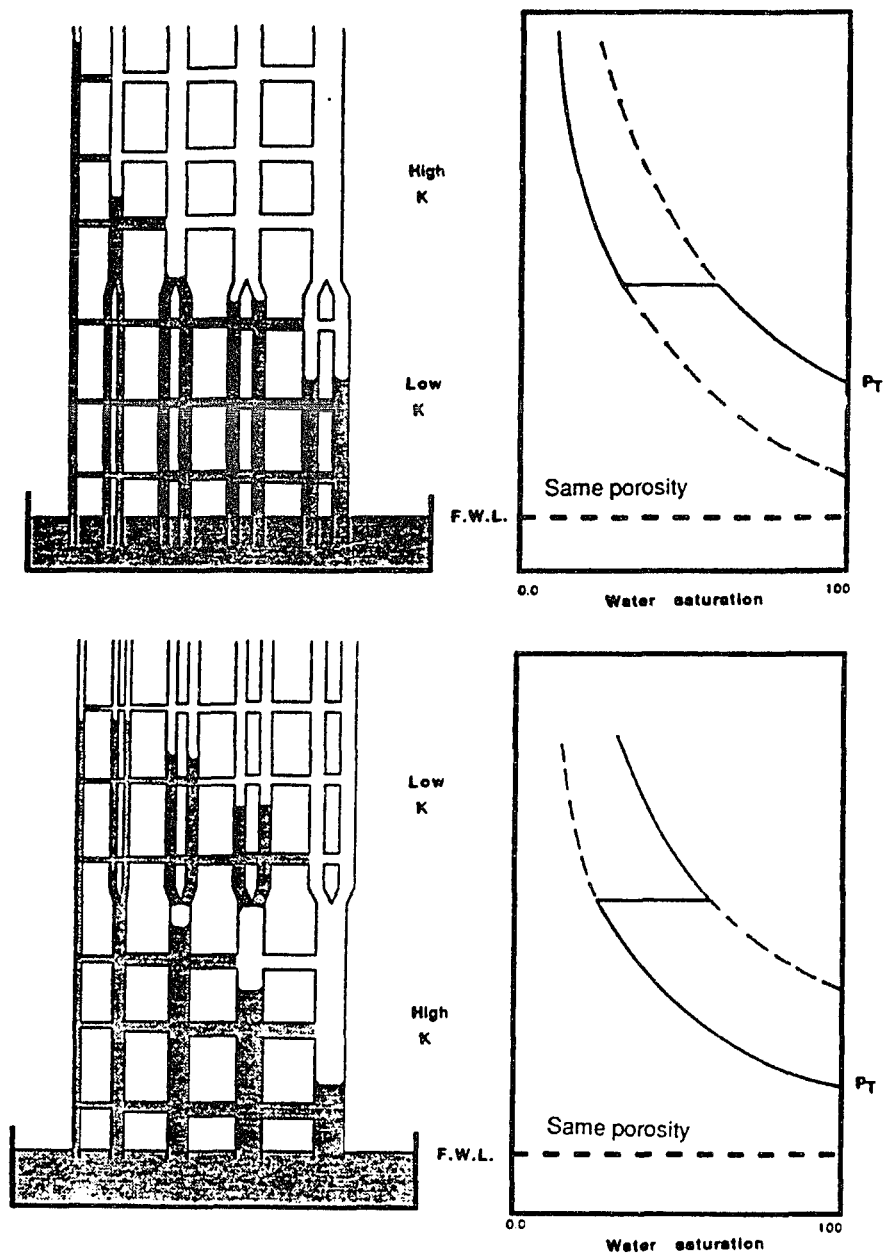
Figure 4.7 Schematic showing the variation in capillary pressure curve due to changes in pore size and permeability.

Since the capillary pressure type curves were measured on cores in drainage conditions, before applying the technique, it was necessary to determine whether the reservoir was undergoing drainage or imbibition regime. For this purpose, the resistivity profile was calculated using the water saturation profile represented in the well logs (**Figure 4.8**). **Figure 4.9** shows the calculated resistivity profile. The lower section of the figure shows a straight-line segments indicating, according to the experimental results, that the reservoir is undergoing a drainage regime.

To apply the technique, the water saturation profile is correlated to capillary pressure type curves developed for the Frio sands that have been normalized to the same porosity (30.5%). Through vertical shifting, the water saturation profile in the lower part of the transition zone is found to match a capillary pressure curve of 1000 md. permeability as shown in **Figure 4.10**. The match also shows the free water level at a depth of 8020 ft., which agrees with the wireline formation tester data.

Using the matching capillary pressure curve, Corey's model is used to calculate the relative permeability in the drainage direction. Plotting the effective water saturation versus the capillary pressure in feet on a logarithmic scale resulted in a pore size distribution index (λ) of 1.8 which has been used in Equations 2.25 and 2.26 to develop the relative permeability curves in the drainage direction. To calculate the relative permeability in the imbibition direction, Pirson's model (Equations 2.49 and 2.50) is used. The irreducible non-wetting phase saturation necessary for Equation 2.49 is calculated using the empirical correlation found by Katz et al. **[1966]** as:

$$S_{nwi} = 0.617 - 1.28 \, \Phi \tag{4.5}$$

where Φ is the porosity.

Reasonable estimation for the irreducible water saturation can be obtained as a function of intergranular porosity and permeability using one of the following empirical models:

$$S_{wi} = \frac{250 \ \Phi^3}{\sqrt{k}} \qquad \text{(Tixier, 1949)} \qquad (4.6)$$

$$S_{wi} = \frac{300 \ \Phi^m}{m^4 \ \sqrt{k}} \qquad \text{(Dumanoir and Coats,1974)} \qquad (4.7)$$

where m is the cementation exponent in Archie's equation.
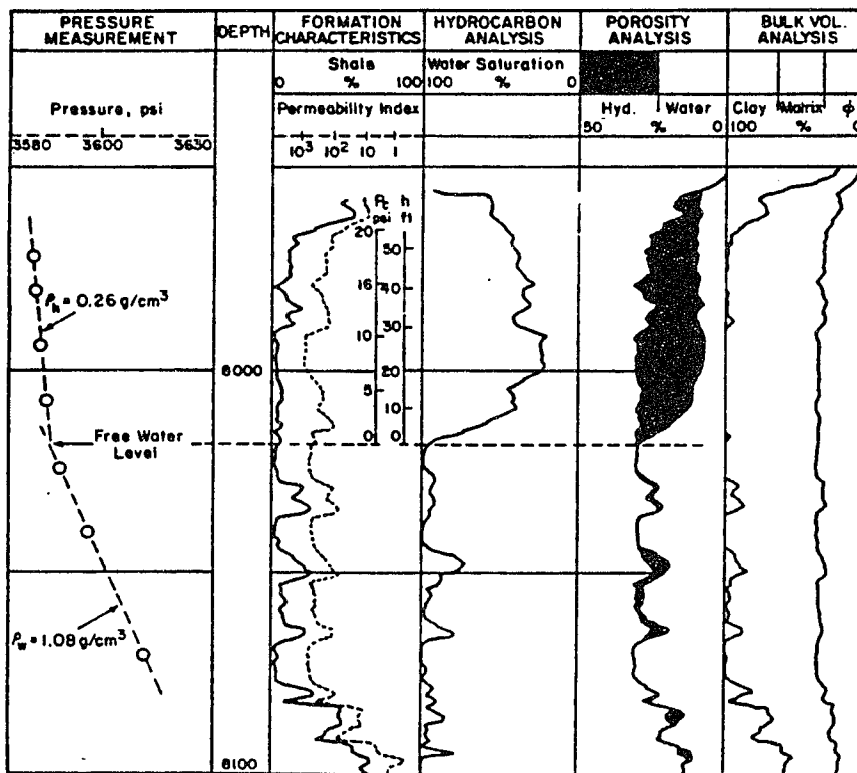
Figure 4.8 Well logs for the Gulf coast field example
[Raymer et al., 1984]
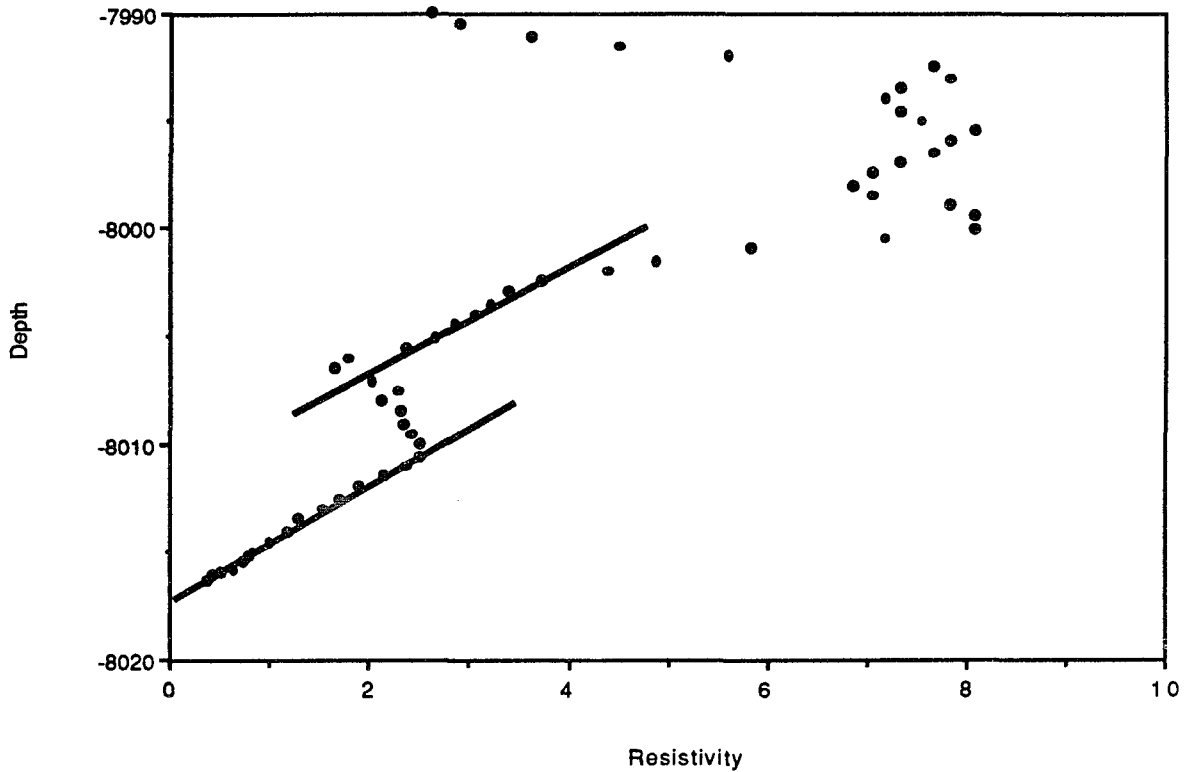
Figure 4.9 Resistivity profile for the Gulf Coast Example.

Figure 4.11 shows the calculated relative permeability for both the drainage and imbibition regimes. Reservoirs either with active water drive or under artificial water flood are usually in an imbibition regime. For such cases, relative permeability curves in the imbibition regime are extremely useful in the reservoir production prediction calculations. In turn, relative permeability curves in the imbibition regime are used to predict the water cut. **Figure 4.12** shows the calculated water cut for the Gulf coast field example in the imbibition regime.
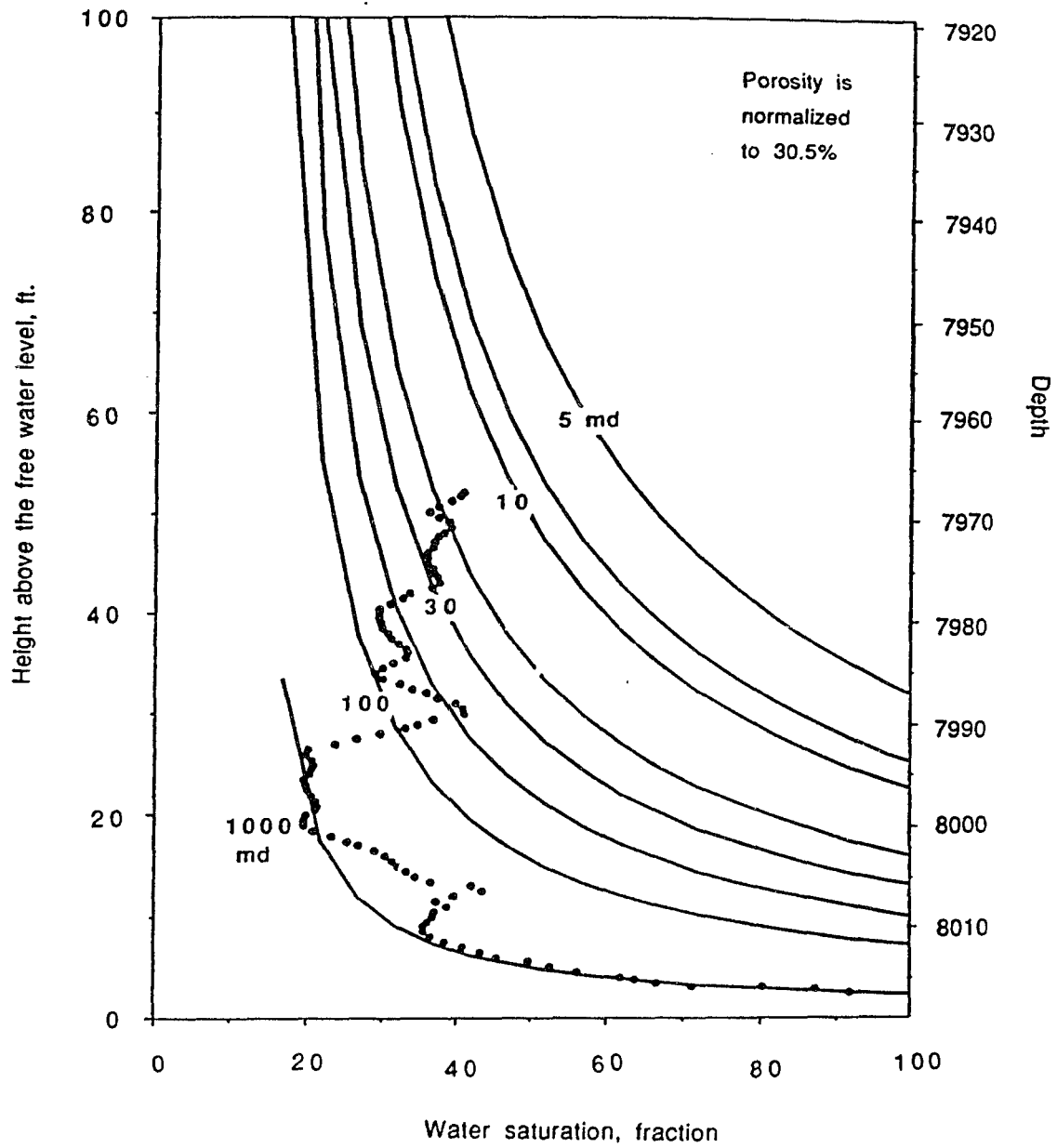
Figure 4.10 Best match for the Gulf coast field example.
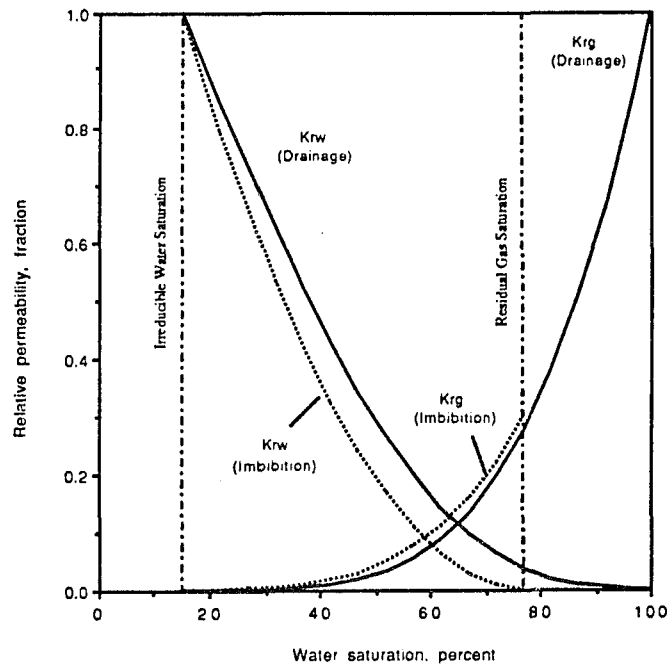
Figure 4.11 Relative permeability curves for the field example in the drainage and imbibition regimes.
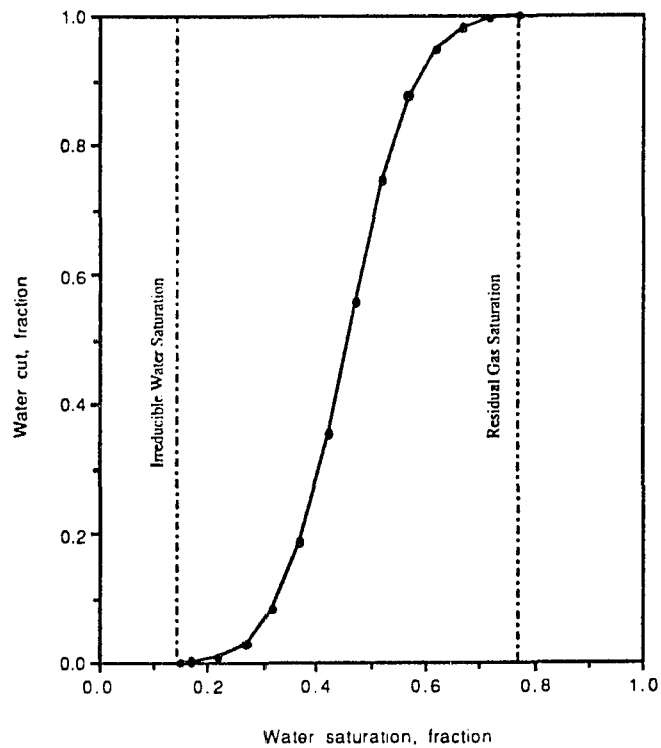
Figure 4.12 Water cut for the Gulf coast field example in the imbibition regime.

4.6 Conclusions

- In the absence of pressure data in the transition zone, generalized capillary pressure curves developed from core samples can be compared to the log derived water saturation profile in the transition zone.

- The capillary pressure-water saturation relationship measured on cores can be used with the J-function to develop generalized capillary pressure type curves typical of the formation under study.

- When matched to the capillary pressure type curves, the log-derived water saturation profile yields reasonable estimates of the absolute permeability, irreducible water saturation, the free water level, and relative capillary pressure characteristics of the reservoir.

- The developed technique can be used in multi-layered as well as homogeneous reservoirs.

CHAPTER V

TIGHT SANDS

5.1 Introduction

Laboratory measurements of relative permeability characteristics of tight sand cores are very complex, time consuming, and of questionable accuracy. A technique that can be used to extrapolate existing core data to cases where such data is absent or not representative of in-situ conditions is of interest. The technique described in the previous chapter is best suited for such cases.

The formulation of the proposed technique for tight gas sand formations requires the development of:

1. A capillary pressure (P_c) to water saturation (S_w) empirical relationship representative of tight sands;

2. Generalized capillary pressure curves for tight sands;

3. A normalization method to reduce the number of variables affecting the log derived water saturation profile; and

4. A water saturation to relative permeability relationship based on the previously developed P_c/S_w relationship.

The core and log data used to develop the proposed relationship are representative of the Cotton Valley, Travis Peak, and Falher formations. Petrophysical data, including the absolute permeability, porosity, and irreducible water saturation, available for nine

core samples are listed in **Table 5.1.** The absolute permeability and porosity of the cores ranged from 30 to 260 microdarcy and from 7.9 to 12.0% respectively.

5.2 Capillary Pressure-Water Saturation Relationship in Tight Sands

An examination of the petrophysical data of available tight sand core samples suggests that the capillary pressure-water saturation relationship can be approximated over most of the saturation range by a linear trend. Thus the P_c/S_w relationship for tight sands can be expressed empirically by:

$$P_c = \frac{a}{(S_w)^b}$$

(5.1)

where:

P_c is the capillary pressure;

S_w is the water saturation in fraction; and

a, b   are coefficients reflecting the formation pore size distribution.

Figure 5.1 shows the P_c/S_w plot for the three core samples representative of the Cotton valley, Travis peak, and Falher formations in log-log scale. The values of the coefficients a, b of Equations 5.1 for these three and the other six tight cores are listed in **Table 5.1.**

Table 5.1 Petrophysical data from tight sand core samples used in this study.

Formation	Core#	K (air) Micro darcy.	Phi %	Swi %	(a) psi	(b)
Cotton Valley	5 A	80	12.0	32.0	35.20	2.304
Cotton Valley	10 B	194	8.20	10.5	9.030	2.167
Cotton Valley	7 A	97	12.5	23.0	35.69	2.132
Cotton Valley	8 A	65	8.80	30.0	11.93	3.400
Cotton Valley	11 A	49	9.00	20.0	21.72	2.348
Cotton Valley	12 A	51	8.50	20.5	29.58	2.236
Cotton Valley	13 A	30	7.90	21.5	43.27	1.909
Travis Peak	17 A	260	9.90	10.5	2.574	2.647
Travis peak	NA	100	9.80	16.0	4.264	1.468
Falher SS.	NA	198	9.40	30.0	19.65	2.623
Falher SS.	NA	136	9.40	32.0	26.16	2.385

$y = 2.2008 - 2.1675x \quad R^2 = 0.993$

$y = 1.4503 - 1.4687x \quad R^2 = 0.994$

$y = 3.2231 - 2.4384x \quad R^2 = 0.992$

▲ Cotton Valley-10
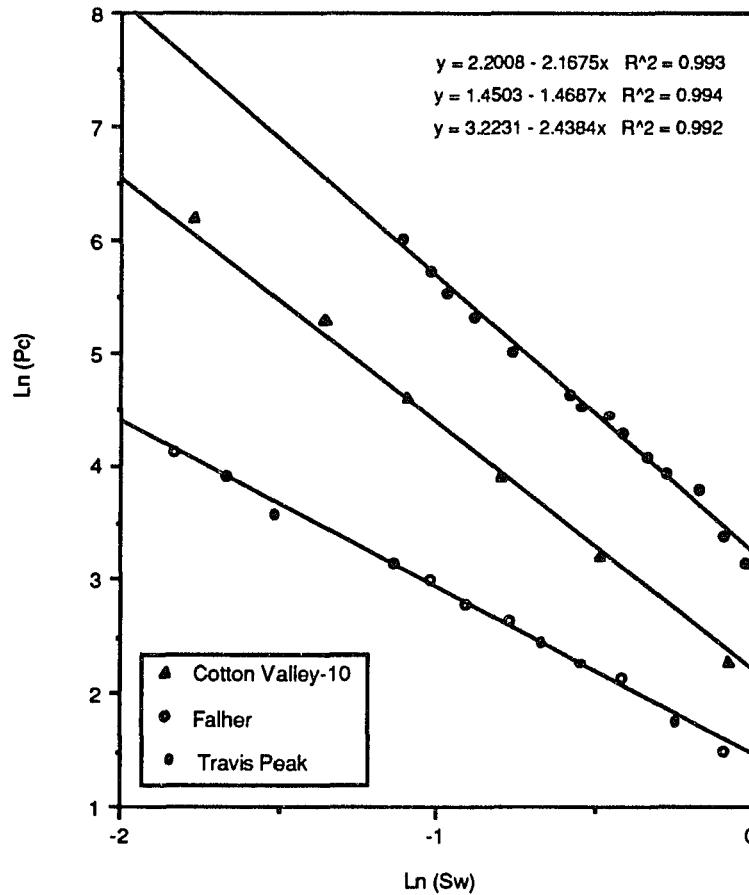
◉ Falher

● Travis Peak

Ln (Pc)

Ln (Sw)

Figure 5.1 Logarithmic P_c vs. S_w plot for three core samples representative of the Cotton Valley, Travis Peak, and Falher tight sands.

5.3 Relative Permeability-Water Saturation Relationship in Tight Sands

5.3.1 Drainage Regime

The empirical expression of P_c/S_w described by Equation 5.1 can be used to solve the integral part of Purcell's model (Equations 2.13 and 2.14), Burdine's model (Equations 2.16 and 2.17), or Wyllie's model (Equations 2.41 and 2.42) and develop much simpler equations to calculate the relative permeability curves for tight sands. Using Wyllie's model, the final expression for the wetting and non-wetting phase are:

$$K_{rwt} = \left\{\frac{(S_w - S_{wi})}{(1 - S_{wi})}\right\}^2 \left\{\frac{(S_w^c - S_{wi}^c)}{1 - S_{wi}^c}\right\}$$

(5.2)

for the wetting phase; and

$$K_{mwt} = \left\{\frac{(1 - S_w)}{(1 - S_{wi})}\right\}^2 \left\{\frac{(1 - S_w^c)}{(1 - S_{wi}^c)}\right\}$$

(5.3)

for the non-wetting phase.

where:

$c = 2b + 1$

b is the slope of the straight line;

S_{wi} is the irreducible wetting phase saturation;

K_{rwt} is the relative permeability for the wetting phase; and

K_{mwt} is the relative permeability for the non-wetting phase.

It is noteworthy, as shown by Corey [1954], that for tight sands, plotting the wetting phase saturation versus $(1/P_c^2)$ does not yield a straight line relationship.

Figure 5.2 shows the deviation of the experimentally determined relative permeability data for tight sand cores from Corey's type curves.
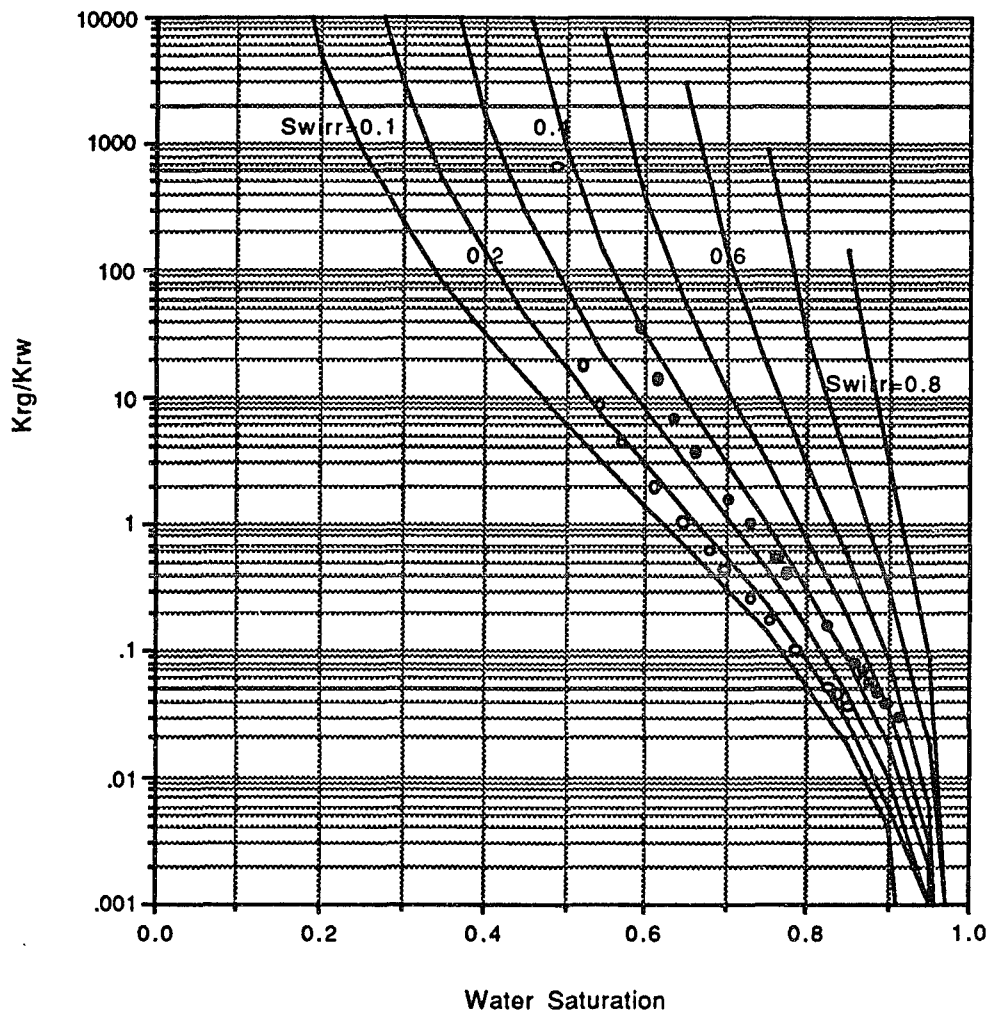
Figure 5.2 Corey's model for relative permeability mismatches the experimental data measured on tight sand cores.

5.3.2 Imbibition Regime

Naar's model expressed by Equation 2.46 to calculate the relative permeability in the imbibition regime requires knowledge of the P_c/S_w relationship in order to be solved. Again, Equation 5.1 is substituted in Equation 2.46 to develop a much easier equation that calculates the relative permeability in the imbibition direction. The final form of the equation is:

$$K_{rw} = \frac{1}{2K} \left\{ \Phi^* S_w^* \right\}^3 \left\{ \frac{\sigma S_w^b}{a} \right\}^2 \tag{5.4}$$

Appendices A and B detail the analytical derivation of Equations 5.2, 5.3, and 5.4.

Figure 5.3 shows the values of the J-function calculated using the capillary pressure data available for tight sand core samples. In these calculations, values of 74 dyne/cm. and zero degrees were used for the interfacial tension, σ, and the contact angle, θ, respectively. When the J-function is plotted versus water saturation on log-log scale, a linear trend emerges as shown by **Figure 5.4**. The best fit of the data results in a correlation coefficient of 0.908 and is represented by the following equation:

$$J = \frac{\alpha}{S_w^\beta} \tag{5.5}$$

where:

$\alpha = 0.039$

$\beta = 2.308$

Equation 5.5 is of the same form as Equation 5.1, as should be expected.

Combining Equations 5.5 and the J-function equation (Equation 2.52) gives:

$$P_c = \frac{\alpha \ \sigma \ \cos \theta}{S_w^\beta \ \sqrt{\frac{K}{\Phi}}} \tag{5.6}$$

A practical presentation of type curves is in terms of height above the free water level, h_{FWL}, which is related to the capillary pressure and water and gas densities by Equation 4.4.

Combining Equations 5.6 and 4.4 and using practical units yields:

$$h_{FWL} = 10.66 \frac{\alpha \, \sigma \, \cos \theta}{S_w^\beta \, (\rho_w - \rho_g) \, \sqrt{\dfrac{K}{\Phi}}}$$

(5.7)

where:

h_{FWL} height above the free water level, ft;

σ interfacial tension, dyne/cm;

θ contact angle, degrees;

S_w water saturation, fraction;

α, β coefficients;

K absolute permeability, md;

Φ porosity, fraction; and

ρ_w, ρ_g water and gas densities, gm/cm^3.
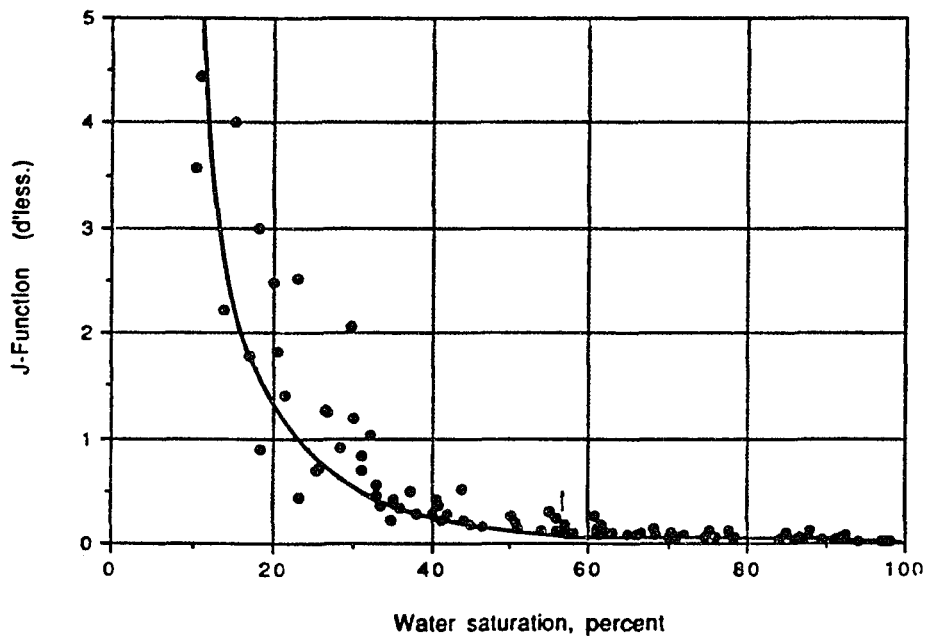
Figure 5.3 Leverett's J-function for tight sands core samples from Cotton Valley, Travis Peak, and Falher formations.
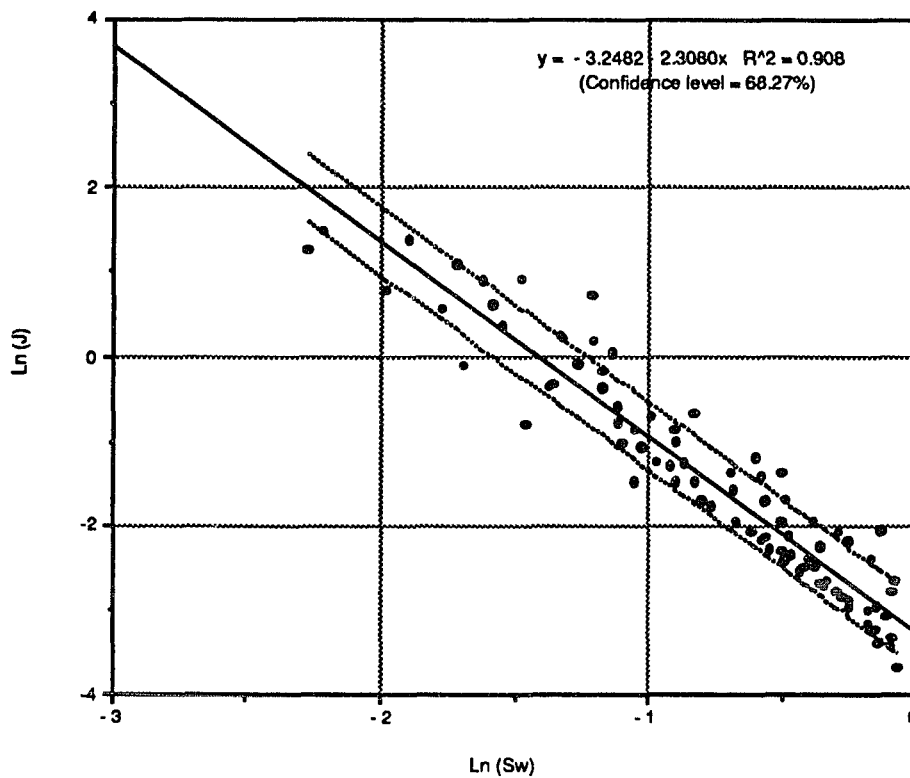
Figure 5.4 Logarithmic plot of the J-function data displayed in **Figure 5.3**.

Figure 5.5 shows an example of type curves generated using Equations 5.7 and the following parameters:

$\alpha = 0.039$

$\beta = 2.308$

$\sigma = 74$ dyne/cm

$\theta = 0.0$ degrees; and

$\Phi = 0.15$

Each curve in the type curves represents a specific absolute permeability value. Each curve is characterized by an irreducible water saturation value derived from the
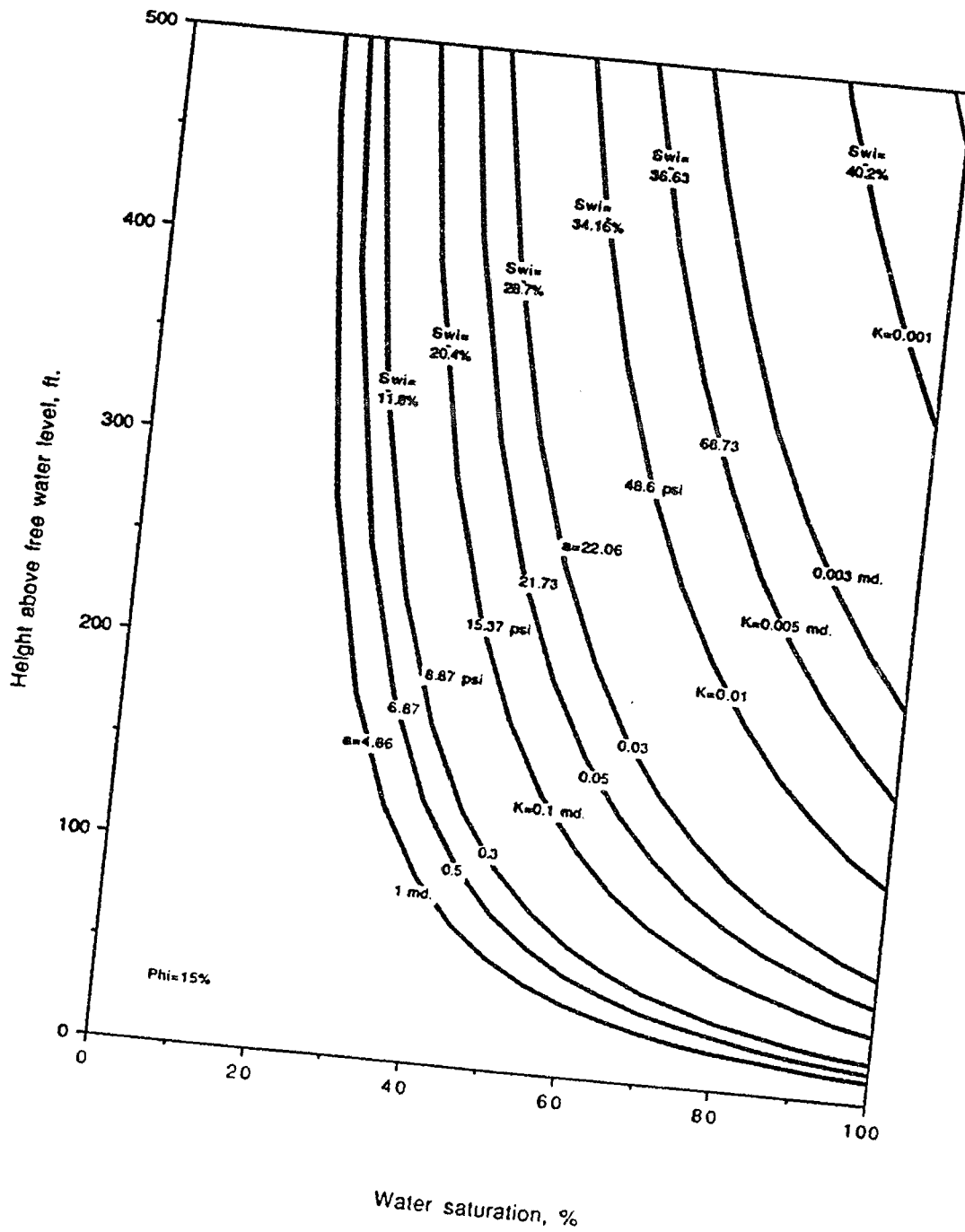
Figure 5.5 Example of capillary pressure type curves.

correlation of **Figure 5.6** obtained for tight sand and core samples studied. Each curve

is also characterized by the value of coefficient a in Equation 5.1. Using the

approximation of b = β, Equations 5.1 and 5.6 can be solved for the coefficient a as:

$$a = \frac{\alpha \ \sigma \ \cos \theta}{\sqrt{\dfrac{K}{\Phi}}}$$

(5.8)
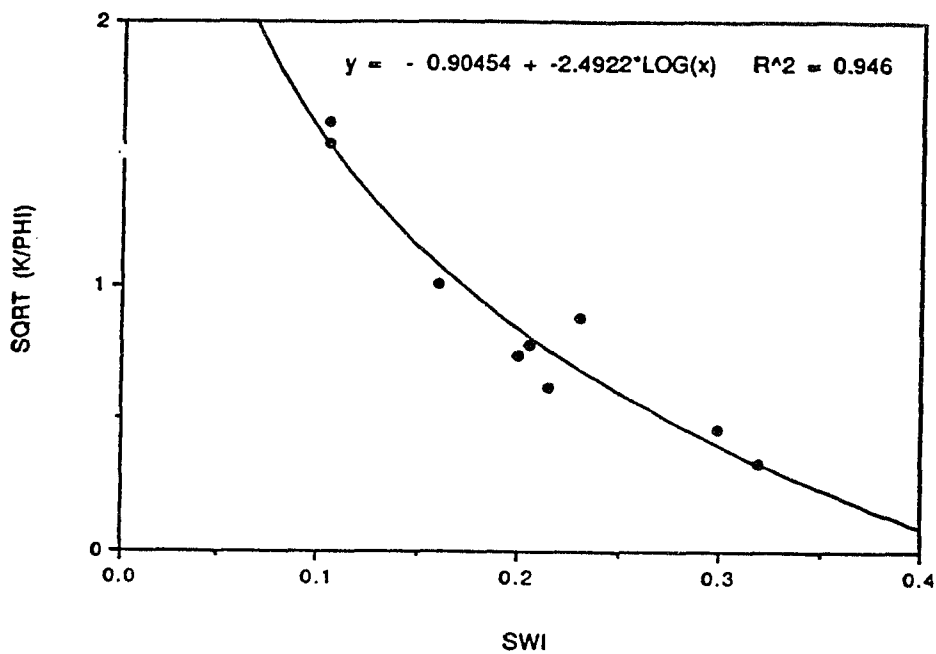
Figure 5.6 Correlation between $\sqrt{\dfrac{K}{\Phi}}$ and Swi for tight sand core samples from Cotton
Valley, Travis Peak, and Falher formations.

5.4   Field Examples

5.4.1 Homogeneous Transition Zone

5.4.1.1   Field Example 1

The well logs obtained in a tight gas-bearing sand formation from a well in Colorado are shown in **Figure 5.7**. **Figure 5.8** shows the porosity, water saturation, and normalized water saturation profiles. The normalization to the average porosity of 7.6% results in a smoother saturation profile. Using the average J-function for tight sands, capillary pressure type curves, similar to those represented in **Figure 5.5**, are generated for average reservoir porosity of 7.6% and other reservoir conditions. Capillary pressure is converted into height above the free water level, h_{FWL}, using the equation:

$$H \text{ (feet)} = 2.18 \ P_c \text{ (psi)} \tag{5.9}$$

The constant 2.18 is calculated using the water salinity and the gas gravity at reservoir conditions.

For the match, the normalized water saturation profile is laid and vertically shifted over the capillary pressure type curves untill a match is found as shown in **Figure 5.9**. The match reveals that over approximately 150 feet of the reservoir, the permeability varies within a narrow range with no distinguished zoning. The following match parameters can be read directly:

Average permeability = 0.08 md.

Irreducible water saturation = 17%

a = 13 psi

Free water level lies at 7,922 ft.
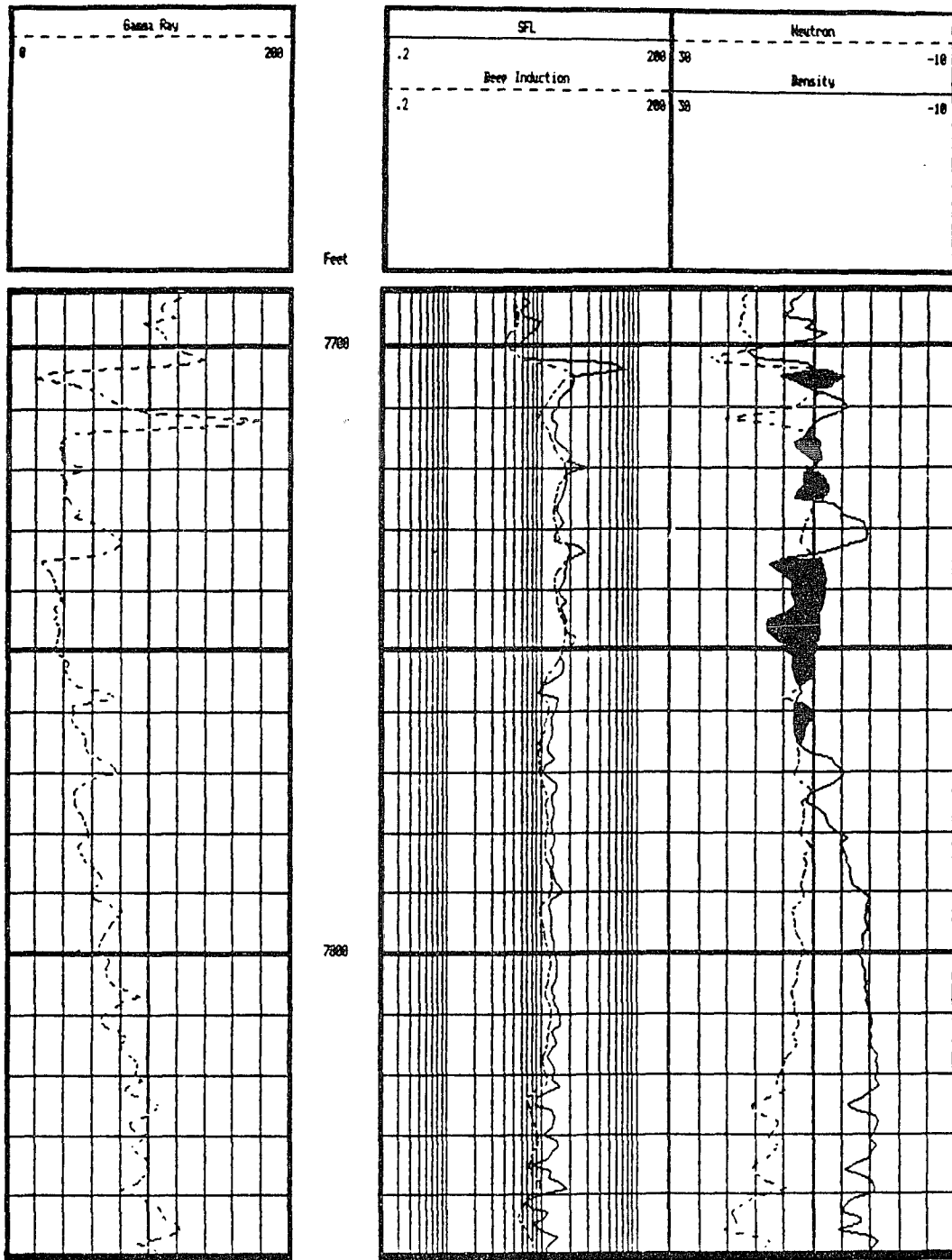
Figure 5.7 Well logs for field example 1

Water Saturation, Fraction

Figure 5.8 Water saturation profile for field example 1.
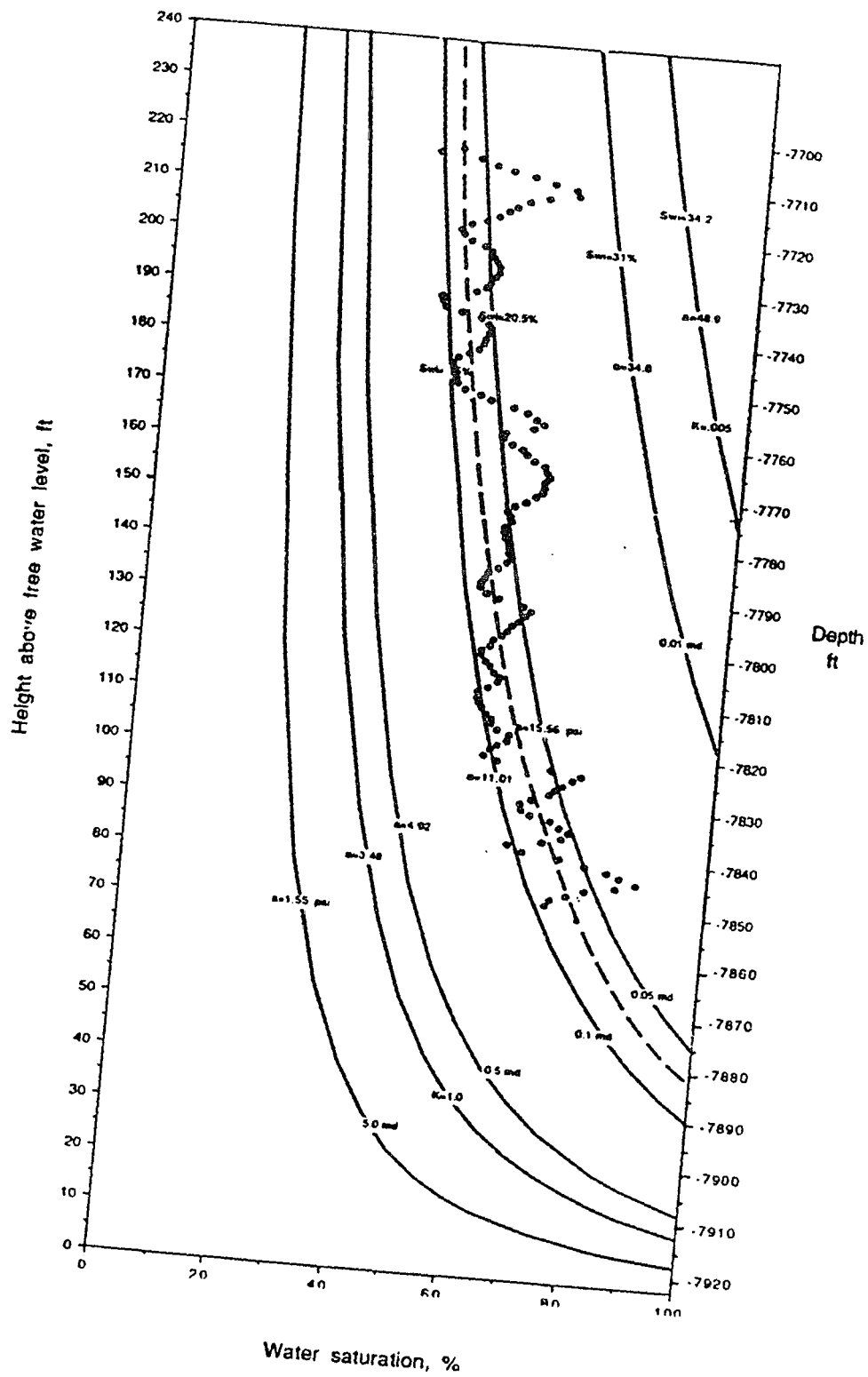
Figure 5.9 Matching normalized water saturation profile to capillary pressure type curves for field example 1.

5.4.2 Multi-Layer Transition Zone

5.4.2.1 Field Example 2

The second field example represents a tight gas bearing sand. **Figure 5.10** shows the well log data and **Figure 5.11** shows the porosity and the calculated water saturation profile. Normalized water saturation profile is calculated for a reference porosity of 7.6% and is also represented in **Figure 5.11**. **Figure 5.12** shows the match obtained when comparing the capillary pressure type curves generated for the same reservoir conditions with the normalized water saturation profile. Unlike example 1, the transition zone of this sand seems to be composed of three strata of distinct properties sharing a common free water level at a depth of 8,130 ft. The match parameters for the three strata are given in **Table 5.2** below:

Table 5.2 Matching parameters for field example 2

	Strata A	Strata B	Strata C
K, md.	0.3	0.08	0.05
Swi, %	6.0	15.0	19.0
a, psi	5.6	10.9	13.8

Gamma Ray

0   200

SFL

.2   200 30   -10

Deep Induction

.2   200 30   -10

Neutron

Density

Feet

8100
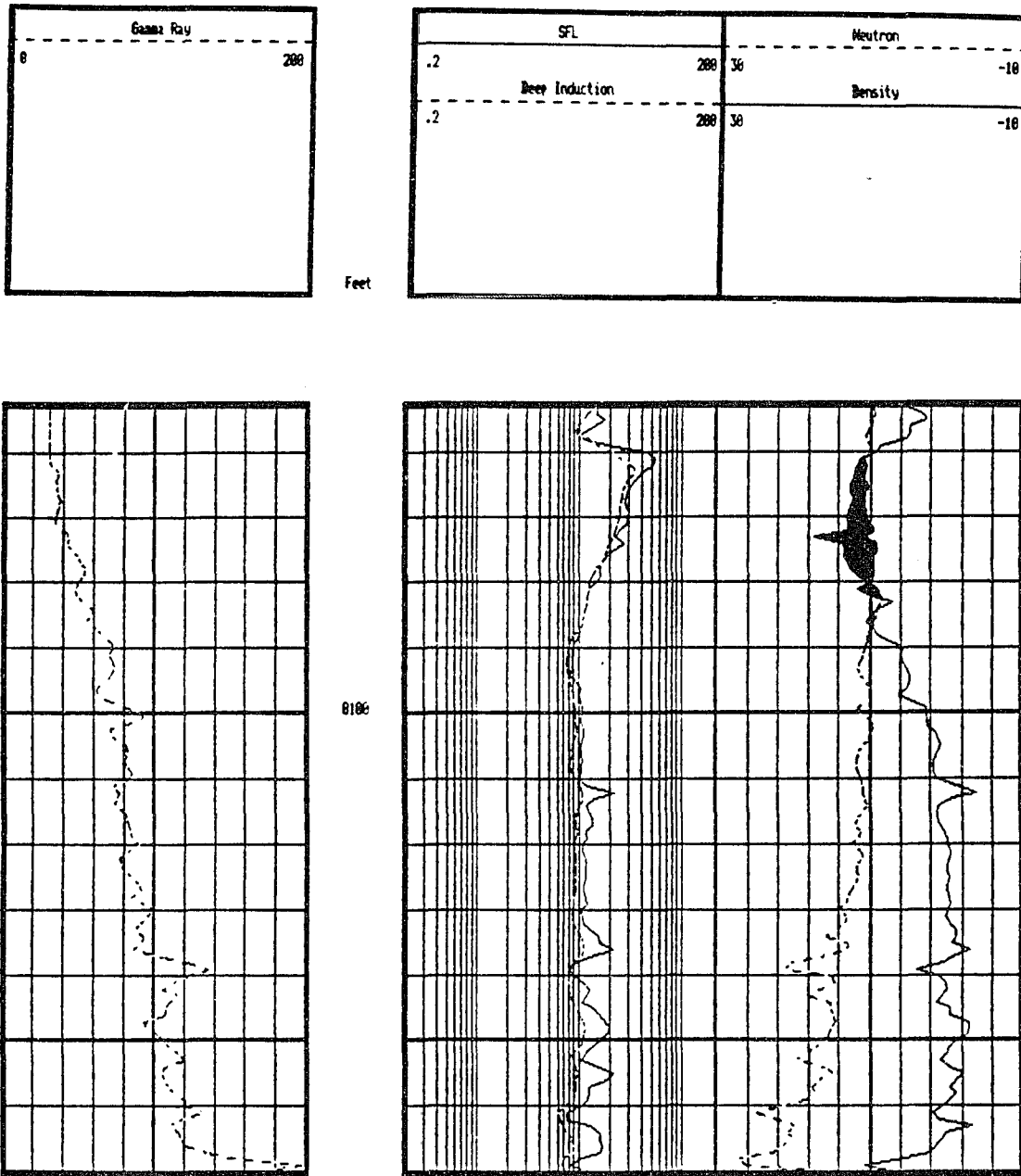
Figure 5.10 Well logs for field example 2.

Water saturation, fraction
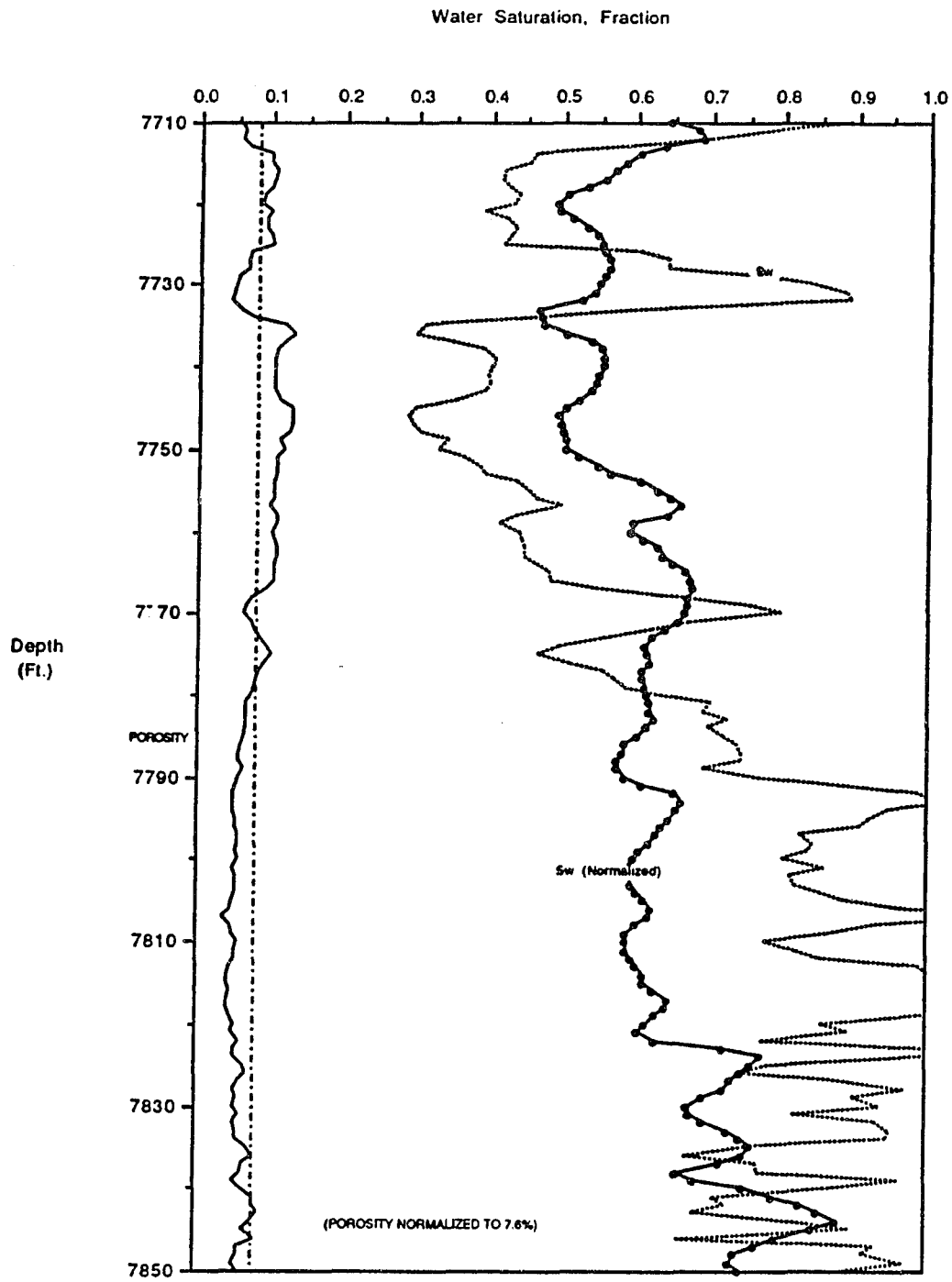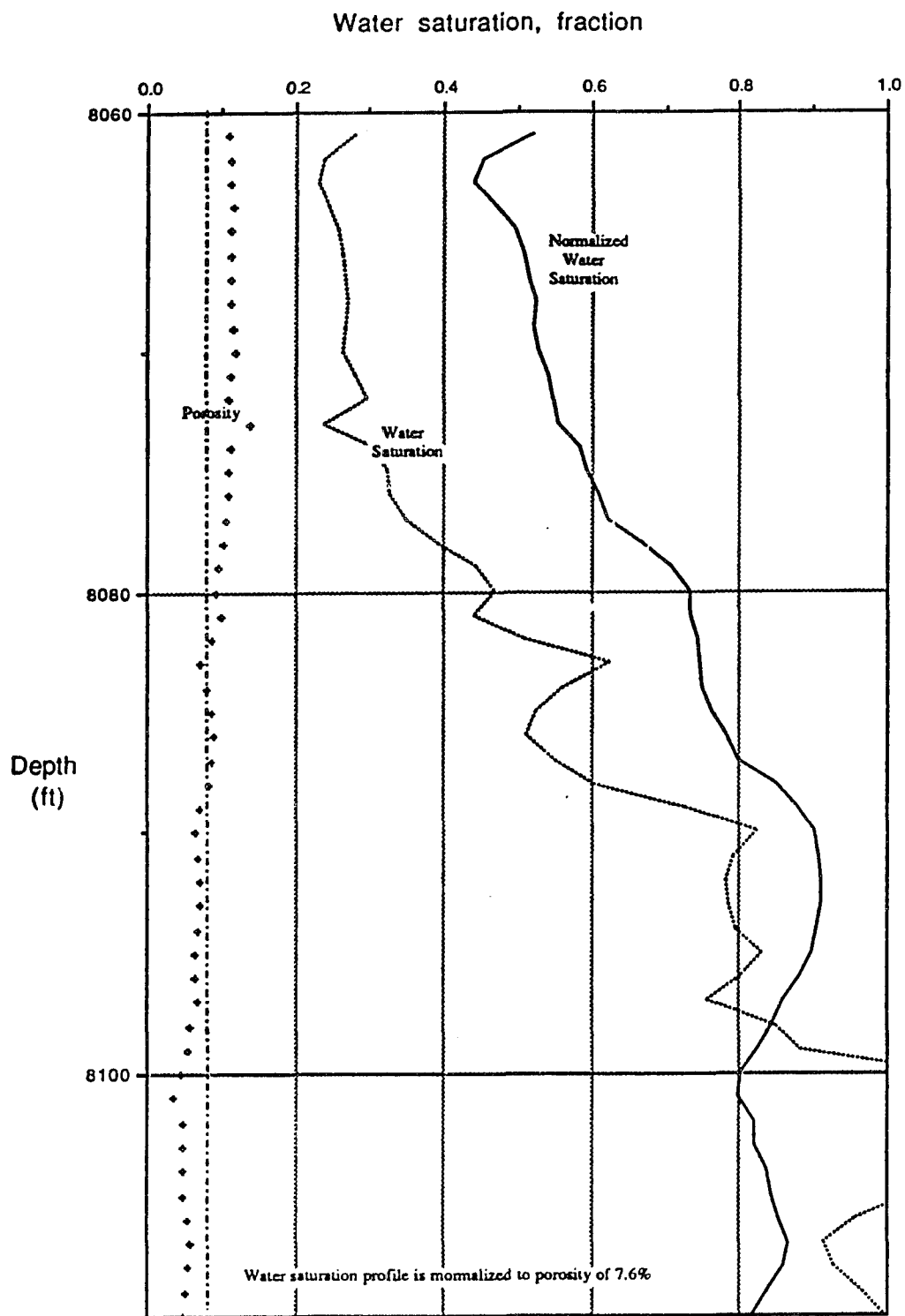

Figure 5.11 Water saturation profile for field example 2.
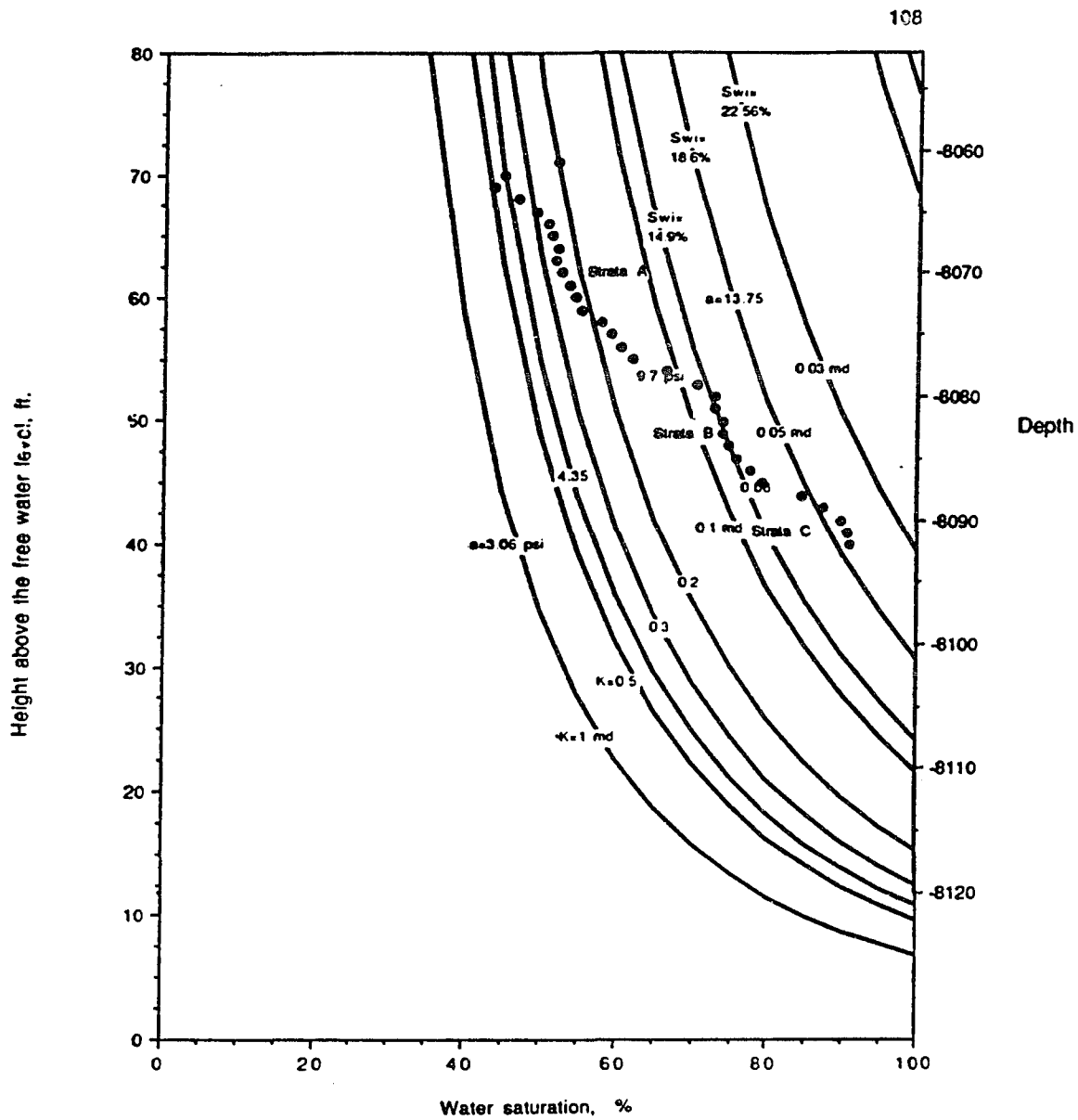
Figure 5.12 Best match of normalized water saturation profile to capillary pressure type curves for field example 2.

5.4.2.2 Field Example 3

The recorded logs for a well in Wyoming, are shown in **Figure 5.13**. The calculated water saturation is normalized to an average porosity of 15.02 % over the transition zone and is shown in **Figure 5.14**. Type curves are generated for the same reservoir conditions and are converted to height above the free water level using the equation:

$$H \text{ (feet)} = 2.665 \; P_c \text{ (psi)} \tag{5.10}$$
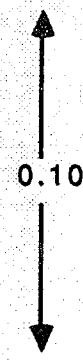
The match shown in **Figure 5.15** shows that the transition zone seems to be composed of at least three strata of different pore structures X, Y, Z. The three strata share a free water level at a depth of 9,126 ft. The match parameters are listed in **Table 5.3** below:

Table 5.2 Matching parameters for field example 2

	Strata X	Strata Y	Strata Z
K, md.	0.05	0.10	0.08
Swi, %	25.0	20.0	22.0
a, psi	21.7	15.4	18.3

Table 5.4. shows a comparison between the permeability measured on cores from strata Y and the estimated permeability through the matching technique. Cores of strata Y shows permeabilities range from 0.08 to 0.16 md. and averaging 0.108 This values agree extremely well with the match permeability.

Table 5.4 Comparison between measured and estimated permeabilities for
strata Y.

Depth (feet)	K air (core) md.	K air (match) md.
9104.5	0.11	
9105.5	0.13	
6106.0	0.10	
9107.0	0.09	
9108.5	0.08	0.10
9109.0	0.10	
9110.5	0.16	
9111.0	0.09	
9112.0	0.10	
9113.0	0.10	

Since the well logs indicate that sand section is reasonably clean, Tixier's method (based on the resistivity gradient) can be used to estimate the permeability of the transition zone. **Figure 5.16** shows the plot of the resistivity gradient, and the calculated resistivity gradient basic factor, a, which is used to calculate the permeability. Tixier's method results in an average permeability of 0.05 md. for the three strata. This value is also in agreement with the match values.

As an example, the relative permeability curves under both drainage and imbibition conditions are calculated using Equations 5.2, 5.3, and 5.4. The resulting curves are shown in **Figure 5.17**.
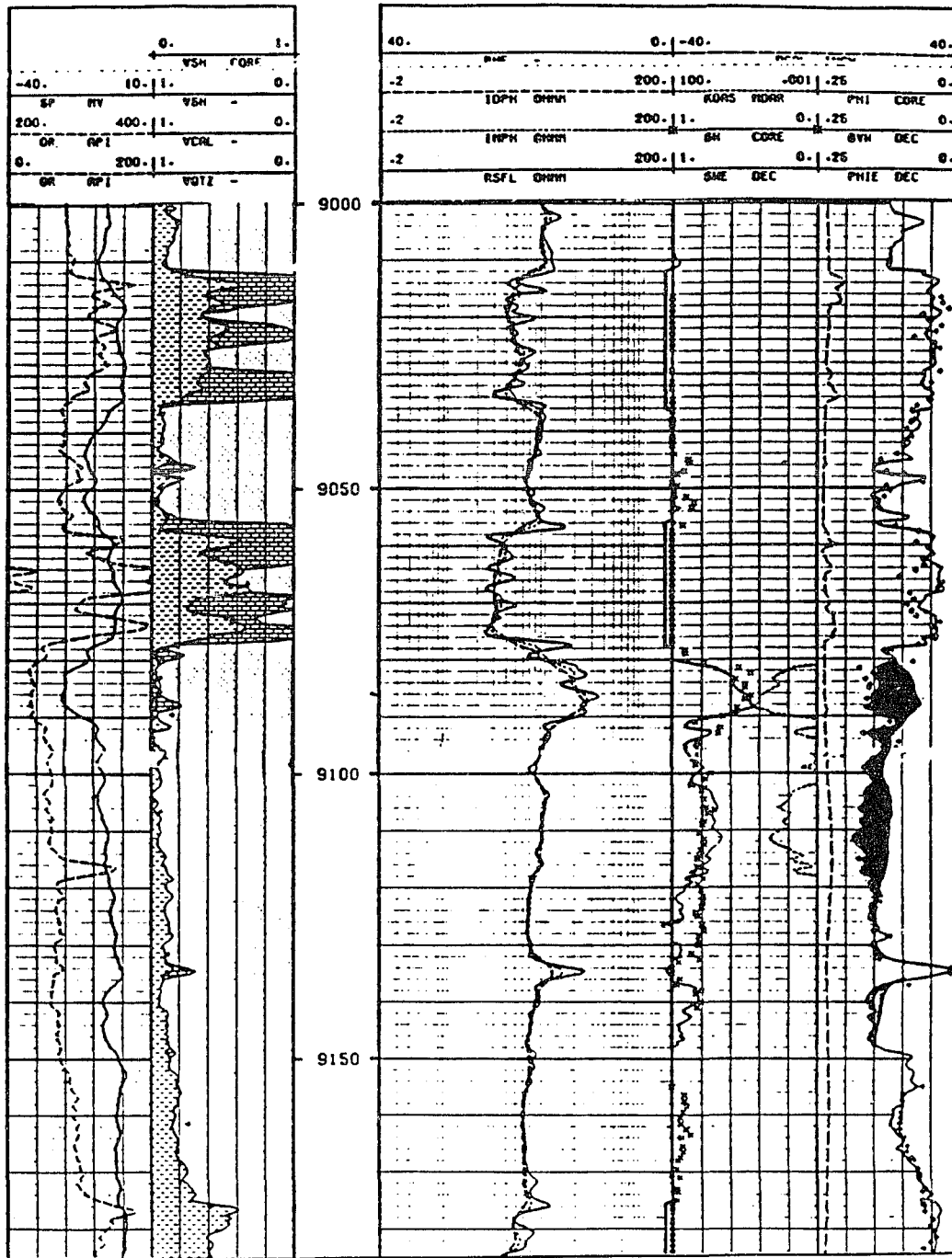
Figure 5.13 Well logs for field example 3.
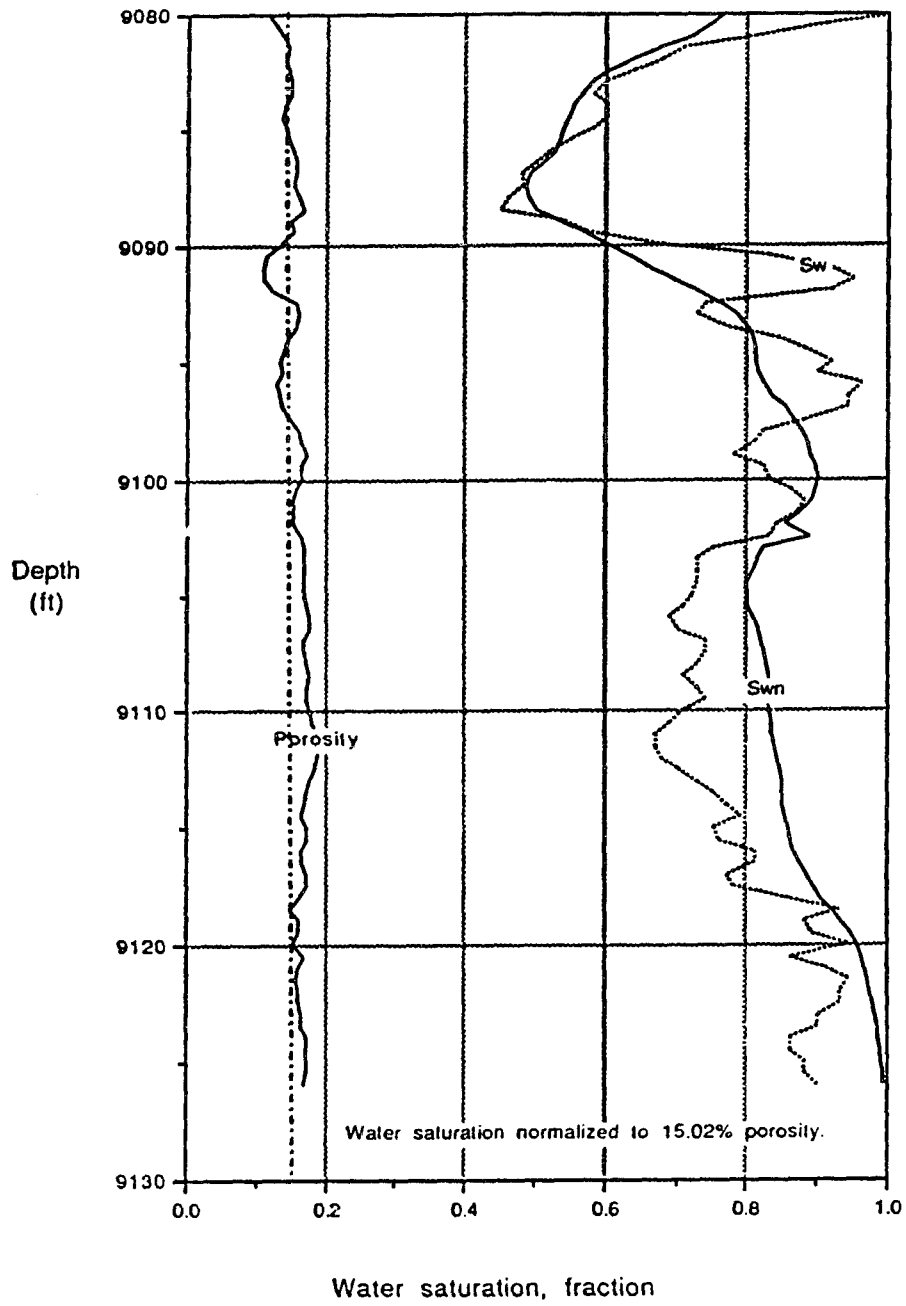
Figure 5.14 Water saturation profile for field example 3.
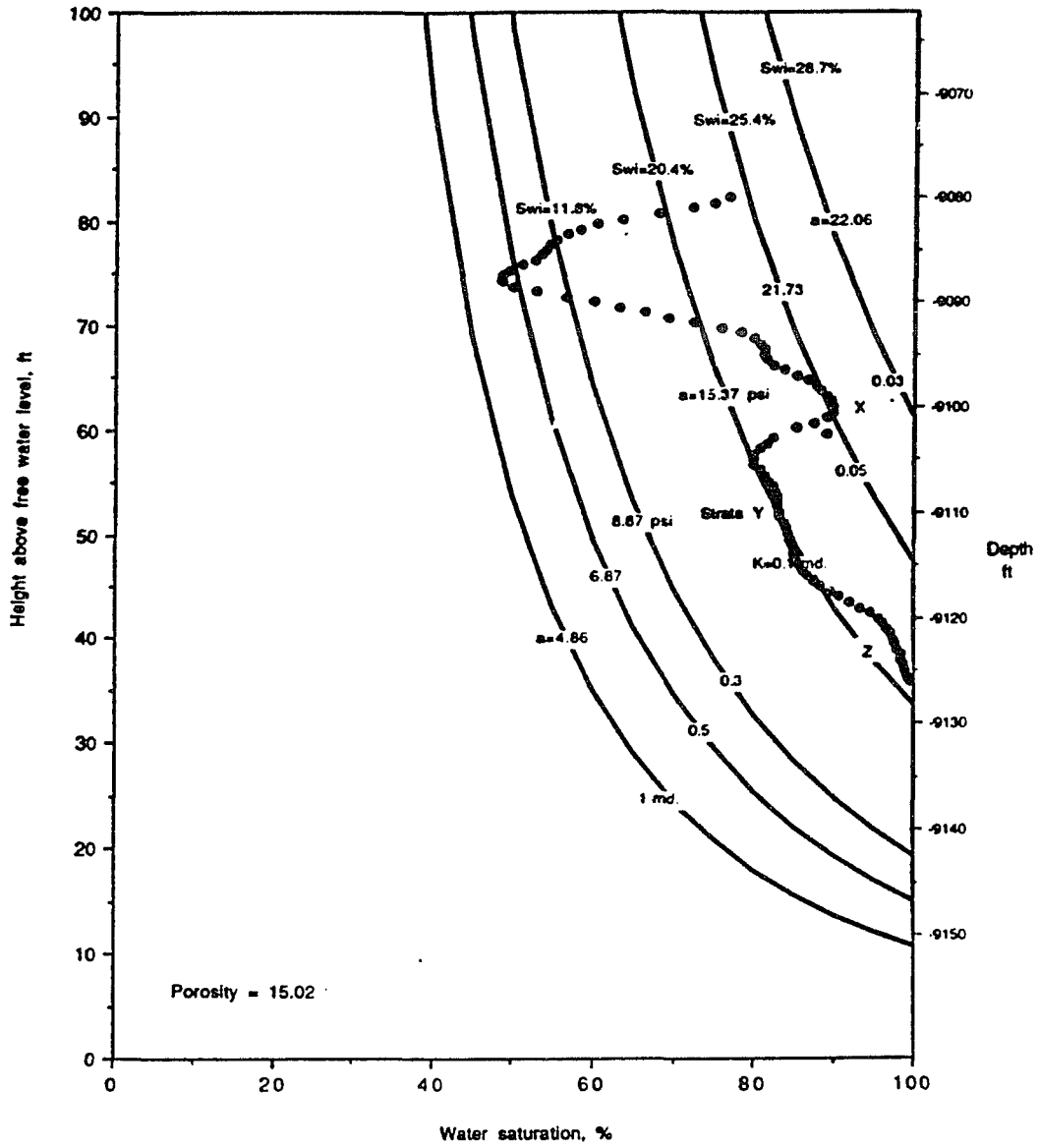
Figure 5.15 Best match for field example 3.
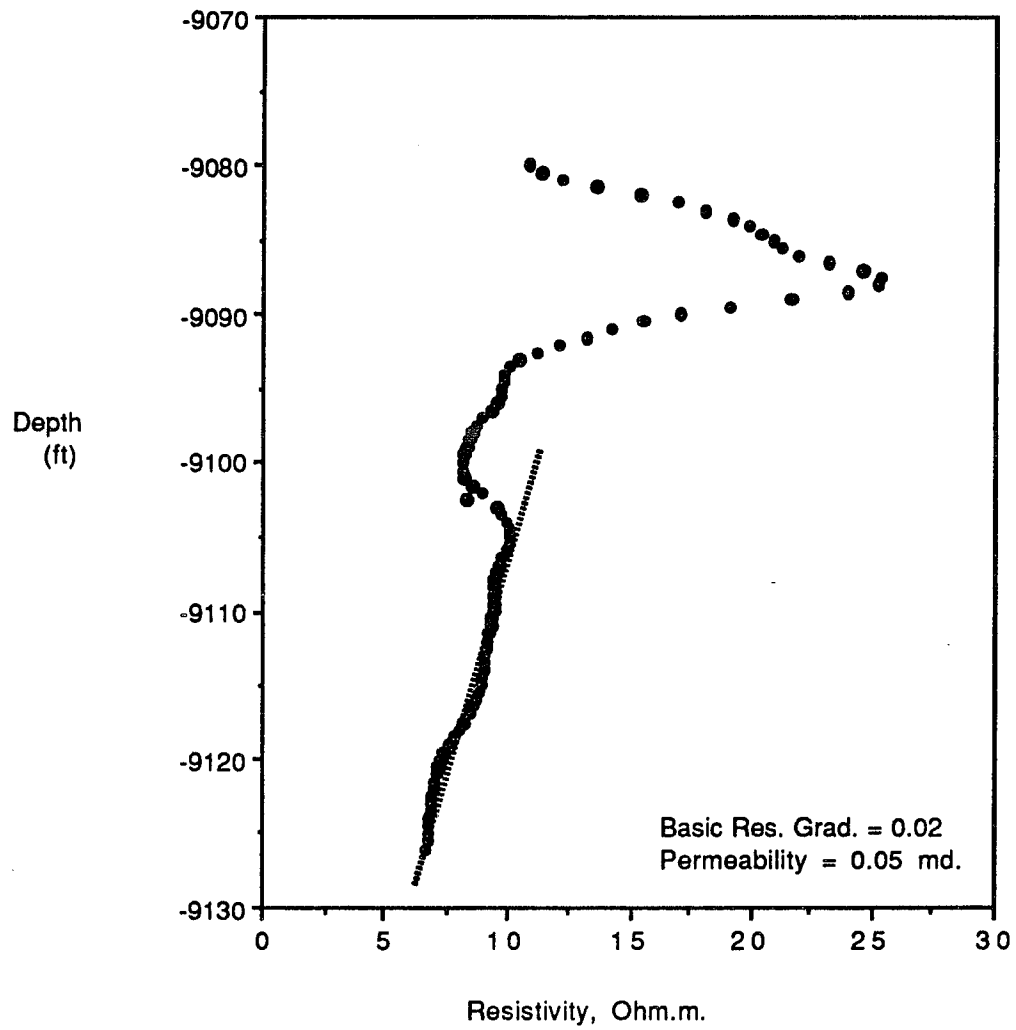
Figure 5.16 Tixier's method to estimate absolute permeability for field example 3.
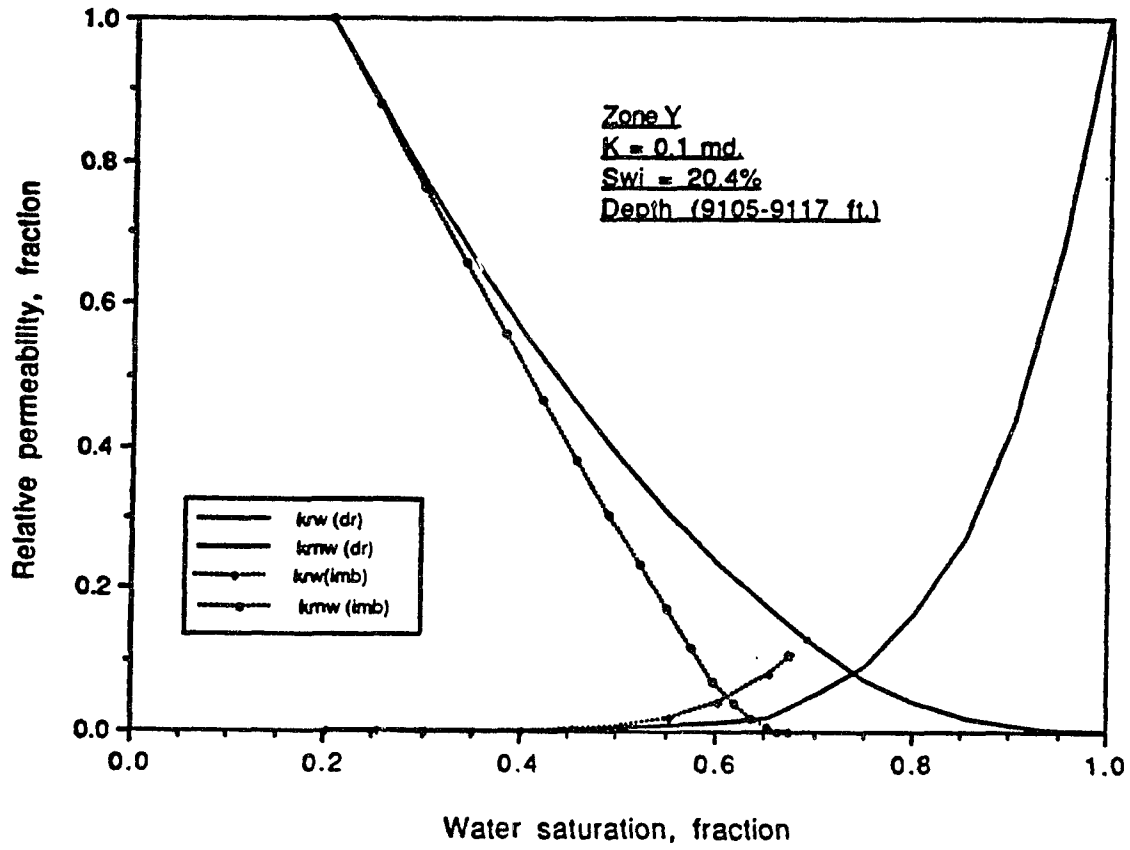
Figure 5.17 Calculated relative permeability curves for strata Y of field example 3.

5.5 Free Water Level Estimation Using Resistivity Gradient in Tight Sands.
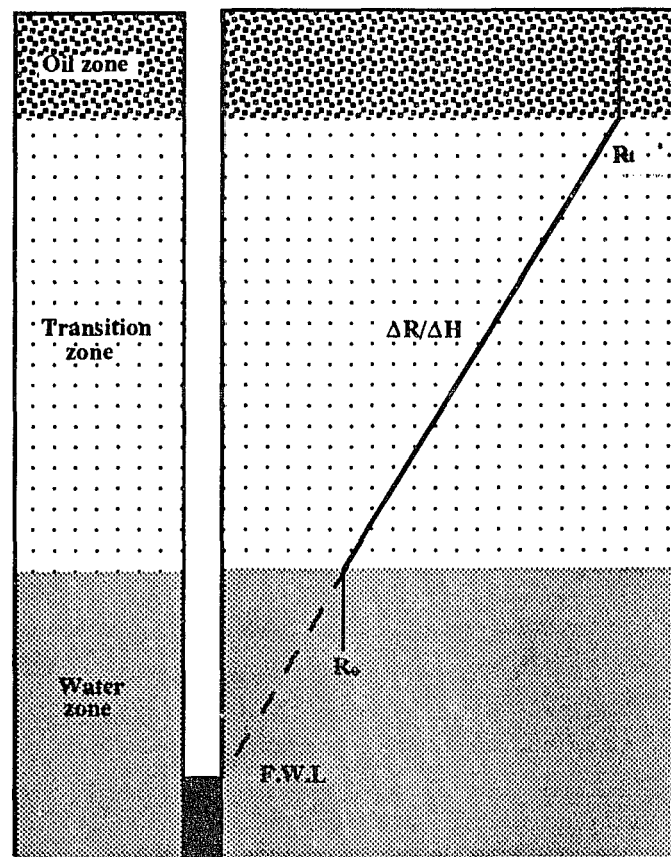
Figure 5.18 Schematic showing free water level estimation using resistivity gradient in tight sands.

For tight sands, the capillary pressure/water saturation relationship is expressed by Equation 5.1 as:

$$P_c = \frac{a}{(S_w)^b} \qquad (5.1)$$

Table 5.1 shows that the exponent b for the nine tight sand core samples studied ranges between 1.46 and 3.4.

Archie's equation to determine the water saturation states:

$$S_w^2 = \frac{F\ R_w}{R_t} \qquad (5.11)$$

Where:

F   is the formation resistivity factor;

R_w is the formation water resistivity; and

R_t is the true formation resistivity.

Assuming the value b = 2 is a representative value for the tight sands, the water saturation term in equation 5.1 is substituted into Equation 5.11. Solving for the capillary pressure:

$$P_c = \frac{a}{F\,R_w}\ R_t \qquad (5.12)$$

For a homogeneous reservoir with the same formation water along the transition zone, the formation factor, F, the cementation exponent, a, and the formation water resistivity, R_w, are constants. Consequently, Equation 5.12 reveals a linear relationship between the capillary pressure and the resistivity in the transition zone of a homogeneous tight sand reservoir.

Capillary pressure can be expressed as a function of the height above the free water level as:

$$H\ (ft.) = \frac{2.3}{(\rho_w - \rho_h)}\ P_c \qquad (5.13)$$

Where:

P_c Capillary pressure (psi)

H Height above free water level (ft.)

ρ_w Density of water (gm. / cc.)

ρ_h Density of hydrocarbon (gm. / cc.)

Now, incorporating equations 5.12 with Equation 5.13 yields:

$$H \text{ (ft.)} = \frac{2.3 \ a}{F \ R_w \ (\rho_w - \rho_h)} \ R_t \qquad (5.14)$$

For constant fluid densities in the transition zone, Equation 5.14 will take the form:

$$H = C \ R_t \qquad (5.15)$$

Where:

C   is constant for a homogeneous reservoir.

Equation 5.15 indicates the linear resistivity gradient over the transition zone. Also the equation indicates that extrapolating the resistivity line untill it intersects with the depth or the capillary pressure axis, $(R_t = 0)$, would define the free water level $(H = 0)$.

Since field example 1 shows a homogeneous transition zone, this observation is applied to its resistivity profile to insure its applicability. Figure 5.19 shows the resistivity profile read from the well logs. The resistivity gradient is established and is extended untill it intersects with the depth axis $(R_t = 0)$. The intersection point reads a free water level at depth 7922 which agrees with the free water level determined through the matching technique.
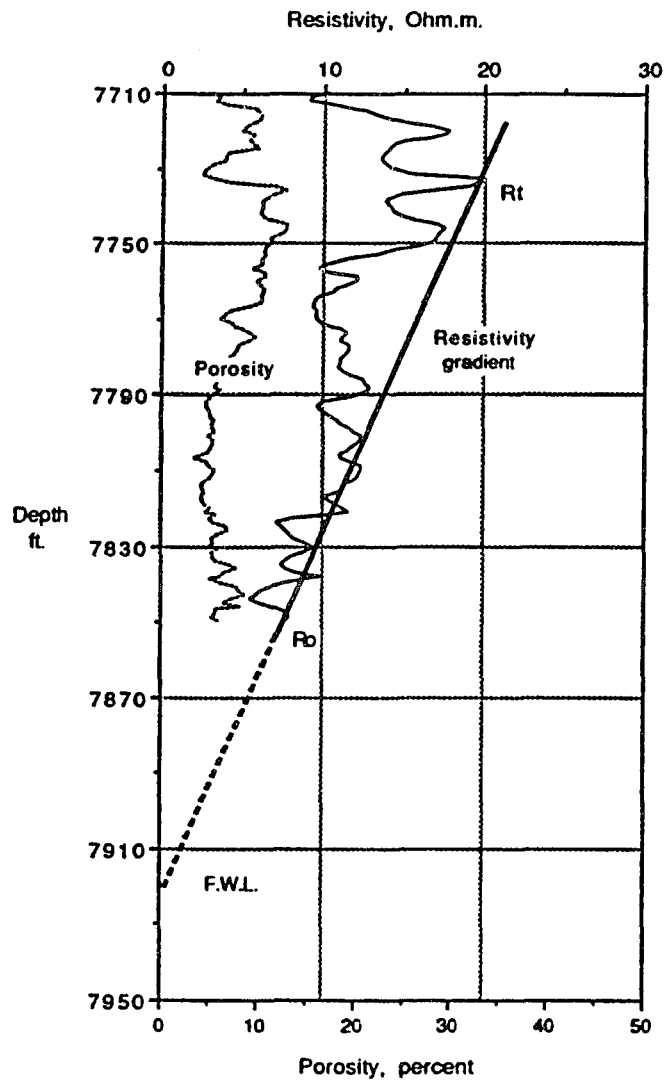
Figure 5.19 Estimation of the free water level using the resistivity gradient for field example 1.

5.6 Technique Limitations

1. The development of type curves is based on petrophysical parameters derived from curve fitting of core data. The parameters used in this study are the average of nine cores representing Cotton Valley, Travis Peak, and Falher formations. The addition of more data

when available should improve the statistical representation of the match results.

2.   The petrophysical models discussed in this chapter should only be used in the analysis of the other tight formations in which petrophysical similarity is demonstrated.

3.   During the course of applying the technique to different reservoirs, it was found that 15 to 20 feet of homogeneous formations are necessary for fitting the saturation profile on the type curves in the case of a layered transition zone. The homogeneous strata can be identified with Gamma Ray log, Microlog, Microlaterolog, or Caliper log.

5.7   Conclusions

■   A capillary pressure-water saturation empirical relationship was developed for tight sand formations. This relationship was used to adapt available relative permeability models to the case of tight sands.

■   The capillary pressure-water saturation relationship was used in conjunction with the J-function to develop generalized capillary pressure type curves typical of tight sand formations.

■   When matched to the capillary pressure type curves, a log-derived water saturation profile yields reasonable estimates of the absolute permeability, irreducible water saturation, the free water level, and relative permeability characteristics.

■ The developed technique can be used in homogeneous as well as multi-layered reservoirs.

■ The linear resistivity gradient in homogeneous tight sand reservoirs can be used directly to determine the free water level.

CHAPTER VI

CONCLUSIONS & RECOMMENDATIONS

6.1 Conclusions

The research work presented in this dissertation was focused on the determination of in-situ capillary pressure and relative permeability. The importance of this is that the measurements of such properties in the laboratory is time consuming and, at times, impossible (e.g.: cases reported for tight sands). The general conclusions of this dissertations may be summarized as follows:

1. Experimental simulation showes that correlating the well log-derived water saturation profile to the pressure data in the transition zone results in a capillary pressure/water saturation (P_c/S_w) curve. The capillary pressure curve can then be used to generate relative permeability curves specific to the formation under study.

2. Experimental results show a linear resistivity gradient under drainage conditions, while a curved profile is observed under imbibition conditions. This observation can be used to determine the reservoir's saturation history, which can help to formulate an understanding of the geological history.

3.   The linear resistivity gradient observed under the drainage regime is used to derive a formula that is used to calculate the in-situ capillary pressure curve for the transition zone using data from well logs.

4.   Brine Imbibition experiments indicates slower imbibition rates as core permeability decreases.

5.   In cases where the pressure gradient data in the transition zone is not available, generalized capillary pressure type curves, developed using capillary pressure measurements on core samples, can be compared to the log-derived water saturation.

6.   The capillary pressure-water saturation relationship is used in conjunction with the J-function to develop generalized capillary pressure type curves characteristic of the formation under consideration.

7.   Well log-derived water saturation can be normalized to a reference porosity, thus, excluding the effect of porosity variations on the saturation profile.

8.   When matched to the capillary pressure type curves, the normalized water saturation profile yields reasonable estimates of the absolute permeability, irreducible water saturation, the free water level, and relative permeability characteristics.

9.   The developed technique can be used in multi-layered as well as homogeneous reservoirs.

10. Examining the petrophysical data collected from three different tight sand fields revealed that the capillary pressure-water saturation relationship can be approximated over most of the saturation range by a linear trend on a log-log scale.

11. General capillary pressure type curves specific to tight sands are developed and matched to well log derived water saturation profiles for three different tight sand formations. Match results agree well with the results obtained with other techniques.

12. Based on the observed linear relationship on a log-log scale, a capillary pressure-water saturation empirical relationship is developed specific to tight sand formations. This relationship is used to adapt available relative permeability models for both the drainage and imbibition regimes to the case of tight sands.

13. In a homogeneous tight sand reservoir, the resistivity gradient is approximated by a straight line in the drainage regime. The extension of this line defines the free water level of the reservoir when it intersects with the zero resistivity axis.

6.2 Limitations & Recommendations

1. The development of type curves is based on petrophysical parameters derived from curve fitting of core data. The parameters used in this study are the average of nine cores representing Cotton Valley, Travis Peak, and Falher

formations. The addition of more data when available should improve the statistical representation of the match results.

2. The petrophysical models discussed in chapter V should only be used in the analysis of the other tight formations in which petrophysical similarity is demonstrated.

3. During the course of applying the technique to different reservoirs, it was found that 15 to 20 feet of homogeneous formations are necessary for fitting the saturation profile on the type curves in the case of layered transition zone. The homogeneous strata can be identified with Gamma Ray, Microlog, Microlaterolog, or Caliper log.

4. The developed technique may be extended to shaly sands, where corrections for shale effects must be considered in the algorithms used.

5. More experience is needed to apply the technique to carbonate reservoirs.

6. Since the matching technique is applicable over the transition zone only, some difficulties may be encountered during curve matching process in highly permeable gas reservoirs. This difficulty is due to their short transition zone. Heavy oil and low permeability reservoirs are good matching candidates because of their long transition zone.

BIBLIOGRAPHY

Alger, R. P., Luffel, D. L., and Truman, R. B., 1987: "New Unified Method of Integrating Core Capillary Pressure Data with Well Logs," SPE Tech. Paper 16793.

Amott, E., 1959: "Observations Relating to the Wettability of Porous Rock," Trans. AIME. vol. 216 156-162.

Amyx, W., Bass, D. M., and Whiting, R. I., 1960: "Petroleum Reservoir Engineering," Mc Graw-Hill, New York.

Anderson, W. G., 1986: "Wettability Literature Survey-Part 1: Rock, Brine Interaction, and the Effects of Core Handling on Wettability," JPT October, 1125-1149.

Anderson, W. G., 1986: "Wettability Literature Survey-Part 2: Wettability Measurement," JPT, November, 1246-1262.

Anderson, W. G., 1986: "Wettability Literature Survey-Part 3: The Effects of Wettability on the Electrical Properties of Porous Media," JPT, December, 1371-1378.

Anderson, W. G., 1987: "Wettability Literature Survey-Part 4: Effects of Wettability on Capillary Pressure," JPT, October, 1283-1299.

Anderson, W.G., 1987: "Wettability Literature Survey-Part 5: The Effect of Wettability on Relative Permeability," JPT, November, 1453-1468.

Aufricht, W.R., and Koepf, E.H., 1957: "The Interpretation of Capillary Pressure Data from Carbonate Reservoirs," AIME, Vol. 210, 402-405.

Berzin, V.M., Yarygina, V.S., and Dubrovina, N.A., 1982: " Adsorption of Asphatenes and Tar From Petroleum by Sandstone," Neftepromysl. Delo. 5, 15017. English translation available from the John Center Library, Translation No. 83-10107-08G.

Bobeck, J. E., Mattax, C.C., and Denekas, M. O., 1958: "Reservoir Rock Wettability—Its Significance and Evaluation," Trans. AIME, Vol. 213, 155-160.

129

Brooks, R. H. and Corey, A. T. 1964: "Hydraulic Properties of porous Media," Colorado State University, March.

Brown, H. W., 1951: "Capillary Pressure Investigations," Petroleum Transactions, AIME, Vol. 192, 67-74.

Brown, R. J. S. and Fatt, I. , 1956: "Measurement of Fractional Wettability of Oil Fields by the Nuclear Magnetic Relaxation Method," Petroleum Transactions, AIME, Vol. 207, 262-264.

Buckley, S. E. and Leverett, M. C., 1942: "Mechanism of fluid displacement in sands," Trans. AIME, Vol.164, 107-116.

Burdine, N. T., Gournay, L. S., and Reicherty,P. O. , 1950: "Pore Size Distribution of Reservoir rocks,"Trans. AIME, Vol. 189, 195-204.

Burdine, N. T., 1953: "Relative Permeability Calculations from Pore Size Distribution Data," Trans. AIME, Vol. 198, 71-78.

Caudle, B. H., Slobod, R. L., and Brownscombe, E. R., 1950: "Further Development In The Laboratory Determination Of Relative Permeability," Petroleum Transaction, AIME, August.

Chilingar, G. V. and Yen, T. F., 1983: "Some Notes on Wettability and Relative Permeabilitis of Carbonate Reservoir Rocks, II," energy Sources 7, No.1, 67-75.

Coates, G. R. and Dumanoir, J. L., 1974: "A New Approach to Improved Log-Derived Permeability," The Log Analyst, January-Febuary 17-31.

Craig, F. F., 1971: "The Reservoir Engineering Aspects of Water Flooding," Monograph series, SPE, Richardson, TX 3.

Corey, A. T., 1954: "The Interrelation Between Gas and Oil Relative Permeabilities," Producers Monthly, November, 38-41.

Donaldson, E. C., Thomas, R. D., and Lorenz, P. B., 1969: "Wettability Determination and Its Effect on Recovery Efficiency," Soc. Pet. Eng. J., March, 13-20.

Fatt, I., and H. Dykstra, 1951: "Relative permeability Studies," Trans. AIME., Vol. 192, 249-256.

Fatt, I., and Klikoff, W. A., 1959: "Effect of Fractional Wettability on Multiphase Flow Through Porous Media," Trans.AIME, 216, 426-432.

Geffen, T. M., Owens, W. W., Parrish, D. R., and Morse, R. A., 1951: "Experimental Investigation of Factors affecting Laboratory Relative Permeability Measurements," Trans AIME, Vol 192, 99-110.

Heseldine, G. M., 1974: "A Method of Averaging Capillary Pressure Curves," SPWLA 15th Annual Logging Symposium, June 2-5

Holbrook, O. C. and Bernard, G. G., 1958: "Determination of Wettability by Dye Adsorption," Trans. AIME, Vol. 213, 261-264.

Honarpour, M., Leonard, K. and Harvey, A. H., 1986: "Relative Permeability of Petroleum Reservoir," CRC Press., Florida, .

Johnson, E. F., Bossler, D. P., and Naumann, V. O., 1959: "Calculation of Relative Permeability from Displacement Experiments," Trans. AIME, Vol. 216, 370-376.

Keelan, D. K., 1972: "A Critical Review of Core Analysis Techniques," Jounal of Canadian Petroleum Technology, Vol 6, 42.

Killins, C. R., Nielsen, R. F., and J. C., 1953: "Capillary Desaturation and Imbibition in Porous Rocks," Producers Monthly, December 18, No. 2, 30-39.

Leas, W. J., Jenks, L. H., and Russell, C. D., 1950: "Relative Permeability to Gas," Trans. AIME, Vol. 189, 65-72.

Leverett, M. C., 1941: "Capillary Behavior in Porous Solids," Trans., AIME, Vol. 142, 152-169.

Lowe, A. C., Philips, M. C., and Riddiford, A. C., 1973: "On the wettability of Carbonate Surfaces by Oil and Water," J. Cdn. Pet. Tech., April-Jun, 12, No. 44, 33-40.

Morgan, W. B. and Pirson, S. J., 1964: "The Effect of Fractional Wettability on the Archie Saturation Exponent," Trans., SPWLA, Fifth Annual Logging Symposium, Midland, TX May 13-15 Sec.B.

Naar, J., and Henderson, J. H., 1961: "An Imbibition Model—Its Application to Flow Behavior and the Prediction of Oil Recovery," Soc. Pet. Eng. J., June, 61-70.

Ong, V., 1990: "An Investigation on Archie Saturation Exponent on Uncosolidated Water wet and Oil-wet Sands," M Sc thesis submitted to Petroluem Engineering Department, Louisiana State University.

Osoba, J. S., Richardson, J. G., Kerver, J. K., Hafford, J. A., and Blair, P. M., 1951: "Laboratory Measurements of Relative Permeability," Petroleum Transaction, AIME, October.

Pirson, S. J., Ed.:1952: "Oil Reservoir Engineering," Mc Graw Hill, New York.

Pirson, S. J., Boatman, E. M., and Nettle, R. L., 1964: "Prediction of Relative Permeability Characteristics of Intergranular Reservoir rocks from electrical resistivity measurements," Trans, AIME, Vol. 231, 564-570.

Purcell, W. R., 1949: "Capillary Pressure—Their Measurement Using Mercury and The Calculation of Permeability Therefrom," AIME, Vol. 186, 39-48.

Rapoport, L.A. and Leas, W. J., 1951: "Relative Permeability to Liquid in Liquid-Gas Systems," Trans. AIME, Vol 192, 83-98.

Raymer, L. L. and Freeman, P. M., 1984: "In-Situ Determination of Capillary Pressure, Pore Throat Size and Distribution, and Permeability from Wireline Data," SPWLA 25th Annual Logging Symposium, June 1-12.

Richardson, J. G., Kerver, J. K., Hafford, J. A., and Osoba, J. S., 1952: "Laboratory Determination of Relative Permeability," Petroleum Transaction, AIME March.

Richardson, J. G.,Perkins, F. M., and Osoba, J.S., 1955: "Differences in behavior of Fresh and Aged East Texas Woodbine Core," Trans. AIME, Vol. 204, 86-91.

Rose, W. and Bruce, W. A., 1949: "Evaluation of Capillary Character in Petroleum Reservoir Rock," Petroleum Transactions, AIME, May.

Salathiel, R. A. , 1972: "Oil Recovery by Surface Film Drainage in Mixed Wettability Rocks," Paper SPE 4104 presented at SPE 47th Annual Meeting, San Antonio, California, October 8.

Somasundaran, P., 1975: "Interfacial Chemistry of Particulate Flotation," Advance in Interfacial Phenomena of Particulate/Solution/Gas systems; Applications to Flotation Research, AICHE Symposium Series 71. No.150, 1-15.

Timur, A., 1968: "An Investigation of Permeability, Porosity, & residual Water Saturation Relationships For Sandstone reservoirs," The Log Analyst, August, 8-17.

Tixier, M. P., 1949: "Evaluation of Permeability From Electric-Log Resistivity Gradients," The Oil and Gas Journal, June, 113-122.

Treiber, L. E., Archer, D. L., and Owens, W. W., 1972: "A laboratory Evaluation of the Wettability of Fifty Producing Reservoirs," SPEJ, December, 531-540.

Welge, H. J., 1952: "A Simplified Method For Computing Oil Recovery By Gas Or Water drive," AIME, Vol. 195, 91-98.

Wyllie, M. R. J. and Rose, W. D., 1950: "Some Theoretical Considerations Related to the Quantitative Evaluation of the Physical Characteristics of Reservoir Rock from Electrical Log Data," Petroleum Transactions, AIME, Vol. 189, 105-118.

Wyllie, M. R. J. and Sprangler, M. B., 1952: "Application of electrical resistivity measurements to problems of fluid flow in porous media," Bull. AAPG, 36, 359.

Wyllie, M.R., and Grander, G. H. F., 1958: "The Generalized Kozeny-Carman Equation," World Oil, April, Production Section, 210-227.

APPENDIX A

Derivation of Relative Permeability Equations

for Tight Sands Under Drainage Conditions

Wyllie [1958] introduced Equations 2.41 and 2.42 that can be used to calculate the relative permeability curves using the capillary pressure data measured on a core sample. These two equations are:

$$K_{rw} = \left(\frac{S_w - S_{wi}}{1 - S_{wi}}\right)^2 \frac{\int_{S_{wi}}^{S_w} \frac{dS_w}{P_c^2}}{\int_{S_{wi}}^{1} \frac{dS_w}{P_c^2}} \qquad (2.41)$$

$$K_{mw} = \left(\frac{1 - S_w}{1 - S_{wi}}\right)^2 \frac{\int_{S_w}^{1} \frac{dS_w}{P_c^2}}{\int_{S_{wi}}^{1} \frac{dS_w}{P_c^2}} \qquad (2.42)$$

Where:

K_{rwt} is the relative permeability for the wetting phase;

K_{mwt} is the relative permeability for the non-wetting phase;

P_c is the capillary pressure; and

S_{wi} is the irreducible water saturation.

To solve the integral term in both equations, the capillary pressure, has to be expressed as a function of water saturation. This will render the integration function in one variable only, and consequently, it can be solved analytically.

Equation 5.1 for tight sands states:

$$P_c = \frac{a}{(S_w)^b}$$ (5.1)

where:

P_c is the capillary pressure;

S_w is the water saturation in fraction; and

a, b   are coefficients reflecting the formation pore size distribution.

The integral terms of equations 2.41 and 2.42 can be calculated using the straight line relationship represented by equation 5.1 as follows:

$$\int \frac{1}{P_c^2} \, dS_w = \int \frac{dS_w}{\left[\frac{a}{(S_w)^b}\right]^2}$$

$$= \frac{1}{a^2} \int (S_w)^{2b} \, dS_w$$

$$= \frac{1}{a^2} \left\{ \frac{(S_w)^{2b+1}}{2b+1} \right\}$$

then, $$\int \frac{1}{P_c^2} \, dS_w = \left\{ \frac{1}{a^2} * \frac{(S_w)^{2b+1}}{2b+1} \right\}$$

The above equation can be used to calculate the relative permeability of both the wetting and the non-wetting phases using Wyllie's model as follows:

a. Wetting phase:

In Wyllie's formula for the wetting phase (Equation 2.41), let the tortuosity factor be:

$$\left\{ \frac{S_w - S_{wi}}{1 - S_{wi}} \right\}^2 = K_1$$

Performing the integration gives:

$$K_{rwt} = K_1 \frac{(S_w)^{2b+1} \Big|_{S_{wi}}^{S_w}}{(S_w)^{2b+1} \Big|_{S_{wi}}^{1}}$$

Now, let $\qquad c = 2b + 1$, then

$$K_{rwt} = K_1 \frac{(S_w)^c \Big|_{S_{wi}}^{S_w}}{(S_w)^c \Big|_{S_{wi}}^{1}} = K_1 \frac{(S_w)^c - (S_{wi})^c}{1 - (S_{wi})^c}$$

Finally,

$$K_{rwt} = \left\{ \frac{(S_w - S_{wi})}{(1 - S_{wi})} \right\}^2 \left\{ \frac{(S_w^c - S_{wi}^c)}{1 - S_{wi}^c} \right\} \qquad (5.2)$$

b. Non-wetting phase:

Similarly, using Wyllie's formula for the non-wetting phase (Equation 2.42), let the tortuosity factor be:

$$K_2 = \left\{ \frac{1 - S_w}{1 - S_{wi}} \right\}^2$$

$$K_{mwt} = K_2 \frac{(S_w)^c \big|^1_{S_w}}{(S_w)^c \big|^1_{S_{wi}}}$$

$$K_{mwt} = K_2 \frac{1 - (S_w)^c}{1 - (S_{wi})^c}$$

Finally,

$$K_{mwt} = \left\{\frac{(1 - S_w)}{(1 - S_{wi})}\right\}^2 \left\{\frac{(1 - S_w^c)}{(1 - S_{wi}^c)}\right\} \tag{5.3}$$

As stated before, Equations 5.2 and 5.3 are much easier to use compared to Wyllie's equations. It should be remembered however, that this two equations are applicable to tight sand reservoirs only.

APPENDIX B

Derivation of Relative Permeability Equations

for Tight Sands Under Imbibition Conditions

Naar et al. [1961] introduced Equation 2.46 to calculate the relative permeability to the wetting phase under the imbibition regime. The equation states:

$$K_{rw \text{ (imb.)}} = \frac{\Phi^{*3} \sigma^2}{K} S^*_{w \text{ (imb)}} \int_0^{S^*_{w \text{ (imb)}}} \frac{S^*_{w \text{ (imb)}} - S}{P_c^2} \, dS \qquad (2.46)$$

where:

Φ^* is the reduced porosity expressed as:

$$\Phi^* = \Phi \, (\, 1 - S_{wi} \,)$$

σ is the interfacial tension;

K is the absolute permeability; and

$S^*_{w \text{ (imb)}}$ is the imbibition effective water saturation.

The effective water saturation is defined as:

$$S^*_w = \frac{S_w - S_{wi}}{1 - S_{wi}}$$

138

where S_{wi} is the irreducible water saturation.

To change the integration limits form effective saturation to "normal" saturation, we have:

$$S^* = \frac{S - S_{wi}}{1 - S_{wi}}$$

$$S = S^* (1 - S_{wi}) + S_{wi}$$

then, $$ds = (1 - S_{wi})\, ds^*$$

or $$ds^* = \frac{ds}{(1 - S_{wi})}$$

From the above equations, we can estimate the new limits as:

@ $S^* = 0$ $S = S_{wi}$

@ $S^* = S_w^*$ $S = S_w$

Introducing the new limits to Equation 2.42 yields:

$$K_{rw} = \frac{\Phi^{*3} \sigma^2}{K (1 - S_{wi})}\, S_{w,\,imb}^* \int_{S_{wi}}^{S_w} \frac{S_w^* - S^*}{P_c^2}\, dS \qquad (2.46b)$$

Now, The term $(S_w^* - S^*)$ also [1]can be changed as:

$$S_w^* - S^* = \frac{S_w - S_{wi}}{(1 - S_{wi})} - \frac{S - S_{wi}}{(1 - S_{wi})} = \frac{S_w - S}{(1 - S_{wi})}$$

then, Equation 2.46b becomes:

$$K_{rw} = \frac{\Phi^{*3}\,\sigma^2 S_w^*}{K\,(1-S_{wi})^2} \int_{S_{wi}}^{S_w} \frac{S_w - S}{P_c^2}\, dS \qquad (2.46C)$$

From Equation 5.1 we have:

$$P_c^2 = \frac{a^2}{S_w^{2b}}$$

Substituting P_c^2 from the above equation into Equation 2.46c yields:

$$K_{rw} = \frac{\Phi^{*3}\,\sigma^2\,S_w^*}{K\,(1-S_{wi})^2} \int_{S_{wi}}^{S_w} \frac{S_w^{2b}\,(S_w - S)}{a^2}\, dS$$

rearranging:

$$K_{rw} = \frac{\Phi^{*3}\,\sigma^2\,S_w^*\,S_w^{2b}}{K\,(1-S_{wi})^2\,a^2} \int_{S_{wi}}^{S_w} (S_w - S)\, dS$$

performing the integration:

$$K_{rw} = \frac{\Phi^{*3}\,\sigma^2\,S_w^*\,S_w^{2b}}{K\,(1-S_{wi})^2\,a^2} \left\{ S_w\,S - 0.5\,S^2 \right\}_{S_{wi}}^{S_w}\, dS$$

$$K_{rw} = \frac{\Phi^{*3}\,\sigma^2\,S_w^*\,S_w^{2b}}{K\,(1-S_{wi})^2\,a^2} \left\{ \left(S_w^2 - 0.5\,S_w^2 \right) - \left(S_w\,S_{wi} - 0.5\,S_{wi}^2 \right) \right\}$$

$$K_{rw} = \frac{\Phi^{*3}\,\sigma^2\,S_w^*\,S_w^{2b}}{K\,(1-S_{wi})^2\,a^2} \left(0.5\,S_w^2 - S_w\,S_{wi} + 0.5\,S_{wi}^2 \right)$$

finally:

$$K_{rw} = \frac{1}{2K} \; (\Phi^* S_w^*)^3 \; \left\{ \; \frac{\sigma S_w^b}{a} \; \right\}^2 \qquad (5.4)$$

VITA

Adel A. Ibrahim was born in Suez, Egypt, on April, 27, 1960. He joined the Department of Petroleum Engineering, Suez Canal University in October, 1979. After obtaining his B.Sc. degree in 1984, he was appointed to work as an assistant lecturer in the same department and he was also accepted in the graduate program to pursue a Master's degree. Adel defended his M.Sc. thesis in May, 1988. The thesis was focused on the effect of temperature and formation water salinity on polymer and surfactants flooding operations in the Egyptian oil fields. Adel's committee recommended him for a Ph.D. program, and he was awarded a governmental fellowship to pursue a Ph.D. degree in the United States.

He joined the Department of Petroleum Engineering, Louisiana State University in August,1989.

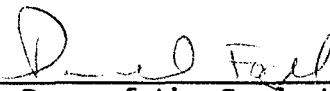# DOCTORAL EXAMINATION AND DISSERTATION REPORT

Candidate: Adel Afifi Ibrahim

Major Field: Petroleum Engineering

Title of Dissertation: IN-SITU DETERMINATION OF CAPILLARY PRESSURE AND RELATIVE PERMEABILITY CURVES USING WELL LOGS

Approved:

Robert Deshandes
Major Professor and Chairman

_D___ D Fxel_
Dean of the Graduate School

EXAMINING COMMITTEE:

Zaki Bassiou

George F. Hart

William Bernard

Philip D. Nunnell

Jine C. Wang

_____

_____
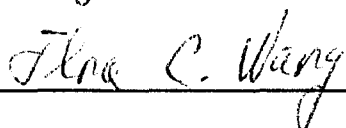
Date of Examination:

November 11, 1992